Engineering of Photosystem I Attachment to Titanium Oxide Nanostructures via Ferredoxin-Fusion Proteins

A Thesis Presented for the

Master of Science

Degree

The University of Tennessee, Knoxville

Tuo Zhu

May 2014

`

Copyright © 2014 by Tuo Zhu
All rights reserved.

`

DEDICATION

This thesis is dedicated to my parents, Shuiquan Zhu and Maili Duan, for their continual and comprehensive support.

ACKNOWLEDGEMENTS

I wish to express my sincere appreciation to my advisor Dr. Barry D. Bruce for giving me the opportunity to pursue this degree. His support, patience, encouragement and valuable advice have guided me along my journey. I would like to thank all my former and current committee members: Dr. Brad Binder, Dr. Engin Serpersu, Dr. Xiaolin Cheng and Dr. Paul Frymier. Their support and advice have helped me finish my project.

I also want to thank my labmates for their valuable advice and help: Richard Franklin Simmerman for teaching me techniques and helping me solve problems; Prakitchai Chotewutmontri for answering my questions; and everyone else that helped me in the Bruce laboratory. I would like to thank my collaborators for their patient help with my projects: Dr. Derek Cashman for teaching me MOE and some computational modeling software; Lijia Wang for providing the titanium oxide nanoparticles for my experiment; and Dr. John Dunlap for taking scanning electron microscope (SEM) images for me.

I would like to thank my parents and friends for always being there for me: my parents for giving me unconditional support, Wanjing Liu for taking good care of me, and everyone else for being nice and patient with me. I feel extremely blessed to have you in my life.

ABSTRACT

Ferredoxins (Fds) are iron-sulfur proteins that mediate electron transfer in a range of metabolic reactions. In the thylakoid membrane of photosynthetic organisms, Fd facilitates electron transfer from the stromal surface of photosystem I (PSI) to the ferredoxin Nicotinamide adenine dinucleotide phosphate oxidoreductase (FNR), which requires that Fd is capable of docking and transferring electrons between these two complexes. In applied photosynthesis, many efforts have been devoted towards re-directing these electrons into either a hydrogen-evolving catalyst or an electron-conducting semiconductor. In this study, the electrons from the PSI complex are directed to a titanium oxide (TiO_2) electrode, and Fd is used to facilitate the electron transfer. In doing so, three different TiO_2 binding peptides (TOBiP) were introduced to Fd in order to provide a specific affinity for TiO_2. The TOBiP-Fd fusion proteins were characterized for their ability to transfer electrons, and optimized for its attachment to TiO_2 nanoparticles. In addition, we have chemically crosslinked PSI to TOBiP-Fd and optimized the attachment of the PSI-Fd-TOBiP complex protein to TiO_2. In the future, we will test and optimize the photocurrent generated by the PSI-Fd-TiO_2 complex.

`

TABLE OF CONTENTS

Chapter 1 Introduction and Literature Review 1

1.1. Origin of Photosynthesis and Cyanobacteria 1

1.2 Electron transport between PSII and PSI 2

1.3 Interaction between PSI and Fd 5

1.4 Applied Photosynthesis 10

1.4.1 Biofuel production 11

1.4.2 Hydrogen production 12

1.4.3 Photocurrent generation 12

1.5 Biological based photovoltaics using hybrid dye-sensitized solar cells 15

1.6 Properties of TiO_2 nanoparticles 19

1.7 Selection of titanium oxide binding peptides and molecular modeling of TiO_2 binding peptides 19

1.8 Conclusion 20

Chapter 2 Material and Methods 22

2.1 Codon analysis and Codon optimization of TeFd 22

2.2 Cloning of TeFd gene 22

2.3 Expression and purification of protein using the IMPACT System 29

2.4 MALDI-TOF mass spectrometry 31

2.5 Difference Spectroscopy 32

2.6 Gel electrophoresis and staining 32

2.7 Production and purification of Fd antibody 34

2.8 Western blotting 35

2.9 Design of in vitro binding assay to TiO_2.....36

2.10 Purification of PSI 37

2.11 Cross-linking of Fd to PSI.....39

2.12 Chl *a* measurement 40

2.13 Computational modeling of PSI and Fd interaction 40

Chapter 3 Results 42

3.1 Introduction.....42

3.2 Computational modeling of the docking site between PSI and Fd.....44

3.3 Cloning of the *Thermosynechococcus elongatus* ferredoxin (TeFd) gene 50

3.4 Generation of TOBiP-TeFd.....54

3.5 Expression, purification and characterization of TeFd. 56

3.6 TOBiP-Fd attachment to TiO_2 nanoparticles 63

3.7 Fd-PSI chemical crosslinking 71

3.8 PSI-TOBiP Fd attachment on TiO_2.....80

Chapter 4 Discussion.....83

4.1 Introduction.....83

4.2 Introduction of TOBiP to Fd 83

4.3 Functional characterize Fd 88

4.4 In vitro binding of TOBiP-Fd to TiO_2 nanoparticle.....89

4.5 PSI attachment to TiO_2 nanostructures via Fd-Fusion Proteins 90

`

Chapter 5 Conclusion and Future Directions 93

List of References 95

Appendix 114

Vita 119

`

LIST OF TABLES

Table 1 Sequence of TOBiPs Used in this study 21

Table 2 Ligation protocol.....26

Table 3 Colony PCR reaction recipe and cycling condition.....27

Table 4 Colony PCR cycling condition 27

Table 5 PCR reaction recipe and cycling condition.....28

Table 6 PCR cycling condition 28

Table 7 Distance restraints used for each docking run 47

Table 8 Interaction energies calculated for PSI/Fd docked complexes.....48

`

LIST OF FIGURES

Figure 1.1 Electron transport pathways of oxygenic photosynthesis.....4

Figure 1.2 Crystal structure of the monomeric PSI 8

Figure 1.3 Structural basis of PSI interaction with PC and Fd 9

Figure 1.4 Reported PSI generated photocurrents over the past eight years 14

Figure 1.5 Schematic overview of a dye-sensitized solar cell 17

Figure 1.6 Model for the hybrid photovoltaic device.....18

Figure 3.1 Sequence of PsaC, D and E subunits and Fd proteins.....46

Figure 3.2 Different docking models between PsaCDE subunits and Fd.....49

Figure 3.3 CAI analyses of WT TeFd and C.O.TeFd 51

Figure 3.4 Digestion of pBSK-C.O.TeFd and pTYB2.....52

Figure 3.5 Colony PCR confirmation of pTYB2-TeFd 53

Figure 3.6 Cloning constructs of pTYB2-TOBiP-TeFd 55

Figure 3.7 Expression Screening.....58

Figure 3.8 Protein purification profile 59

Figure 3.9 Protein purification result 60

Figure 3.10 MALDI-TOF Spectra for purified proteins.....61

Figure 3.11 Difference spectrum of purified Fd.....62

Figure 3.12 Optimization of TOBiP-Fd attachments to TiO_2 nanoparticle 65

Figure 3.13 SEM images of TiO_2 nanoparticles 68

Figure 3.14 Purification of anti-TeFd.....73

Figure 3.15 Crosslink results 74

Figure 3.16 Optimization of the crosslinking reaction..... 75

Figure 3.17 Optimized crosslink results 79

Figure 3.18 PSI Standard curve..... 81

Figure 3.19 Relative amount of PSI-TOBiP Fd that is bound on TiO_2..... 82

Figure 4.1 Crystal Structure of Fd from different organisms 87

Figure 4.2 Model for PSI attachment to TiO_2 nanostructures..... 92

`

Chapter 1 Introduction and Literature Review

1.1. Origin of Photosynthesis and Cyanobacteria

Photosynthesis is an ancient process which converts light energy into chemical energy that can be used for metabolic processes (Blankenship & Hartman, 1998). It is known that photosynthesis is the only significant solar energy storage process on Earth. In addition, it is the source of all of our food and most of our energy resources (Blankenship, 2010). Considering the importance of this process, a great amount of research has been done to investigate photosynthesis, including its origin. Even through numerous hypotheses have been made on where and how photosynthesis originated, there is no direct evidence to support any of these predictions (Blankenship, 2010; Des Marais, 2000; Govindjee, 2009; John M. Olson, 2004; Wang et al., 2006). Evidence from previous research suggests that photosynthesis may have arisen approximately 3.5 to 3.2 billion years ago in bacteria and has evolved to form the photosynthetic organisms present today (Blankenship, 2010; Des Marais, 2000; Govindjee, 2009), including land plants and algae (Des Marais, 2000; Govindjee, 2009).

Among all the photosynthetic organisms, cyanobacteria are the only known prokaryotes which perform oxygenic photosynthesis (photosynthesis that release oxygen) (Altermann & Kazmierczak, 2003; Mulkidjanian et al., 2006). Due to their rapid life cycle and relatively ease in manipulating their genetic

background, cyanobacteria have long served as model organisms for photosynthesis research (Jan Zarzycki, 2012). Cyanobacteria comprise an extremely diverse phylum and have colonized a wide range of environmental niches, including some extreme environments like high temperature (Shih et al., 2013; Yamaoka et al., 1978).

Thermosynechococcus elongatus (*T.e*) strain BP-1 is a unicellular rod-shaped cyanobacterium originally isolated from a hot springs at Beppu on Kyushu Island in Japan and has an optimum growth temperature of approximately 55 ºC (Yamaoka et al., 1978). Previous studies have provided a complete genome sequence for *T. elongatus* (Nakamura et al., 2002). In addition, the Photosystem I and II complexes of this organism are highly stable and have been structurally solved by X-ray crystallography (Jordan et al., 2001a; Zouni et al., 2001). Considering all these advantages, *T. elongatus* was selected for this project.

1.2 Electron transport between PSII and PSI

It is commonly known that photosynthesis occurs in two stages: light-dependent reactions and light-independent reactions. During the light-dependent reactions, light is captured and utilized to generate ATP and NADPH while the light-independent reactions use these products to capture and reduce carbon dioxide (Clayton, 1976). The light-dependent reactions of photosynthesis mainly

occur in the thylakoid membranes and are mediated by photosystem II (PSII) and photosystem I (PSI) which are linked by a series of proteins and protein complexes as described below (Rochaix, 2011).

As shown in Figure 1.1, PSII uses light energy to split water and create a charge separation across the thylakoid membrane. Electrons from PSII are then transferred to the plastquinone (PQ) pool and used to generate PQH_2. The PQH_2 reduces cytochrome b_6f (Cyt b_6f) and is recycled back to the PQ pool (Rochaix, 2011). The electrons from the Cyt b_6f complex are transported to PSI through a soluble electron carrier in the lumenal space (Hippler et al., 1998). This electron carrier may be plastocyanin (PC) and / or cytochrome c (Cyt c) depending on the organism (Bryant & Frigaard, 2006; Katoh et al., 1962).

Photosynthetic electron transfer creates a proton gradient across the thylakoid membrane which is used by the ATP synthase to generate ATP. These ATP are then used for CO_2 fixation and for other cellular processes (Rochaix, 2011).

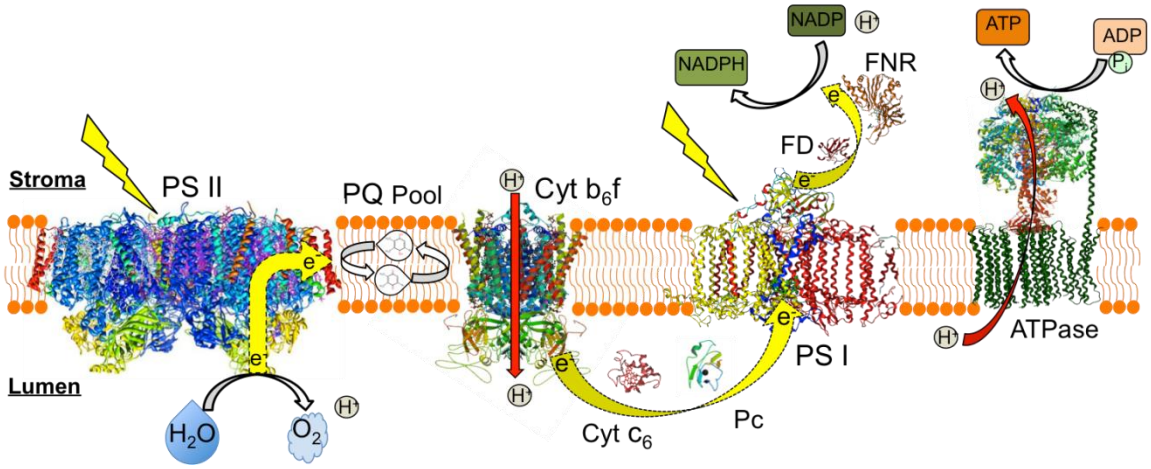

Figure 1.1 Electron transport pathways of oxygenic photosynthesis

The thylakoid membrane with PSII, Cyt b_6f, PSI, and ATP synthase is shown. Electron transport pathways are shown by the yellow arrow to indicate the direction of electron flow. PSII uses light energy to split water and create a charge separation across the thylakoid membrane. Electrons are transferred from PSII through the PQ pool to Cyt b_6f and further transferred to PSI via the soluble electron carrier PC and / or Cyt c. Ultimately FNR reduces $NADP^+$ to NADPH with the electrons transported from PSI via Fd (adopted from Rohaix *et al.,* 2011).

`

1.3 Interaction between PSI and Fd

The structure of cyanobacterial PSI was first solved to 2.5 Å in 2001 (Jordan et al., 2001b). In most cyanobacteria the PSI complex is a trimer with a molecular weight (MW) nearly a megadalton. Each monomer of PSI contains 12 subunits and many cofactors (including 22 carotenoids, 96 chlorophylls, 2 phylloquinones, 3 [4Fe4S] centers, 4 lipids, and approximately 200 water molecules) (Figure 1.2). A common feature of PSI is the presence of a stromal domain which is composed of three subunits: PsaC, PsaD, and PsaE. It was determinated that the stromal subunit PsaC coordinates two [4Fe-4S] centers (F_A and F_B), which participated in rapid electron transfer to ferredoxin (or flavodoxin) (Figure 1.3) (Golbeck, 1999), and the detailed electron transfer process is described below.

As mentioned previously, electrons flow from PSII to PSI via soluble electron carrier proteins, Cyt c or PC (Bryant & Frigaard, 2006; Katoh et al., 1962). Upon excitation at the P700 reaction center of PSI (Hippler et al., 1998), the excited electron transfers through the [4Fe-4S] center, F_X, into F_A and F_B in the PsaC subunit (Zanetti & Merati, 1987; Zilber & Malkin, 1988). The electron is then transferred out of the PSI membrane complex to the [2Fe-2S] cluster of Fd or to flavodoxin under iron-limiting conditions (Godman & Balk, 2008; Ragsdale & Ljungdahl, 1984) (Figure 1.3). Fd transports the electron to FNR, and FNR reduces $NADP^+$ to NADPH, which functions as a reductant in reactions of the Calvin Cycle and several other metabolic processes (Berg et al., 2007; Rochaix,

2011). The process that electron transport from PSII to FNR is called the noncyclic electron transport (Raven, 1969). Besides noncyclic electron transport, there is a cyclic electron transport which starts at PSI. PSI passes electrons to its primary acceptor Fd, then to Cyt b_6f complex, and then to PC before returning to PSI. This transport chain produces an H^+ concentration gradient that can be used to synthesis ATP (Raven, 1969, 1970). Considering the important role Fd plays in electron transfer during photosynthesis, it is very important to understand the interactions between Fd and PSI.

Ferredoxin has been extensively studied ever since it was first sequenced in 1967 (Matsubara et al., 1967; Sasaki & Matsubara, 1967). Fd belongs to a group of [Fe-S] proteins. Functional analysis has indicated that Fd is an electron transport protein which is involved in various electron transfer reactions, including photosynthesis (D. O. Hall, 1973). Studies have shown that plant Fds are red in color and possess absorption maxima at 465, 420 and 330 nm. The absorption of the protein in the visible region is mainly due to the iron-sulfur center and is lost on treatment with reagents which remove iron or sulfur (D. O. Hall, 1973).

In addition, many studies have been performed to investigate the interaction between PSI and Fd. Early crosslinking studies in spinach identified subunits with a molecular weight around 20 kDa (Zanetti & Merati, 1987; Zilber & Malkin, 1988) that can crosslink to Fd. This subunit has been identified as PsaD, a stromal subunit of PSI (Sonoike et al., 1993). Several years later, similar results were observed in the cyanobacterium *Synechocystis sp.* PCC 6803 which

supports the hypothesis that interactions exist between PSI stromal subunits (PsaC, D and E) and Fd (Andersen et al., 1992; Lelong et al., 1994). Many key residues that contribute to the interaction between PSI and Fd have been identified using site directed mutagenesis and chemical crosslinking (Hanley et al., 1996; Lelong et al., 1996b; Sonoike et al., 1993; Zanetti & Merati, 1987). These results suggested that the docking site would allow close proximity between the [2Fe-2S] center of Fd and the terminal [4Fe-4S] center of PSI (Hanley et al., 1996; Lelong et al., 1996a; Lelong et al., 1994; Setif et al., 2010a).

Although there have been many approaches to elucidating the interactions between PSI and Fd, the lack of a high-resolution crystal structure of a PSI-Fd complex has prevented a detailed model (Cashman et al., 2014). In the present work, computational approaches enable the integration of experimental data into predictive models describing how Fd can dock to PSI. The “Protein Frustratometer” (EMBNet, http://www.frustratometer.tk/) utilizes energy landscape theory (Jenik et al., 2012) and provides a computational algorithm that identifies these regions of high localized energetic frustration in protein structures. The highly frustrated regions in protein structures can be used to identify possible binding sites between proteins (A. Das & Plotkin, 2013).

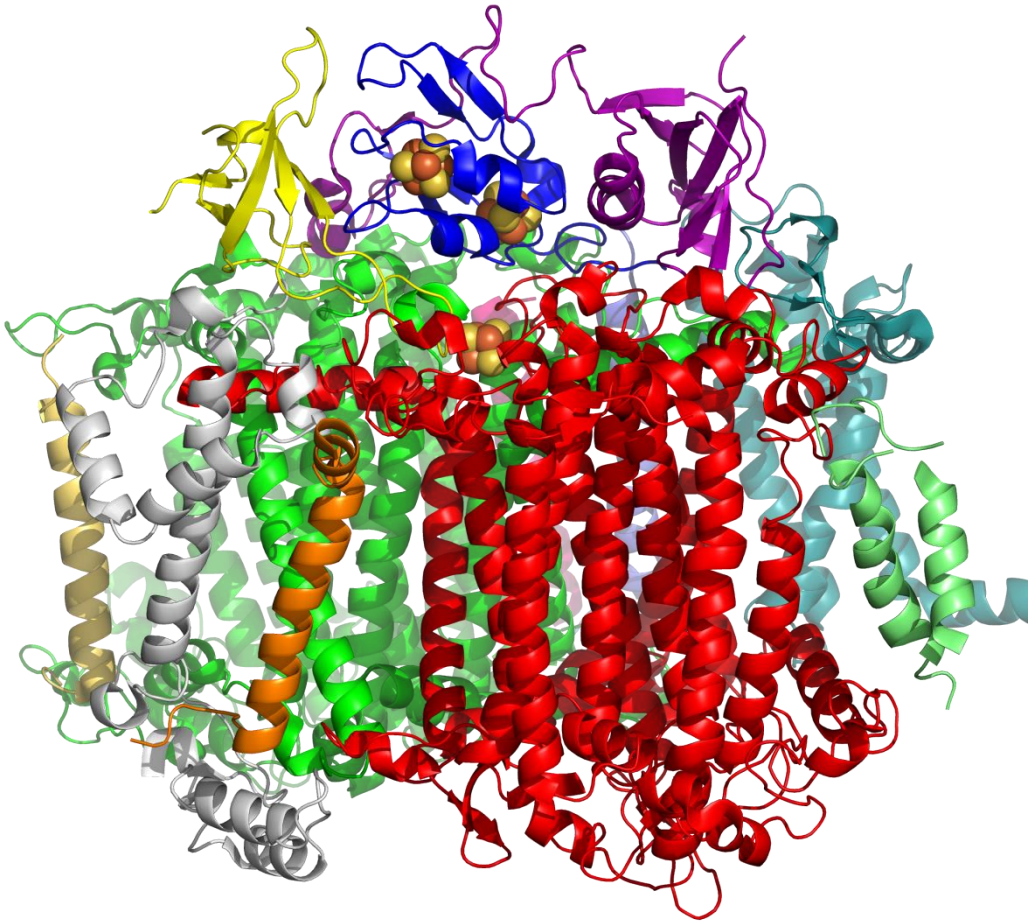

Figure 1.2 Crystal structure of the monomeric PSI

The backbone of *T. elongatus* PSI (PDB ID: 1JB0) is represented in ribbons and each subunit is colored differently: PsaA (red), PsaB (green), stromal subunits PsaC (blue), PsaD (purple), and PsaE (yellow). The [4Fe–4S] centers F_X, F_A and F_B, are represented in space filling and colored by element, Fe (red) and S (yellow).

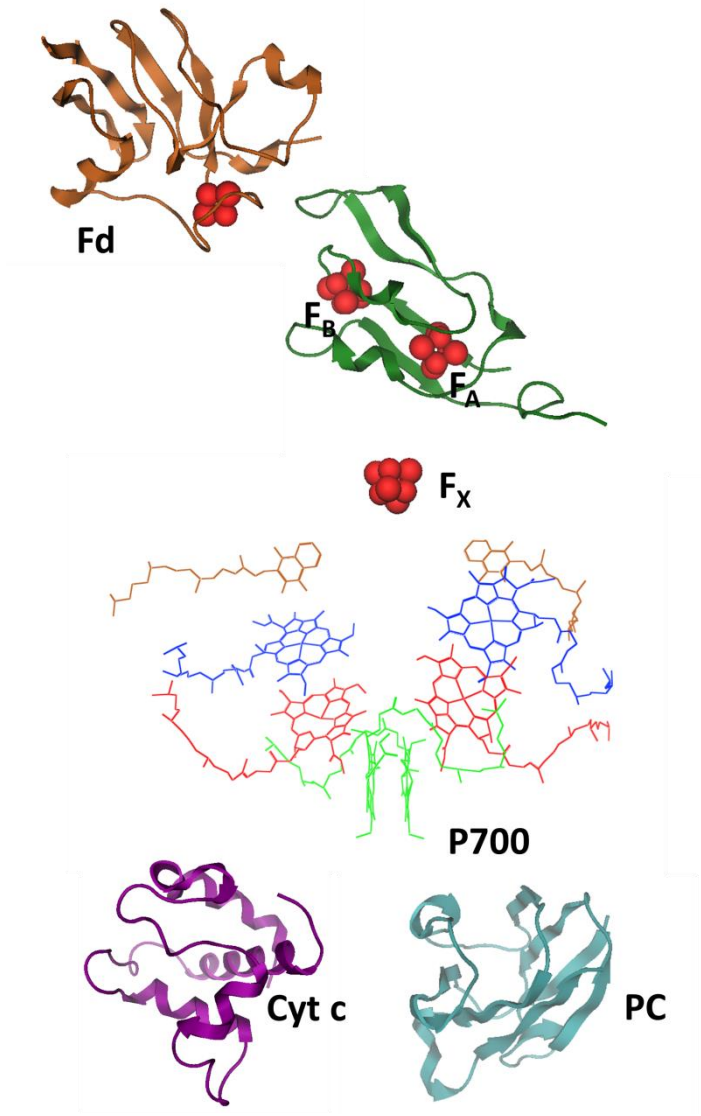

Figure 1.3 Structural basis of PSI interaction with PC and Fd

Electrons from PC (cyan) or Cyt c (purple) are transported to the P700 reaction center (green) where they are energized and transported to [4Fe-4S] clusters FX, FA and FB (red cubes) in PsaC (green). Finally, the electrons arrive at Fd (brown) which is docked on the stromal side of PSI. PSI (PDB ID: 1JB0), Fd (PDB ID: 2CJN), Cyc c (PDB ID: 4EIC) and PC (PDB ID: 2PLT).

1.4 Applied Photosynthesis

Over 85% of world energy demands are met by the combustion of fossil fuels like coal, oil, and natural gas, unfortunately current oil reserves have been estimated to be sufficient for only the next 42 years (Govoni et al., 2008). Considering the limited fossil fuel resources and the heavy pollution caused by their use, finding alternative, sustainable and clean sources of energy is a striking and urgent need (Andreiadis et al., 2011; Berardi et al., 2014; Govoni et al., 2008; Gust et al., 2009).

Of the potential energy sources that might meet these criteria, sunlight is the most promising one. The sun delivers energy to the earth's surface at an average rate of 120,000 trillion watts per year, which is about 4 orders of magnitude larger than the current rate of worldwide technological energy use by humans (Gust et al., 2009). Even though some methods have been developed to convert sunlight into electricity, several disadvantages persist, making it hard for solar energy conversion to compete with fossil fuels (Berardi et al., 2014). Discovery of a fundamental scientific basis for new solar fuel technologies is desired.

Photosynthesis, through billions of years of evolution, is a process that sustainably converts light into chemical energy. Investigations have been performed using the fundamental science underlying photosynthetic energy conversion to design systems that convert light into stored chemical energy, and this field is called applied photosynthesis. There are several general approaches

in applied photosynthesis which include biofuel production, hydrogen production and photovoltaic cells (Berardi et al., 2014; Hammarstrom & Hammes-Schiffer, 2009).

1.4.1 Biofuel production

Any fuel derived directly from living organisms or from their metabolic byproducts is defined as a biofuel. The potential of using photosynthetic organisms to produce biofuel is of particular interest. Several desirable features of photosynthetic microorganisms have made them attractive for biofuel production, including ease of cultivability, a relative high growth rate (compared to land plants), and the capability of accumulating a very large amount of feedstock for biofuel production (Scott et al., 2010).

Many cyanobacterial strains have been metabolically engineered to produce desired biofuels including ones that produce isobutyraldehyde and isobutanol (Atsumi et al., 2009; Lan & Liao, 2011), ethanol (Deng & Coleman, 1999), or isoprene (Lindberg et al., 2010). In the past few years, the production of biodiesel from algae and cyanobacteria has been an area of considerable interest (Miao & Wu, 2006; Scott et al., 2010).

1.4.2 Hydrogen production

The metabolism of hydrogen by photosynthetic microorganisms such as algae has been studied since 1939. It was observed that H_2 can be photo produced by treating algae with electron transport inhibitors (Gaffron, 1939). Later research explained this observation and claimed that the H_2 production was achieved by directing electron flow from PSI to a hydrogenase (Stuart & Gaffron, 1972).

Since then, photosynthetic microorganisms have been extensively studied for their ability to produce H_2 from sunlight and water (D. Das & Veziroglu, 2001; Ghirardi et al., 2005). In addition to these *in vivo* studies, several *in vitro* studies have succeeded in producing H_2 by coupling the PSI complex to either platinum nanoparticles or a hydrogenase (Evans & O'Neill, 2004; Ihara & Nakamoto, 2006; Ifeyinwa Jane Iwuchukwu et al., 2010; Millsaps et al., 2001).

1.4.3 Photocurrent generation

As mentioned earlier, PSI is capable of generating a charge separation with an internal quantum efficiency approaching one (Hogewoning et al., 2012). Due to the high light conversion efficiency and rapid charge separation of PSI, researchers from around the world have investigated the redirection of light excited electrons into photovoltaic devices.

In an earlier study, Greenbaum's group immobilized PSI on fiberglass filter paper which had direct contact with a metal electrode and generated sustained photocurrent under light illumination (Greenbaum, 1989). This result revealed the possibility of using photosynthetic biological materials (like PSI) for the direct conversion of solar energy to electricity. Several groups have now used PSI as a photoactive material for photocurrent generation (G. Chen et al., 2013; Mershin et al., 2012c).

Over the past 10 years, numerous groups have worked to improve artificial electron transfer to and from PSI in photovoltaic devices. For example, several attempts have been made to replace the electron acceptor Fd with an organic or inorganic semiconductor (like TiO_2) to develop a biologically-based photovoltaic device (R. Das et al., 2004; Mershin et al., 2012a; Yehezkeli et al., 2013). Due to the extensive research in this field, a 10-fold increase in photocurrent per year has been observed in this field (Figure 1.4) (Nguyen & Bruce, 2014).

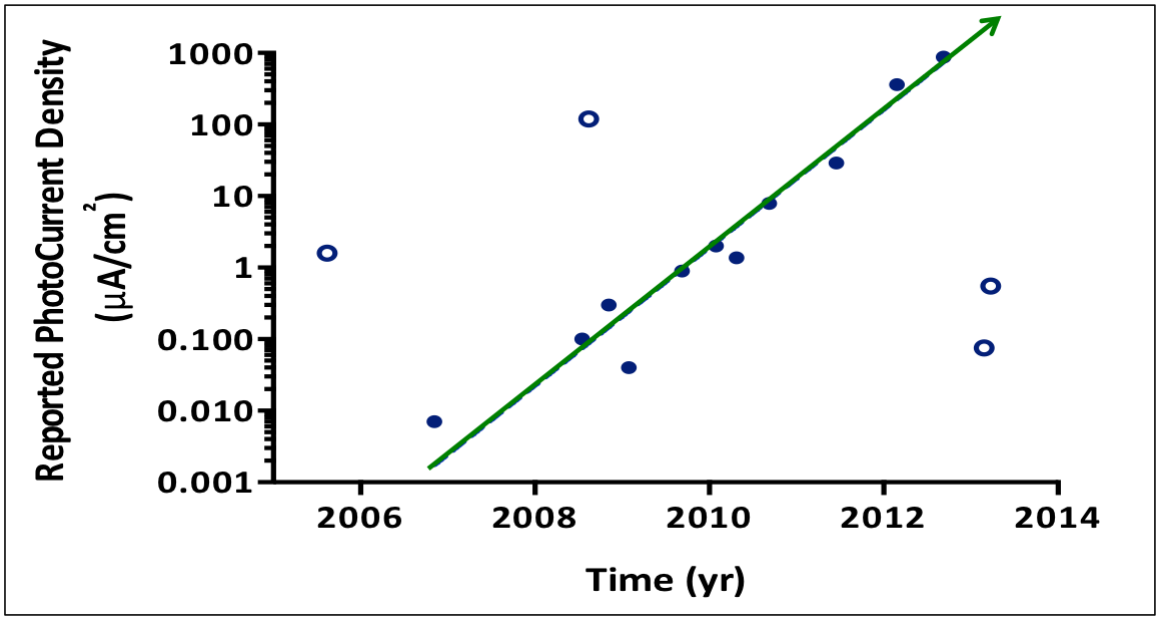

Figure 1.4 Reported PSI generated photocurrents over the past eight years

Photocurrent density extracted from PSI studies over the past eight years. On average, a 10-fold increase in rate (μA/cm2) per year has been observed with the fitted trend line (open points excluded) (Nguyen & Bruce, 2014).

1.5 Biological based photovoltaics using hybrid dye-sensitized solar cells

In order to build a photovoltaic device, the dye-sensitized solar cell (DSC) was selected as a model, and several modifications were applied to generate a biological based hybrid dye-sensitized solar cell.

The DSC, also known as the Grätzel cell, was originally invented by Grätzel's group (Brain O' Regan & Michale Gratzel, 1991). The DSC is composed of 3 primary components as shown in Figure 1.5. A mesoporous semiconductor layer was used to establish electronic conduction and is deposited on conductive glass. A monolayer of dye (also called molecular photosensitizer), which is capable of light driven charge separation, is coated on the surface of the semiconductor. Upon photo excitation, the dye injects electrons into the mesoporous semiconductor, leaving the dye in its oxidized state. The dye molecule is then regenerated by the liquid electrolyte. The redox system passes electrons through electrolytes to cathode and completes its regenerative cycle (Brain O' Regan & Michale Gratzel, 1991; Hagfeldt et al., 2010).

Even through the DSC is widely used, it still has several problems to be solved: 1. the dye is unstable; 2. the dye, platinum and conducting glass are expensive; and 3. the electrolyte solution and platinum are hazardous to human health and the environment (Chang et al., 2014). To overcome these problems, a low cost, highly efficient and environmentally friendly assembly is desired. Using biological materials, like PSI, to replace the costly and unstable dye in the DSC

could help solve some of these problems. The PSI from photosynthetic organisms can be easily harvested and remains functionally active for months or even years (I. J. Iwuchukwu et al., 2011; Kiley et al., 2005; Toporik et al., 2012). The high efficiency of light conversion and the fact that it is non-hazardous also make PSI an attractive alternative for the synthetic dye molecule.

Previous research has incorporated PSI in some bio-hybrid devices to create electrical power (Blankenship et al., 2011; Mershin et al., 2012c). It is of critical importance to optimize the process of transferring the electrons from the P700 reaction center within PSI to the electrodes. Since it may be difficult to further minimize the distance between the [4Fe-4S] centers in PsaC and the electrodes, Fd may be used as intermediary to connect PSI and the electrode, thus facilitating electron transfer. By directly linking Fd to the PsaC, D and E subunits of PSI, it may be possible to build a hybrid photovoltaic device. The principle of operation and energy level scheme of the hybrid photovoltaic device is shown in Figure 1.6. Photo-excitation of the P700 reaction center of PSI is followed by electron transport within PSI to its stromal [4Fe-4S] centers F_A and F_B. The electron is then transferred into Fd and injected into the conduction band of the TiO_2 nanoparticles. The dye molecule (PSI) is regenerated by the redox system (Cyt c), which itself is regenerated by sacrificial electron donor ascorbate.

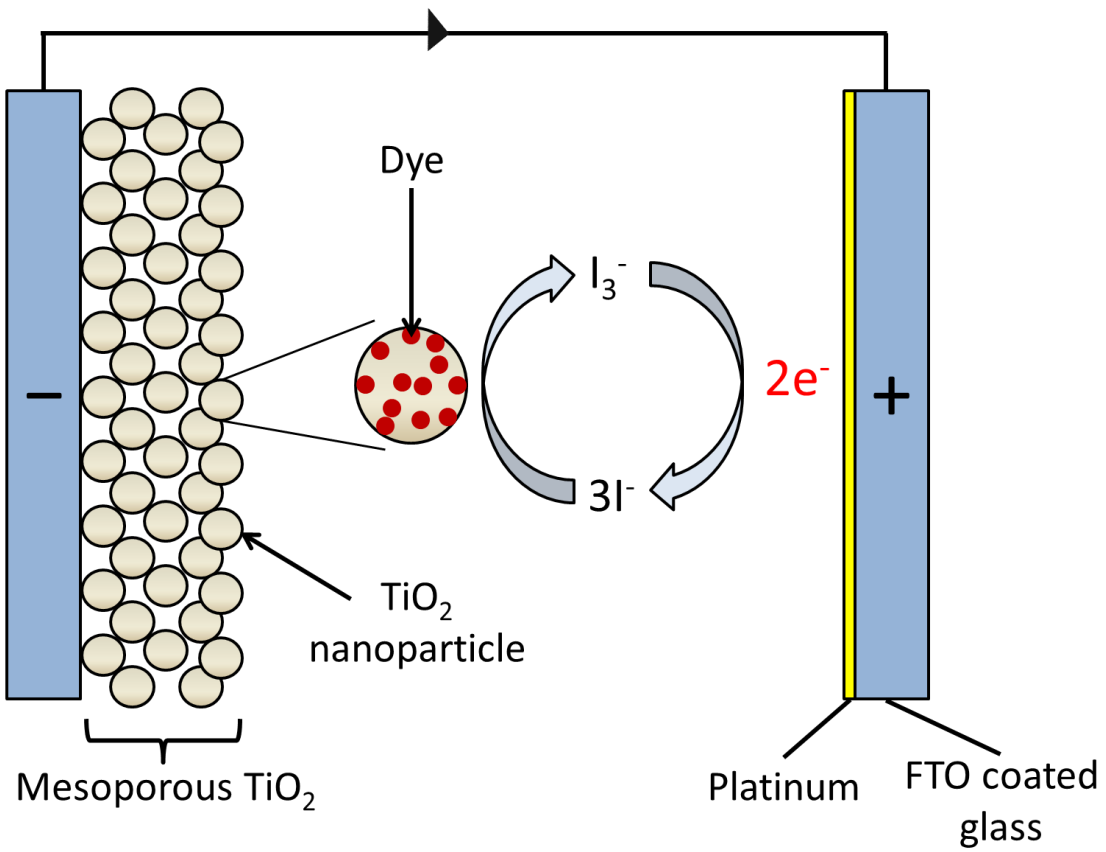

Figure 1.5 Schematic overview of a dye-sensitized solar cell

Photo-excitation of the dye is followed by electron injection into the mesoporous metal oxides semiconductor. The dye molecule is regenerated by the iodide/triiodide redox system, while the redox system is regenerated by receiving electrons through the electrolyte from the anode. The anode is coated with a thin layer of platinum catalyst and is deposited on a transparent conducting oxide on a glass or plastic substrate. The most commonly used substrate is glass coated with fluorine-doped tin oxide (FTO).

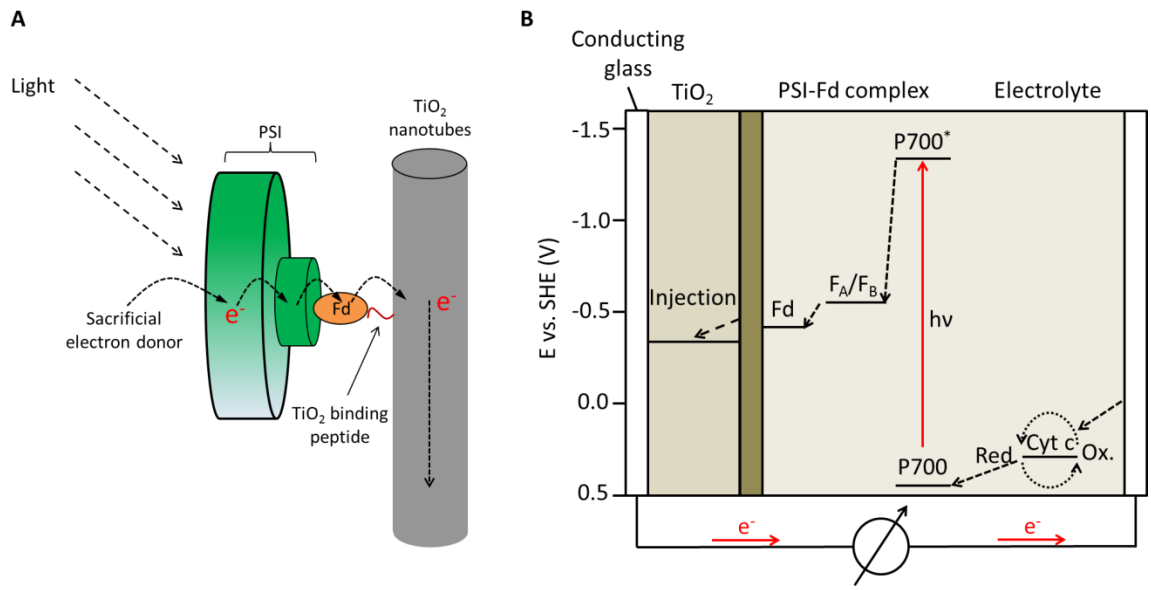

Figure 1.6 Model for the hybrid photovoltaic device

A) The stromal side of PSI is connected to the TiO_2 electrode via the TiO_2 binding peptide-Fd fusion protein. Upon exposure to light, excited electrons from PSI will be injected into the TiO_2 electrode via Fd. B) Principle of operation and energy level scheme of the hybrid photovoltaic device. Photo-excitation of the P700 reaction center of PSI is followed by electron transport within PSI to its stromal [4Fe-4S] centers F_A and F_B. The electron is then transferred into Fd and injected into the conduction band of the TiO_2 nanoparticles. The dye molecule is regenerated by the redox system (Cyt c), which itself is regenerated by sacrificial electron donor ascorbate. Potentials are referred to the standard hydrogen electrode (SHE).

`

1.6 Properties of TiO_2 nanoparticles

Titanium dioxide (TiO_2) is the naturally occurring oxide of titanium. Several forms of TiO_2 exist in nature. Among those, anatase and rutile are the two common forms. TiO_2 is almost an ideal semiconductor because of its high stability, low cost and safety with respect to both humans and the environment (Macwan et al., 2011).

The performance of TiO_2 based biophotovoltaics is largely influenced by the size of the TiO_2 nanoparticle. The high surface-to-volume ratio achieved by nanoparticles can provide more area for PSI adsorption and light harvesting (Macwan et al., 2011; Mershin et al., 2012b). To achieve a higher surface-to-volume ratio of the particle, various techniques have been used (Sugimoto et al., 2003). As a result, TiO_2 nanoparticle was chosen as the electrode in our study.

1.7 Selection of titanium oxide binding peptides and molecular modeling of TiO_2 binding peptides

A growing number of peptides capable of specifically recognizing inorganic materials have been reported, yielding a library of peptides that can be utilized as biological linkers to conjugate biomolecules to inorganic materials at the nano scale (Thai et al., 2004). These inorganic-binding peptides can be inserted into protein structures and used as “molecular erector sets” that will direct the assembly of hybrid materials (Sarikaya et al., 2003). Recently, much

effort has been directed at identifying short peptides that bind with high affinity and specificity to certain inorganic materials, like titanium oxide binding peptides (TOBiPs) (Haibin Chen; Su, 2008).

As mentioned in the previous section, Fd will be attached to a TiO_2 nanoparticle. To enable this design, three TOBiPs were tested to determine which one would provide Fd with the highest affinity to the TiO_2 nanomaterial (Table 1). However, due to the lack of a detailed model between PSI and Fd, work was first conducted to generate a method that would allow incorporation of TOBiP into Fd without interrupting the interactions between PSI and Fd.

1.8 Conclusion

The goal of this project is to help solve the energy crisis human beings are facing by generating a low cost, high efficiency photovoltaic device using biological materials. The interaction between PSI and Fd will be studied using computational modeling. TOBiP will be engineered to Fd, and the fusion protein will be characterized and optimized for its attachment to the TiO_2 nanoparticle. Finally, PSI will be crosslinked to TOBiP-Fd and attached to the TiO_2 electrode, creating a photovoltaic device.

`

Table 1 Sequence of TOBiPs Used in this study

TOBiP	Sequence
STB1	CHKKPSKSC
STB2	CTKRNNKRC
LSTB1	AHKKPSKSA

`

Chapter 2 Material and Methods

2.1 Codon analysis and Codon optimization of TeFd

The complete genome information of *T. elongatus* was provided by the National Center for Biotechnology Information (NCBI Reference Sequence: NC_004113.1). The wild type ferredoxin (petF) gene sequence was found within the genome (locus tag: tsl1009) with a total length of 297 bp (Appendix 1). The codon optimization was performed by online software provided by JAVA Codon Adaptation Tool (JCat, http://www.jcat.de/Start.jsp) (Carbone et al., 2003). The WT *T. elongatus* Fd (TeFd) gene sequence was set as input sequence, and *E. coli* was selected as output organism. Then, the codon optimized TeFd gene sequence was generated. In order to insert Fd gene into a pTYB2 expression vector, an NdeI (CAT ATG) restriction site at 5' and an XmaI (CCC GGG) restriction site at 3' were introduced to the codon optimized ferredoxin gene sequence (before the stop codon). The codon optimized TeFd (C.O.TeFd) gene was synthesized by Epoch Life Science (Epoch, Sugar Land, TX) and received as a pBSK-C.O.TeFd plasmid was dissolved in TE buffer (1 mM EDTA, 10 mM Tris, pH 8.0) with concentration of 150 ng/μL.

2.2 Cloning of TeFd gene

The synthesized pBSK-C.O.TeFd plasmid and pTYB2 vector (New England Biolabs, Beverly, MA) were digested with NdeI and XmaI for 2 hrs at 4

ºC, and enzymes were heat-killed at 65 ºC for 20 min. Digested pTYB2 vectors were incubated with 1 µL of calf intestine alkaline phosphatase (CIAP) (Promega, madison, WI) for 1 hr at 37 ºC to remove phosphate overhangs inhibiting self-ligation. The digested C.O.TeFd and CIAP treated pTYB2 vector were purified using the Wizard SV Gel and PCR Clean-Up System (Promega, Madison, WI).

The purified digested C.O.TeFd was ligated to the CIAP treated pTYB2 vector (Table 2) for 2 hrs at room temperature. After ligation, the product was added to *E. coli* GC10 competent cells (Genesee Scientific, San Diego, CA) and kept on ice for 30 min. The mixture was then heat shocked at 42 ºC for 45 sec, 500 µL of SOC medium (20 g/L Tryptone, 5 g/L Yeast Extract, 4.8 g/L MgSO4, 3.603 g/L dextrose, 0.5g/L NaCl, and 0.186 g/L KCl) (Orkin, 1990) was added, and incubated at 37 ºC for 1 hr. The transformed cells were spread on 1.5% Luria Broth (LB) agar plates containing 150 µg/ mL ampicillin.

Colony PCR was used to confirm resulting colonies using T7 Promoter F and T7 Terminator R primers (Appendix 2) under the conditions shown in Table 3 and Table 4. All primers used in this project were synthesized by Integrated DNA Technologies (IDT; Coralville, IA) and received as lyophilized powder. The primers were resuspended to 100 µM in deionized, autoclaved water (ddH_2O). These 10x stocks were kept at -20 ºC. The working stocks of primers were prepared by diluting the 10X stock to 1X stock (10 µM) with ddH_2O to avoid contamination of the primer stocks.

One positive colony was picked, grown overnight in LB with 150 µg/mL ampicillin using 37 ºC shaking incubator and harvested. The cell pellet was then used for a midi-prep (Wizard Plus, Promega, Madison, WI) to extract the pTYB2-TeFd plasmid. The extracted plasmid was then sequenced.

The titanium oxide binding peptides (TOBiPs) were introduced to the N-terminus of Fd. Three forward primers and one reverse primer (Appendix 2) were designed to introduce 3 different TOBiPs (STB1, STB2 and LSTB1) (H. Chen et al., 2006, 2008) at the 5' end of the TeFd.

The high fidelity DNA polymerase ExTaq (Takara Bio Inc., Shiga, Japan) was used for PCR. The reaction was set up according to Table 5 and Table 6, and the PCR product was analyzed using 0.8% agarose gels. The product was purified using Wizard SV Gel and PCR Clean-Up System (Promega, Madison, WI).

The purified PCR product was then ligated into the pGEM-T Easy vector (Promega, Madison, WI) using T4 DNA Ligase for 2 hrs at room temperature (Table 2). After ligation, the product was transformed to *E. coli* GC5 competent cells (Genesee Scientific, San Diego, CA) using the method described above. The transformed cells were spread on 1.5% LB agar plates containing 150 µg/mL ampicillin. In addition, 500 µL of 20 mg/mL 5-bromo-4-chloro-3-indolyl-β-D-galctopyranoside (X-gal) and 100 µL of 100 mM Isopropyl β-D-1-thiogalactopyranoside (IPTG) were added on the top of the LB plate.

The white colonies were further screened using colony PCR (Table 3 and Table 4). M13 forward and M13 reverse primer (Appendix 2) were used for the reaction. One confirmed colony was selected and used for mini-prep (Wizard Plus, Promega, Madison, WI) to extract the pGEM-TOBiP TeFd plasmid. These plasmids were sequenced and then inserted into pTYB2 vector (New England Biolabs, Beverly, MA) to generate pTYB2-STB1 TeFd, pTYB2-STB2 TeFd, and pTYB2-LSTB1 TeFd constructs using the same method as mentioned above.

Table 2 Ligation protocol

Ingredient	Volume (µL)
T4 DNA Ligase (3 Units/µL)	1
2x Rapid Ligation Buffer	5
Vector (100 ng/µL)	1
Insertion (25 ng/µL)	3
Total Reaction Volume	10

`

Table 3 Colony PCR reaction recipe and cycling condition

Ingredient	Volume (µL)
GoTaq Polymerase (5 Units/µL)	0.1
5x GoTaq Buffer	5
dNTP mix (2.5 mM each)	2
Forward Primer (10 µM)	0.5
Reverse Primer (10 µM)	0.5
30% Triton X-100	0.2
ddH_2O	16.7
Total Reaction Volume	25

* *E. coli* colonies were suspended in ddH2O in the PCR tube before adding remaining ingredients

Table 4 Colony PCR cycling condition

Step	Temperature (ºC)	Reaction Time (sec)
1	94	300
2	94	30
3	55	30
4	72	90
5	Repeat steps 2-4 for 35 times	
6	72	300
7	4	Hold

Table 5 PCR reaction recipe and cycling condition

Ingredient	Volume (µL)
ExTaq (5 Units/µL)	0.25
10x ExTaq Buffer	5
10 mM dNTP mix (2.5 mM each)	4
Forward Primer (10 µM)	1
Reverse Primer (10 µM)	1
Template DNA (200 ng/µL)	0.4
ddH_2O	39.35
Total Reaction Volume	50

Table 6 PCR cycling condition

Step	Temperature (ºC)	Reaction Time (sec)
1	94	300
2	94	30
3	45	30
4	72	30
5	Repeat steps 2-4 for 35 times	
6	72	300
7	4	Hold

`

2.3 Expression and purification of protein using the IMPACT System

The IMPACT system (New England Biolabs, Beverly, MA), which was designed to purify proteins using a self-cleavable intein tag, was used to purify Fd proteins. The pTYB2-TOBiP TeFd (pTYB2-STB1-TeFd, pTYB2-STB2-TeFd, and pTYB2-LSTB1-TeFd) and pTYB2-TeFd constructs were transformed into *E. coli* ER2566 competent cells (New England Biolabs, Beverly, MA) and spread on 1.5% LB agar plate with 150 µg/mL ampicillin.

Induction screens were performed in order to find the colonies that best expressed the desired proteins. Three colonies were picked and grown at 37 ºC with shaking at 225 rpm in 5 mL LB liquid medium tubes with 150 µg/mL ampicillin until OD_{600} is between 0.4 to 0.6, and IPTG was then added (1 mM final) to start the induction. The *E. coli* cells were harvested by centrifugation (6000g for 2 min) after 3 hrs induction. The cell pellets were resuspended in 150 µL ddH_2O and 50 µL of 4X SDS sample buffer (4X SSB, 400 mM DTT, 40 mM Tris-HCl pH 6.8, 20% glycerol, 4% SDS). The samples were boiled for 3 min and analyzed by SDS-PAGE.

The colony that expressed the most fusion protein was used to purify the protein. The purification process used a modified protocol from the IMPACT Kit Instruction manual (https://www.neb.com/products/e6901-impact-kit). The selected colony was grown at 37 ºC with shaking at 225 rpm in 2X 1L LB liquid medium flasks with 150 µg/mL ampicillin and 56 mg/L FeSO4 (Wittenberg et al., 2013). When the OD_{600} reaches 0.4, the cells were then moved to 20 ºC for 20

min. 1 M IPTG stock was added to a final concentration of 1 mM to induce fusion protein production. The *E. coli* cells were harvested by centrifugation at 6000 g for 10 min in 4 X 500 mL centrifuge tubes after 16 hrs induction. The cell pellets were then resuspended in 25 mL of 1X Cell Lysis Buffer (20 mM Tris-HCl, pH 8.5, 500 mM NaCl, 1 mM EDTA, and 0.3% Triton X-100) per 2 L cell culture. Protease inhibitor cocktail (0.2 mM PMSF, 1 μM Leupeptin, and 1 μM Pepstatin) was also added to the solution to help protect the desired protein.

The cells were lysed with 3 passes through French Press (Thermo Electron Corporation, Waltham, MA) at an internal pressure of 25,000 psi. The lysate was then collected and centrifuged using the Sorvall SS-34 rotor at 36,000 g for 30 min. The supernatant was collected and used for protein purification while the pellet was resuspended in 25 mL 1X Cell Lysis Buffer. 60 μL of the resuspended pellet was collected for further analysis (as described in Gel electrophoresis and staining section).

The supernatant was then loaded onto a chitin matrix column (New England Biolabs, Beverly, MA) at 0.5 mL/min. The column was washed with 20 column volumes (CVs) of ice-cold column buffer (20 mM Tris-HCl, pH 8.5, 500 mM NaCl, and 1 mM EDTA) to remove unbound proteins at 2 mL/min. The column was then washed with 3 CVs of ice-cold column buffer supplemented with 50 mM β-mercaptoethanol (β-ME) to induce the self-cleavage of the intein tag. The column was then incubated at 4 ºC for 20-40 hrs. The proteins were eluted with 5 mL column buffer at 4 ºC. The elution was dialyzed in 0.1X

phosphate buffered saline (0.1X PBS, 13.7 mM NaCl, 0.27 mM KCl, 1 mM Na_2HPO_4 and 0.18mM KH_2PO_4 at pH 7.2) 3 times for 4 hrs each. Sample was collected from the dialyzed protein and analyzed using SDS-PAGE (as described in Gel electrophoresis and staining section). The remaining protein was frozen in liquid nitrogen and stored at -80 ºC for long term storage.

2.4 MALDI-TOF mass spectrometry

The purified ferredoxin proteins were analyzed by the matrix-assisted laser desorption ionization-time of flight (MALDI-TOF) mass spectrometry (MS) to confirm their molecular weight. MALDI-TOF MS was performed using a Bruker Daltonics Microflex™ mass spectrometer. The MALDI-TOF MS was calibrated using ProteoMass™ Protein MALDI-MS Calibration Kit (Sigma-Aldrich, St. Louis, MO). The protein samples (or standard) were mixed with 10 µL of 60% (v/v) sinapinic acid (3-(4-hydroxy-3,5- dimethoxyphenyl)prop-2-enoic acid, Sigma-Aldrich, St. Louis, MO) in a 1:1 ratio. The MS plate was spotted with 1 µL of the sample (or standard) at each spot and air-dried thoroughly at room temperature. The resulting mass/charge data was exported into a text file (.txt) and analyzed using GraphPad Prism 6 (GraphPad Software, La Jolla, CA).

2.5 Difference Spectroscopy

The Fd proteins were also analyzed by a Cary 300 Bio UV-Visible Spectrophotometer (Agilent Technologies, Santa Clara, CA) to characterize their representative absorbances at 330nm, 424nm and 460nm under oxidized and reduced states (D. O. Hall, 1973). The protein sample was diluted in 0.1X PBS (pH 7.2) to a final concentration of 100 μM, and the scanning mode measurement from 250 nm to 550 nm was performed in triplicate at 60 nm/min averages at 0.5 nm intervals. The oxidized state ferredoxin measurement was performed using 0.1X PBS as a blank, while the reduced state was measured using 0.1X PBS containing 10 mM sodium dithionite as blank and 100 μM protein with 10 mM sodium dithionite as sample. The results were exported into an excel file and the average of the 3 replicates was calculated. GraphPad Prism 6 (GraphPad Software, La Jolla, CA) was used to analyze the results.

2.6 Gel electrophoresis and staining

To analysis the protein samples, a tris-glycine system was used. The gel casting apparatus used 0.75 mm thick spacer plates and short plates from the Protean-3 system (Bio-Rad Hercules, CA). For the resolving solution, 3.5 mL of 15% acrylamide (in 1X resolving gel buffer) was mixed with 20 μL of 10% w/v ammonium persulfate (APS) and 10 μL of tetramethylethylenediamine (TEMED). Isopropanol was added to the top of the resolving solution to help exclude air

bubble from the resolving gel. After polymerization the isopropanol was removed, and 2 mL of the stacking solution (4.8% acrylamide in 1X stacking gel buffer) was mixed with 20 µL APS and 10 µL TEMED and poured on top of the resolving solution.

A 0.75 mm thick comb is then inserted into the stacking solution. The polymerization takes about 5 min, and then the comb is removed from the gel. The gels were run at 15 mA per gel using SDS running buffer (0.1% SDS, 25 mM Tris and 275 mM glycine, pH 8.3) until the bromophenol blue from the 1X SSB reached the bottom (usually takes about 1.5 hrs).

For Coomassie Brilliant Blue staining, the gels were stained in 10% acetic acid, 50% methanol and 0.25% Coomassie Brilliant Blue R 250 for 1 hr and then washed with water and incubated in destain (10% acetic acid, 50% methanol) for 2 hrs.

Silver staining was also performed when a more sensitive stain was required (Chevallet et al., 2006). The proteins were fixed to the gel for 45 min with 200 mL of fixing solution (50% ethanol 10% acetic acid) and then washed with 200 mL of ddH_2O for 4 min (repeat wash 4 times). The gel was exposed to 100 mL silver nitrate (0.5% $AgNO_3$) for 30 min and quick rinsed with 200 mL ddH_2O for 10-15 sec. The gel was developed in 100 mL developing buffer (236 mM Na_2CO_3, 0.02% formaldehyde) for 15 min and washed in 200 mL ddH_2O for 5 min (3 times). 100 mL of the Farmer's reducer (685 µM $K_3Fe(CN)_6$ and 12 mM $Na_2S_2O_3$) was used to treat the gel for 45 min and washed with ddH_2O for 6 min

(repeat wash 4 times). The gel was then stained with silver nitrate again for 25 min and rinsed with ddH_2O for 15 sec. Finally, the gel was incubated with developer and stopped when the band was optimally visible by adding destain buffer. The results were analyzed with Quantity One software version 4.4 (Bio-Rad, Hercules, CA), and bands were quantitated by photon counting.

2.7 Production and purification of Fd antibody

The polyclonal antibody was made in rabbits (Pocono Rabbit Farm, Canadensis, PA) using recombinant forms of Fd expressed and isolated from *E. coli* as mentioned above. The characterization and specificity of the antibody was confirmed with Western blotting analysis.

The anti-Fd antibody was further purified using cyanogen bromide (CNBr)-1activated Sepharose 4B (GE Healthcare Life Sciences, Piscataway, NJ). 1 gram of the CNBr-activated Sepharose 4B was loaded in an empty column and activated using 20-50 mL cold HCl for 15 min at 4 °C. The column was then washed with 200 mL of 1 mM HCl at 1 mL/min. 1 mL of 1 mg/mL Fd was incubated on the activated Sepharose beads overnight at 4°C and washed with 15 mL of coupling buffer (500mM NaCl, 100 mM $NaHCO_3$, pH 8.3) the following day. The uncoupled sites on the beads were blocked with 3 mL of 1 M Tris-HCl buffer (pH 8.0) for 2 hrs at room temperature. The beads were then washed with 10 mL 1X PBS buffer and incubated with serum (produced by Pocono Rabbit

Farm) overnight at 4°C. The flow-through from the column was saved for Western blot testing. The column was washed again with 10 mL 1X PBS buffer and 5 mL 150 mM NaCl-HCl (pH 5) solution. The purified antibody was eluted with 6 mL elution buffer (150mM NaCl, pH 2.5) and neutralized with saturated phosphate buffer (add Na_2HPO4 to PBS buffer until saturation: 1 mL of elution buffer requires 50 µL of saturated phosphate buffer). The antibody solution was kept in a 50% glycerol solution with 0.1% sodium azide (w/v) at -20 °C. The anti-PsaD and anti-PsaE antibody were purified in the same way as described above.

2.8 Western blotting

Immobilon PVDF membrane (Millipore, Billerica, MA) was cut into the size of the Tris-glycing gel, activated in pure methanol for 5 min, and then soaked in transfer buffer (48 mM Tris, 390 mM glycine, 20% methanol) for another 5 min.

Gels were run with pre-stained markers (EZ-Run Prestained, Fisher Scientific, Fair Lawn, NJ; or SeeBlue, Invitrogen, Carlsbad, CA). Proteins were transferred to the pre-soaked PVDF using Mini Trans-Blot® Electrophoretic Transfer Cell (BioRad, Hercules, CA) at 100 V for 1.5 hrs at 4 ºC. The immobilon was removed from the cell and incubated with Tris-buffered saline and Tween 20 (TBST, 137 mM NaCl, 3 mM KCl, 0.1% v/v Tween-20 and 25 mM Tris-HCl, pH 8.0) containing 3% w/v non-fat milk (NFM) with shaking for 1 hr at room temperature. The immobilon was then incubated with the primary antibody

(1:10,000 dilution) in TBST-NFM solution overnight at 4 °C. The immoblion was washed 3 times with TBST-NFM (10 min each time) and then incubated with the donkey-anti-rabbit horseradish peroxidase conjugated (DAR-HRP) (Thermo Scientific, Rockford, IL) for 1 hr at 1:25,000 dilution in TBST-NFM. The immobilon was again washed 3 times with TBST for 10 min and once with TBS for 10 min.

The immobilon was then incubated with 1:1 volume mix of HRP substrate and Luminol (Millipore) at 2 mL total volume for 5 min avoiding light. The results were captured using a Chemidoc XRS (Bio-Rad, Hercules, CA) for 360 sec taking images every 10 sec. The results were analyzed with Quantity One software version 4.4 (Bio-Rad, Hercules, CA), and bands were quantitated by photon counting.

2.9 Design of in vitro binding assay to TiO_2

In order to test the binding affinity of Fd to the TiO_2 nanoparticles, an *in vitro* binding assay was performed. TiO_2 nanoparticle (0.5 mg) and 10 µL of the 1 mg/mL Fd (WT Fd and TOBiP-Fd) was mixed in a 1.5 mL Eppendorf tube (Eppendorf, Hamburg, Germany) and raised to 100 µL with 0.1X PBS buffer. The mixture was incubated at 4 °C for 3 hrs and centrifuged at 1,000 g for 1 min. The supernatant was then discarded while the pellet was collected and washed twice with an equal amount of buffer, after that 50 µL of 4X SSB was added to the final pellet and boiled for 2 min to denature the sample. The protein samples

(supernatant and pellet) were analyzed using SDS-PAGE, gel staining, or Western blotting. Various conditions was performed, inlcuding pH, additives, TOBiPs and TiO_2 nanoparticle species to detect the optimium codition for the assay.

2.10 Purification of PSI

Purification of trimeric PSI was carried out following the protocol used by Iwuchukwu *et al* with minor modifications (Ifeyinwa Jane Iwuchukwu, 2011). The frozen *T. elongatus* cells were thawed and resuspended in 30 mL of lysozyme buffer (10 mM $CaCl_2$, 10 mM $MgCl_2$, 500 mM sorbitol and 50 mM HEPES, pH 8.0) using a large Dounce homogenizer. The resuspended cells were transferred back to a 50 mL conical tube and adjusted to 1 mg/mL chlorophyll a (Chl *a*). Chl *a* concentration was calculated using methods described in Chapter 2.14 (Arnon, 1949).

Lysozyme was then added to a final concentration of 0.25% (w/v) and incubated in the dark at 37 ºC for 45 min. The resulting mixture was centrifuged for 10 min at 5,000 g and the supernatant was discarded. The pellet was resuspended in lysis buffer (20 mM MES, 500 mM Sorbitol, 10 mM $CaCl_2$, and 10 mM $MgCl_2$, pH 6.4) to 1 mg/mL Chl a. The solution was passed twice through a French Press (SLC Aminco) with an internal pressure of 25,000 psi to lyse the

cells. The cell lysate was then centrifuged using an SS-34 rotor at 40,000 g for 20 min, and the supernatant was discarded.

The pellet was collected and washed with wash buffer (10 mM $CaCl_2$, 10 mM $MgCl_2$ and 20 mM MES, pH 6.4) and then washed in buffer containing 3 M NaBr, and then finally in the initial wash buffer. The final washed membrane fragments were adjusted to 1.06 mg/mL Chl *a*, and 10% dodecyl–maltoside (DM) was added to a final concentration of 0.6% (w/v). The mixture was incubated at 20 ºC for 30 min with gentle shaking in darkness. The insoluble material was removed from the solubilized membrane mixture by centrifugation at 40,000 g for 20 min. The supernatant was separated from the pellet and then loaded onto 10 - 30% sucrose gradients containing wash buffer and 0.03% DM. Density gradient centrifugation was performed using an SW28 rotor at 24,000 rpm at 10 ºC for 16 hrs. The lowest green band contained the trimetric PSI complex.

The PSI samples were then diluted with 20 mM MES pH 6.4 with 0.02% DM to about 4X the original volume and loaded onto a POROS 20HQ (Invitrogen, Carlsbad, CA) anion exchange column (S/N 500, SpectraLab Scientific, Ontario, CA). The PSI was purified using HPLC following the method shown in Appendix 3. The Chl *a* concentration was measured and dialyzed and concentrated into wash buffer to make the final concentration 1 mg/mL Chl *a,* and it stored at -80 ºC for long term storage.

2.11 Cross-linking of Fd to PSI

T. elongatus PSI and TeFd was mixed at a molar ratio of 1:1 in 0.1 x PBS (pH7.2) with 0.03% DM solution. The mixture of PSI and Fd was then incubated for 30 min on ice before adding the chemical crosslinking agent, EDC (Thermo Scientific, Rockford, IL) and/or NHS (Thermo Scientific, Rockford, IL). The crosslinker was added to the mixture to make the final concentration 5 mM NHS and 2.5 mM EDC in a total volume of 50 µl. Equal volume of 20 mM glycine in 0.03% DM was added to quench the crosslinking reaction.

Following this, a multilayer sucrose gradient (3 layers, 5%, 20% and 60% sucrose in 0.03% DM, 0.1X PBS, pH7.2) was made in a microfuge tube (Beckman coulter Inc., Pasadena, CA). The crosslinking product was then loaded on the top of the sucrose gradient to separate free Fd from PSI and PSI-Fd crosslinked product using a TLA-55 rotor (Beckman coulter Inc., Pasadena, CA) and Optima^{TM} Ultracentrifuge (Beckman coulter Inc., Pasadena, CA) at 150,000 g for 2 hrs. After sucrose gradient separation, 100 µL of the green layer (PSI and PSI-Fd complex) was isolated and mixed with 4X SSB and incubated at 42 ºC for 30 min to denature the PSI. The protein sample was then analyzed using 15% Tris-Glycine SDS-PAGE and immuno-detected by Western blotting. The immunoblots were probed with different antibodies, including anti-Fd, anti-PsaD and anti-PsaE (Cashman et al., 2014).

`

2.12 Chl *a* measurement

The concentration of PSI was measured by its Chl *a* concentration. The concentration of Chl *a* was determined by chlorophyll extraction with 985 µL 90% methanol and 15 µL of sample. The mixture was vortexed and incubated at 60 ºC for 2 min and then centrifuged at 21,000 g for 2 min to remove debris. 800 µL of the supernatant was collected and measured its absorbance at 665 nm and used to calculate total chlorophyll content using the following equation.

$$[\text{Chl } a] = \frac{\text{Abs}_{665} \times 13.5}{15 \times 1000}$$

2.13 Computational modeling of PSI and Fd interaction

This section was performed with the collaboration of Dr. Derek Cashman, the results of which have been submitted for publication in the Journal of Molecular Recognition (Cashman et al., 2014). The protein structure files of TePSI and TeFd were downloaded from the Protein Data Bank (PDB) with PDB accession coordinates number 1JB0 (PSI) and 2CJN (Fd). Program MOE V. 2012 (Chemical Computing Group, Inc., Montreal, Quebec, Canada) was used to extract the stromal subunits of PSI from the PDB file, and hydrogen atoms were added to the structure according to standard residue protonation (Cashman et al., 2014).

The extracted stromal subunits from PSI as well as Fd were analyzed using the Protein Frustratometer (EMBNet, http://www.frustratometer.tk/) to

calculate the regions that exhibit local configurational frustration. The regions (or key residues) that were highly frustrated were mapped on the PSI and Fd protein structures using MOE V. 2012. In addition, residues that were experimentally determined by site-directed mutagenesis, crosslinking, and other studies were also identified (Bottin et al., 2001; Fischer et al., 1999; Setif et al., 2002; Setif et al., 2010b).

The modeling of the interaction between PSI and Fd was performed by rigid body docking using the Energy Minimize function in MOE with the CHARMM27 force field. The extracted stromal subunits of PSI (PsaC, D and E) and the Fd protein were treated as separate rigid bodies with the predicted interaction surfaces facing each other.

Certain distance restraints were set between an atom of a residue on PSI and another atom of a residue on Fd to ensure that the 2 residues would be in proximity to the docked complex structure (Cashman et al., 2014). These distance restraints were set to calculate potential models for the PSI-Fd interaction complex, bringing together the residues that have been experimentally proposed to be involved in PSI-Fd interactions and/or the regions of high energetic frustration. Docking models were generated with different sets of distance restraints, and each of these models was then subjected to energy minimization in MOE for future analysis (Cashman et al., 2014).

`

Chapter 3 Results

3.1 Introduction

Solar energy is the most abundant energy source available in the world (Hammond, 1972; Mussgnug et al., 2007); however, we cannot effectively harvest this energy. Traditional inorganic solar cells are costly, energy intensive to manufacture, and have limited absorption of solar radiation. It is desirable to develop flexible and lightweight solar cells that can compete with inorganic semiconductor cells, yet remain inexpensive. This can be accomplished by combining biological materials to build a hybrid dye synthetized cell.

Energy conversion from light to electrical energy in photosynthesis and in photovoltaic devices is initiated by the charge separation, which generates a photovoltage in the system (Blankenship et al., 2011; Gur et al., 2005). Nature provides excellent systems of the charge separation, such as the photosynthetic reaction center PSI, which evolved over billions of years to become a highly efficient light energy converter (Brettel & Leibl, 2001; Nelson, 2009). Located in the thylakoid membranes of plants and cyanobacteria species, PSI contains a special pair of chlorophyll (P700), which undergoes light-induced charge separation and generates a light activated electron. The electron is then transferred through the PSI to ferredoxin (Brettel & Leibl, 2001; D. O. Hall, 1973). Ferredoxin is an electron transfer protein with an iron-sulfur center that facilitates

electron transfer between PSI and the ferredoxin:NADP+ oxidoreductase (FNR) in photosynthesis (Tagawa & Arnon, 1962).

In applied photosynthesis, many efforts have been directed towards using these electrons in either a hydrogen-evolving catalyst or an electron-conducting photovoltaic cell device (Ifeyinwa Jane Iwuchukwu et al., 2010; Mershin et al., 2012c). In this project, efforts have been made to shuttle these light induced electrons from PSI to a TiO_2 electrode. Ferredoxin was used to connect PSI to the TiO_2 electrode in a directional manner and facilitate electron transfer from PSI to the electrode. To help this process, a TOBiP was engineered to the N-terminus of the Fd to provide specific binding to TiO_2. In addition, a chemical crosslinking reaction was performed, linking PSI and TOBiP-Fd to generate a PSI-Fd-TOBiP protein complex. The crosslinked product can attach to TiO_2 electrodes in a directionally-specific way and generate a photovoltaic device.

T. elongatus is a thermophillic cyanobacterium that was isolated from hot springs, and its PSI and Fd were shown to be stable at ambient as well as increased temperatures (Frenkel et al., 1950). A further advantage is the availability of a high-resolution X-ray diffraction crystal structure (Hatanaka et al., 1997; Jordan et al., 2001a). Therefore, PSI and Fd from *T. elongatus* was selected and tested.

`

3.2 Computational modeling of the docking site between PSI and Fd

The docking surface between PSI and Fd was characterized by its local potential energy surface using the Protein Frustratometer (EMBNet, http://www.frustratometer.tk/) (Cashman et al., 2014). The Frustratometer is used to understand the biological behavior of a protein by analyzing how the energy is distributed in protein structures (Onuchic et al., 1997). Residues of high local frustration usually suggest biologically important regions such as binding or allosteric sites, while the minimally frustrated regions indicate a stable folded region of the molecule (Bryngelson & Wolynes, 1987).

All subunits from the stromal domain of PSI (PsaC, D and E) and Fd with a potential energy surface characterized by a local frustration density of 20% or greater are highlighted in red (Figure 3.1). These highly frustrated regions are labeled as RI through RV in the PsaCDE complex, and RVI and RVII are in Fd. After labeling these regions in the structural model, the RI region on PsaC and RV region on PsaE were shown to have direct contacts with core subunits PsaA and PsaB of PSI (deleted from the model in the present calculations). Residues that have been experimentally identified via site-directed mutagenesis, crosslinking, and other studies to be involved in interactions between PSI and Fd were labeled blue (Figure 3.2) (Bottin et al., 2001; Fischer et al., 1999; Setif et al., 2002; Setif et al., 2010b).

The modeling of the interaction between PSI and Fd was performed by rigid body docking using MOE V. 2012 (Chemical Computing Group, Inc.,

Montreal, Quebec, Canada). The extracted PsaC, D and E subunits and Fd protein were treated as individual rigid bodies with the predicted interaction surfaces facing each other. Several restraints between the experimentally identified residues and frustrated residues (one atom of a residue on PSI and another atom of a residue on Fd, Table 7) were set for each docking run and the interaction energies were calculated for PSI/Fd docked complexes (Table 8). The distance between the closest iron atoms of the [2Fe-2S] center in PSI and Fd was between 9.7 to 14.9 Angstroms which suggests that the docking configuration may provide an adequate proximity for rapid electron transfer (Page et al., 1999). Using the method described in Chapter 2.13, a total of 12 models were generated which can be grouped into two categories with opposite orientations of Fd (Figure 3.2) (Cashman et al., 2014).

PsaC:

1- AHTVKIYDTCIGCTQCVRACPTDVLEMVPWDGCKAGQIASSPRTEDCVGCK

RCETACPTDFLSIRVYLGAETTRSMGLAY -80

RI

PsaD:

1- TTLTGQPPLYGGSTGGLLSAADTEEKYAITWTSPKEQVFEMPTAGAAVMRE

GENLVYFARKEQCLALAAQQLRPRKINDYKIYRIFPDGE TVLIHPKDGVFPEKV

RII **RIII**

NKGREAVNSVPRSIGQNPNPSQLKFTGKKPYDP -138

RIV

PsaE:

1- MVQRGSKVKILRPESYWYNEVGTVASVDQTPGVKYPVIVRFDKVNYTGYSG

RV

SASGVNTNNFALHEVQEVAPPKKGK -75

Fd:

1- ATYKVTLVRPDGSETTIDVPEDEYILDVAEEQGLDLPFSCRAGACSTCAGK

RVI

LLEGEVDQSDQSFLDDDQIEKGFVLTCVAYPRSDCKILTNQEEELY – 97

RVII

Figure 3.1 Sequence of PsaC, D and E subunits and Fd proteins

Cysteine residues are highlighted in yellow. Residues that have frustration density of 20% or greater are highlighted in red. Interaction residues predicted by site directed mutagenesis experiments are colored in blue.

`

Table 7 Distance restraints used for each docking run

4 to 7 restraints were set between amino acids from the PsaC, D and E subunits of PSI and the Fd protein.

1	PsaE: R39 Fd: D27	PsaE: R39 Fd: E31	PsaE: R39 Fd: D35	PsaC: C13 Fd: C40	PsaD: R73 Fd: D66	PsaD: K104 Fd: D68	PsaD: K76 Fd: E71
2	PsaD: R73 Fd: R35	PsaD: K76 Fd: E30	PsaC: C13 Fd: C40	PsaE: R39 Fd: D66	PsaE: R39 Fd: D68	PsaC: K34 Fd: E71	
3	PsaE: R39 Fd: E31	PsaC: K34 Fd: D35	PsaC: C13 Fd: C40	PsaD: R73 Fd: D66	PsaD: R18 Fd: D68	PsaD: K104 Fd: D68	PsaD: K76 Fd: E71
4	PsaD: R18 Fd: E30	PsaD: K76 Fd: E31	PsaC: C13 Fd: C40	PsaE: R39 Fd: D66	PsaC: K34 Fd: E71		
5	PsaD: R73 Fd: E30	PsaD: K76 Fd: D35	PsaC: C13 Fd: C40	PsaE: R39 Fd: D66	PsaE: R39 Fd: D67	PsaE: I37 Fd: I70	
6	PsaE: R39 Fd: E31	PsaC: C13 Fd: C40	PsaD: K104 Fd: D66	PsaD: R73 Fd: D67	PsaD: K76 Fd: E71		
7	PsaD: R73 Fd: E30	PsaD: K104 Fd: E30	PsaD: K76 Fd: D35	PsaC: C13 Fd: C45	PsaC: K34 Fd: D67		
8	PsaC: K34 Fd: E31	PsaC: K34 Fd: D35	PsaC: C13 Fd: C45	PsaD: R73 Fd: D66	PsaD: K76 Fd: D67	PsaD: K104 Fd: E71	
9	PsaC: K34 Fd: E31	PsaC: K34 Fd: D35	PsaC: C13 Fd: C45	PsaD: R73 Fd: D66	PsaD: K76 Fd: D67		
10	PsaE: R39 Fd: E30	PsaE: R39 Fd: E31	PsaC: C13 Fd: C45	PsaD: R73 Fd: D66	PsaD: K104 Fd: D68	PsaD: K76 Fd: E71	
11	PsaC: C13 Fd: C40	PsaD: K104 Fd: D66	PsaD: K76 Fd: E71	PsaD: R39 Fd: E31			
12	PsaE: R39 Fd: E30	PsaE: V55 Fd: F38	PsaC: C13 Fd: C40	PsaD: R73 Fd: D66	PsaD: K76 Fd: D67	PsaD: K104 Fd: E71	

`

Table 8 Interaction energies calculated for PSI/Fd docked complexes

The interaction energy was calculated in kcal/mol and the distance between the closest iron atoms of the [2Fe-2S] center in PSI and Fd was measured in Angstroms.

Docked Complex	1	2	3	4	5	6	7	8	9	10	11	12
Total Interaction Energy	-315.5	-404.5	-500.6	-337.6	-370.2	-395.7	-314.9	-268.0	-290.0	-395.5	-241.1	-319.8
F_B - F_{Fd} Distance	11.4	11.0	9.7	11.3	11.7	11.0	13.5	14.2	14.9	10.6	12.3	11.1

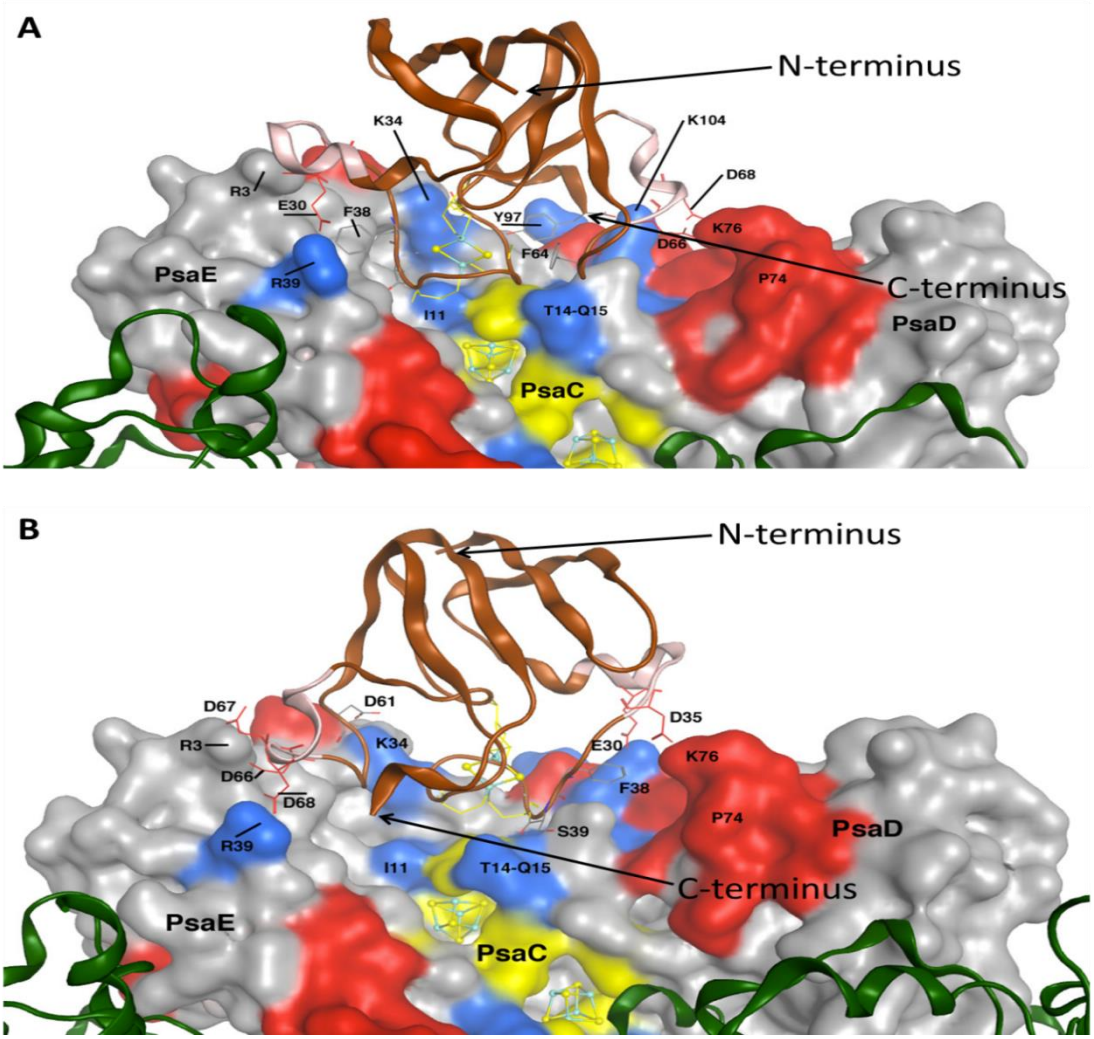

Figure 3.2 Different docking models between PsaCDE subunits and Fd

Fd is represented as a brown ribbon, with purple ribbons representing frustration residues. The black arrows denote the N- and C- terminus of Fd. PsaC, D and E are drawn as a grey surface with blue patches representing interaction residues predicted by experimental data and red patches representing frustration residues. The [4Fe-4S] centers of PSI and [2Fe-2S] center of Fd are represented as ball-and-stick models. Strands of PsaA and PsaB are drawn as green ribbons.

`

3.3 Cloning of the *Thermosynechococcus elongatus* ferredoxin (TeFd) gene

The wild type *T. elongatus* ferredoxin (WT TeFd) gene sequence (locus tag: tsl1009) was retrieved from its genome DNA (Appendix 1). Since the useage of codon for a certain amino acid varies from organism to organism (*E. coli* and *T. elongatus*), the codon adaptation index (CAI) of *E. coli* was used to analyze the TeFd gene (Figure 3.3). CAI measures the relative percentage of the codon usage of a gene (TeFd) against the codon usage of highly expressed genes (in *E. coli*) (Jansen et al., 2003). The CAI values range from 0 to 1, with higher values indicating a codon more commonly used to code for a particular amino acid. The CAI score of the WT TeFd is 0.26 in *E. coli* and indicates a potential expression problem. To solve this problem, WT TeFd gene was codon optimized using online software (shown below) and characterized with CAI (Figure 3.3). The codon optimized TeFd sequence is shown in Appendix 1 and is used in all experiments.

Codon optimized TeFd (C.O.TeFd) was then artificially synthesized (pBSK-C.O.TeFd), digested with NdeI and XmaI, and ligated into identically cut pTYB2 vector to generate pTYB2-TeFd (Figure 3.4). Colony PCR screening was used to confirm the insertion of C.O.TeFd into the pTYB2 vector with the size of a positive colony being 585 bp (Figure 3.5).

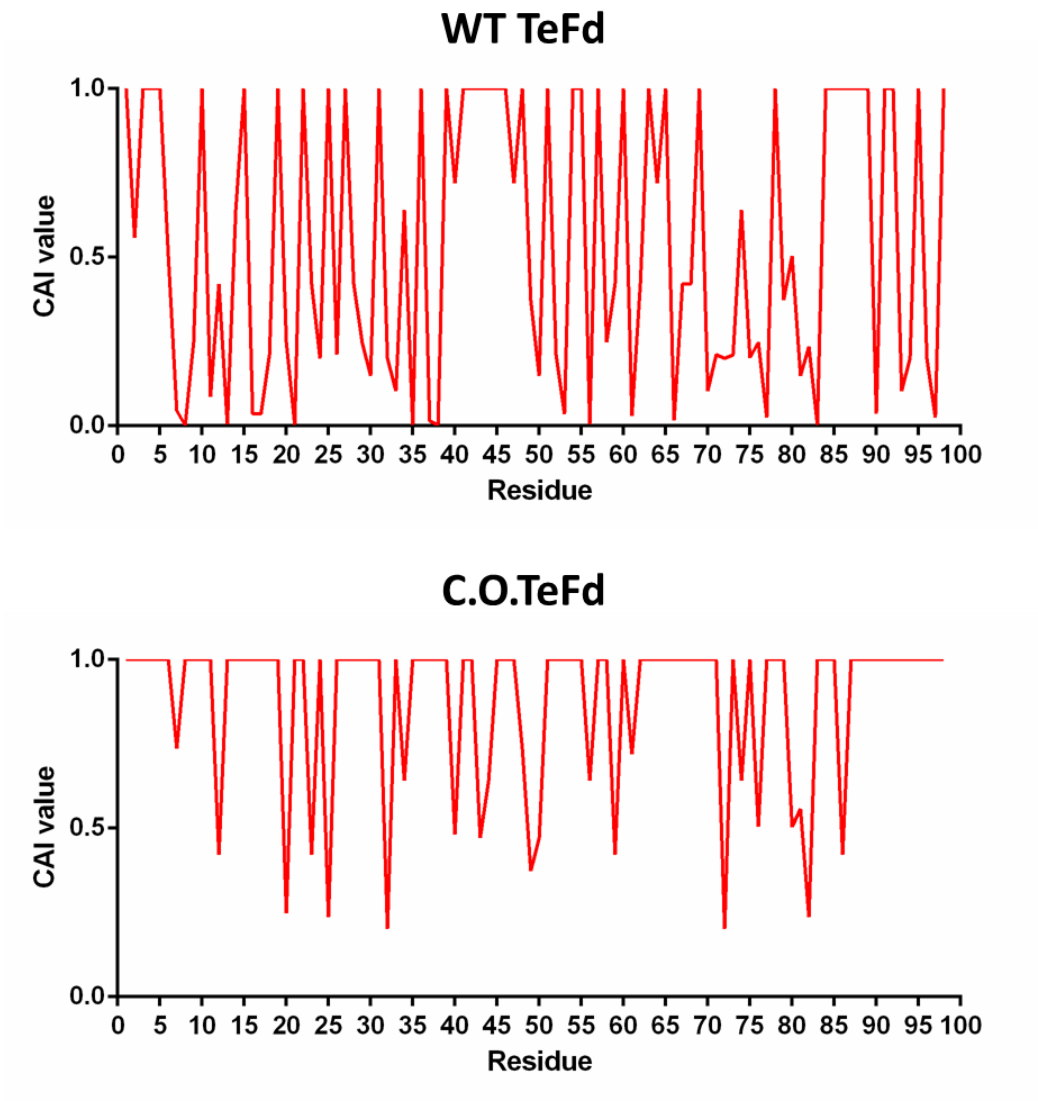

Figure 3.3 CAI analyses of WT TeFd and C.O.TeFd

Codon adaptation index was used to characterize codon usage of WT TeFd and C.O.TeFd as described in the method section. The CAI value for WT TeFd is 0.26 while for C.O.TeFd is 0.77. The residues with low CAI value indicated the rarely used codons in *E. coli* and are likely to cause expression problem (or low expression).

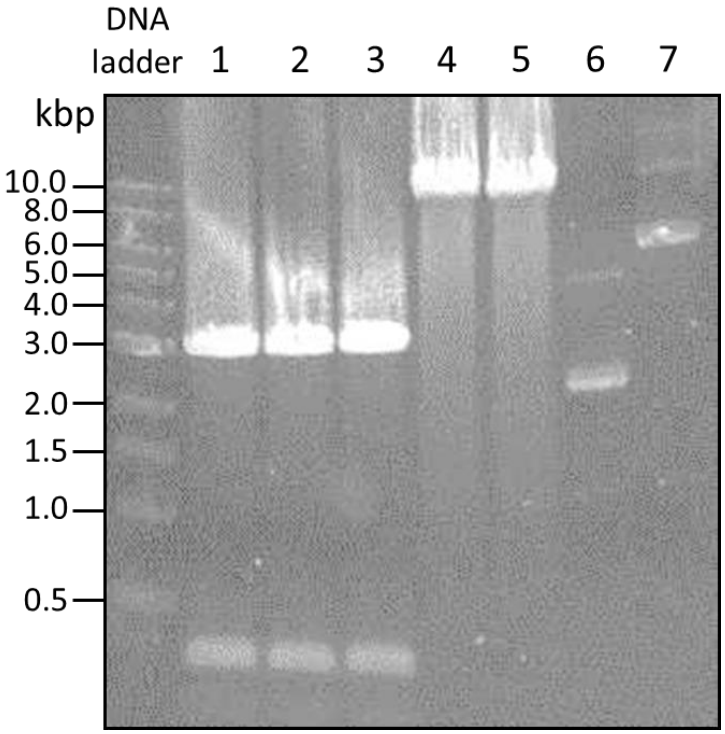

Figure 3.4 Digestion of pBSK-C.O.TeFd and pTYB2

NdeI and XmaI were used to digest pBSK-C.O.TeFd and pTYB2. Multiple lanes were used in order to provide enough samples for gene clean and later ligation experiment. Lanes 1-3 were enzyme digested pBSK-C.O.TeFd, and the upper band is pBSK (~3Kbp) while the lower band is C.O.TeFd (~300bp). Lane 4 and 5 are digested pTYB2. Lane 6 and 7 are pBSK-C.O.TeFd and pTYB2 without restriction enzyme digestion respectively.

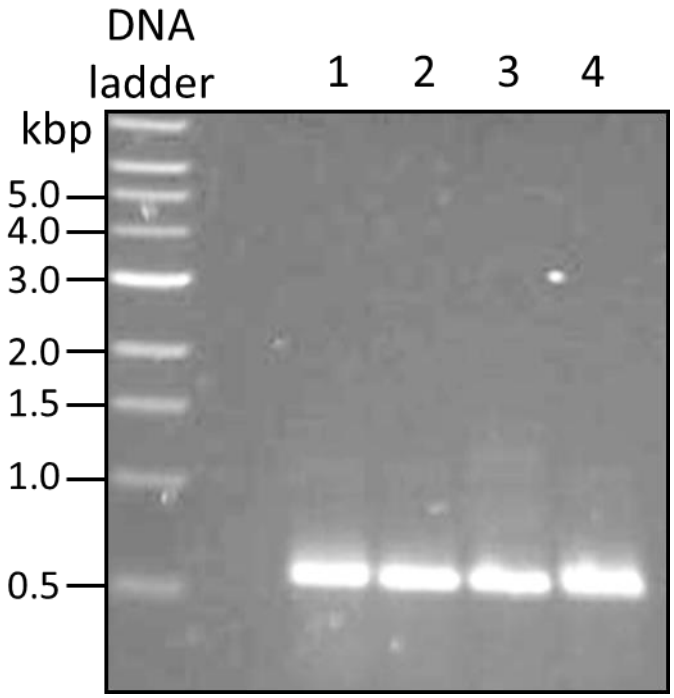

Figure 3.5 Colony PCR confirmation of pTYB2-TeFd

Colony PCR results confirmed insertion of TeFd into pTYB2. Lanes 1-4 are colonies screened for C.O.TeFd insertion with the expected size of the insertion of 585 bp.

3.4 Generation of TOBiP-TeFd

Short titanium oxide binding peptides (TOBiP) that bind specifically to TiO_2 (H. Chen et al., 2006, 2008), was engineered to the terminus of Fd.

Based on the PSI-Fd docking models (Figure 3.2), the C-terminus of Fd is located in the middle of the interaction site between PSI and Fd, while the N-terminus of Fd was further away from the interaction site. Thus, TOBiP was placed on the N-terminus of Fd to avoid interference with the interaction between Fd and PSI.

Three TOBiPs were selected for incorporation into TeFd, and the final fusion constructs are shown below in the pTYB2 expression vector (Figure 3.6). The eight amino acid long TOBiPs, followed by a short linker to increase the flexibility, was cloned onto the 5' end of the pTYB2-TeFd plasmid. Using PCR techniques as previously described (Chapter 2.5), 3 constructs were generated: pTYB2- STB1-TeFd, pTYB2- STB2-TeFd, and pTYB2- LSTB1-TeFd.

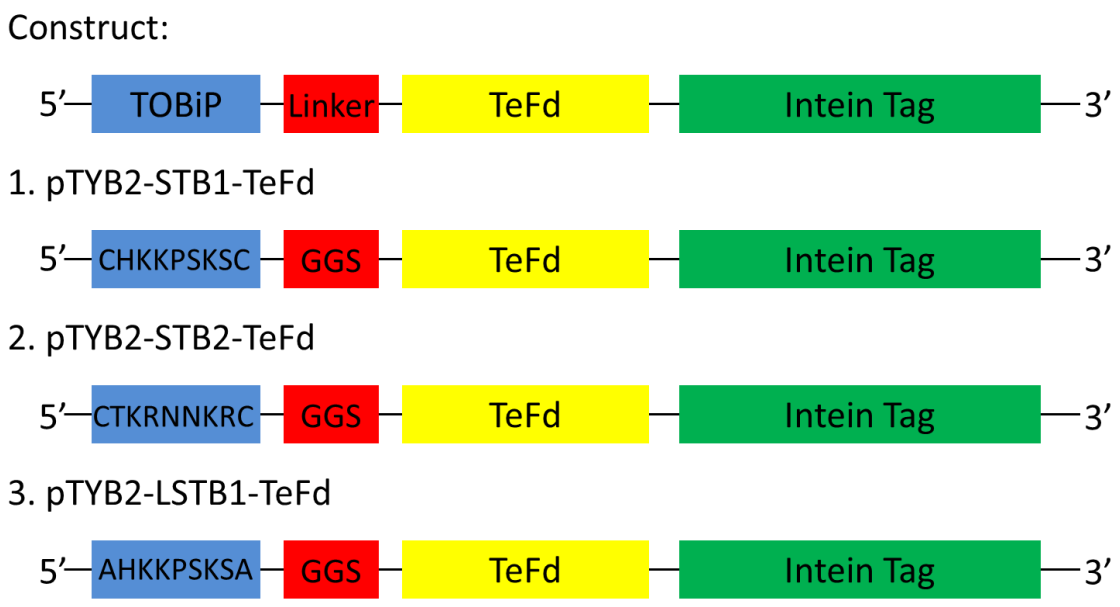

Figure 3.6 Cloning constructs of pTYB2-TOBiP-TeFd

Three constructs were engineered using different TOBiPs. The TOBiPs were cloned onto the 5' end of the TeFd gene (followed by a three amino acid linker GGS). The Fd gene was followed by a intein Tag which is used for affinity purification of Fd.

`

3.5 Expression, purification and characterization of TeFd.

The constructed plasmids (pTYB2- TOBiP- TeFd and pTYB2- TeFd) were transformed into chemically competent ER2556 *E. coli* cells. Expression screening was then performed to select the colonies that had the highest expression pattern of our desired proteins. Since the Fds were produced with a 55 kDa intein tag, the expected molecular weight (MW) of the fusion protein is roughly 66 kDa (Figure 3.7).

The purification of TeFd and TOBiP-TeFd was performed using IMPACT system (New England Biolabs, Beverly, MA) following the protocol in Chapter 2.6. Samples from each purification step were collected and analyzed by SDS-PAGE (Figure 3.8), while elutions are shown in Figure 3.9A. Some contamination bands were present in the elutions, which are most likely residual intein tag used to purify the proteins. The contamination was removed by passing the elution through a 50 kDa Centrifugal Concentrator, which allowed passage of TeFd and TOBiP-TeFd, but not contaminant (Thermo Fisher Scientific Inc., Rockford, IL) (Figure 3.9B).

The apparent MW from SDS-PAGE was larger than the predicted MW based on its amino acid composition. To confirm the size of our purified protein, MALDI-TOF MS was used to measure the mass to charge value (Figure 3.10). For WT TeFd, STB1-TeFd, STB2-TeFd, and LSTB1-TeFd, the difference between predicted MW and MALDI calculated MW was within ±1 Da. Some of

the MALDI results showed a second peak larger than predicted, which is likely to be inclusion of beta-mercaptoethanol (β-ME, 78 Da) used during purification.

Spinach Fd exhibits absorption maxima at 465, 420, 330 and 278 nm. The absorption of the protein in the visible region is mainly due to the iron-sulfur center. The absorption is lost when the iron-sulfur center is removed from Fd (Bayer et al., 1967; D. O. Hall, 1973; Rao et al., 1971).

Since the iron-sulfur center in Fd is critical for the electron transfer process from PSI to the electron acceptor Fd, a difference spectrum was taken to confirm that purified WT TeFd contains the [2Fe-2S] center and that the addition of TOBiP does not interfere with the [2Fe-2S] center (Figure 3.12). The oxidized form of Fd (exposed in air) shows four peaks at 460, 424, 330 and 278 nm. The slight difference in the maxima absorbance may be caused by the different species of Fd (spinach vs. *T. elongatus*). The Δ absorbance between oxidized Fd (WT TeFd and TOBiP- TeFd) and reduced Fd (added 10mM sodium dithionate) shows two peaks at 424nm and 460nm, respectively, and confirms that both WT TeFd and LSTB1-TeFd contain a [2Fe-2S] center and suggests that they are functionally capable of transferring electrons from PSI to an electron acceptor.

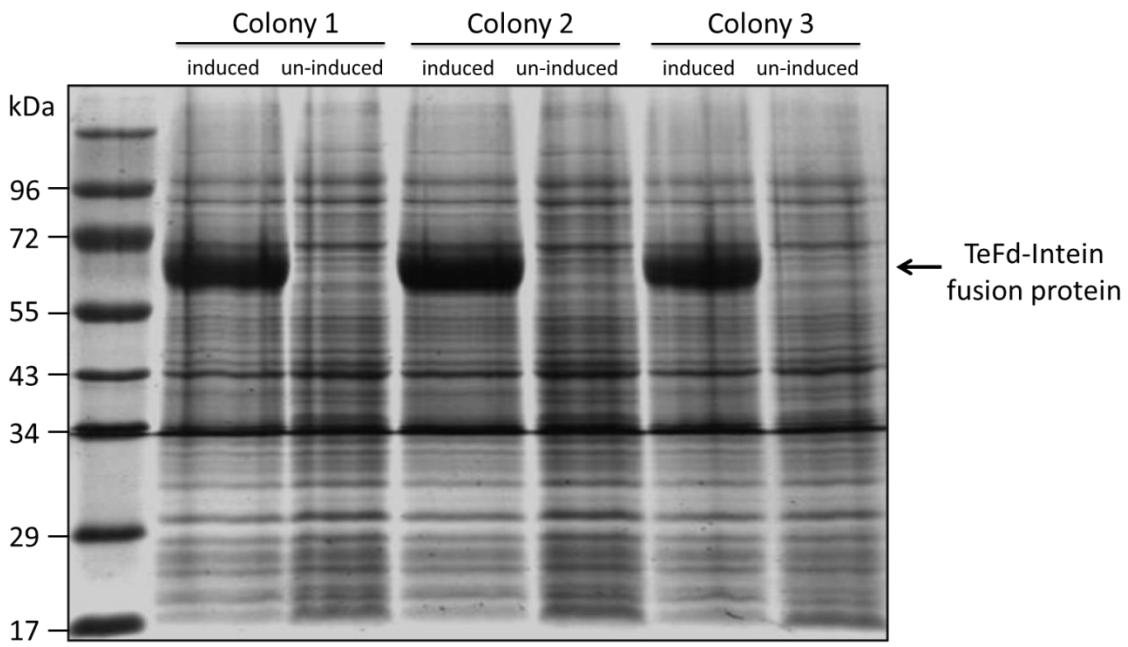

Figure 3.7 Expression Screening

Expression screening was performed to confirm the expression of WT Fd-intein fusion protein with put expected MW of 66 kDa (shown here as an example). Three colonies were grown, induced at 37 ºC for 4 hrs, and analyzed using SDS-PAGE on a 15% tris-glycine gel.

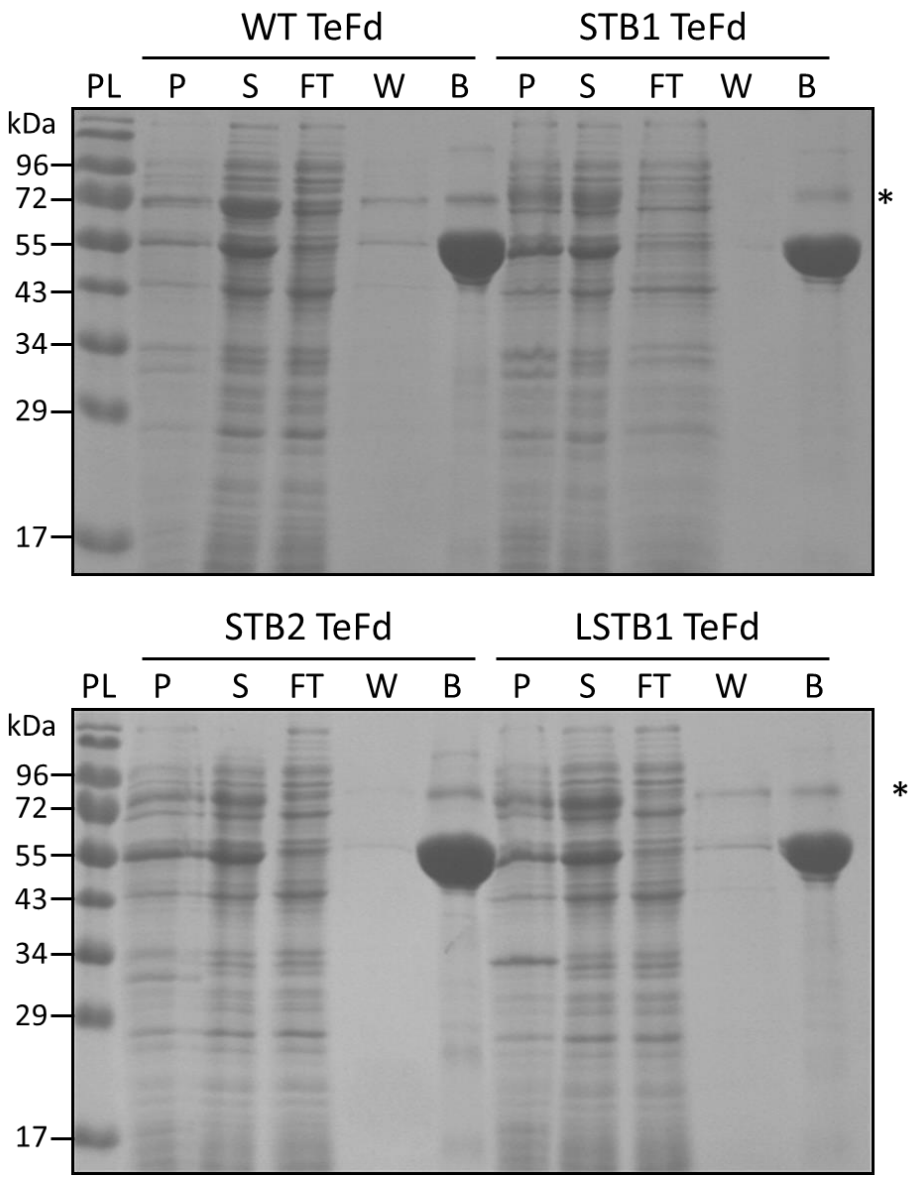

Figure 3.8 Protein purification profile

Protein ladder (PL), insoluble fraction (P), soluble fraction (S), flow-through (FT), wash (W), and column beads (B) of the WT TeFd and TOBiP-TeFd purification were run on a 15% tris-glycine gel. The Fd-fusion protein is represented by the * species.

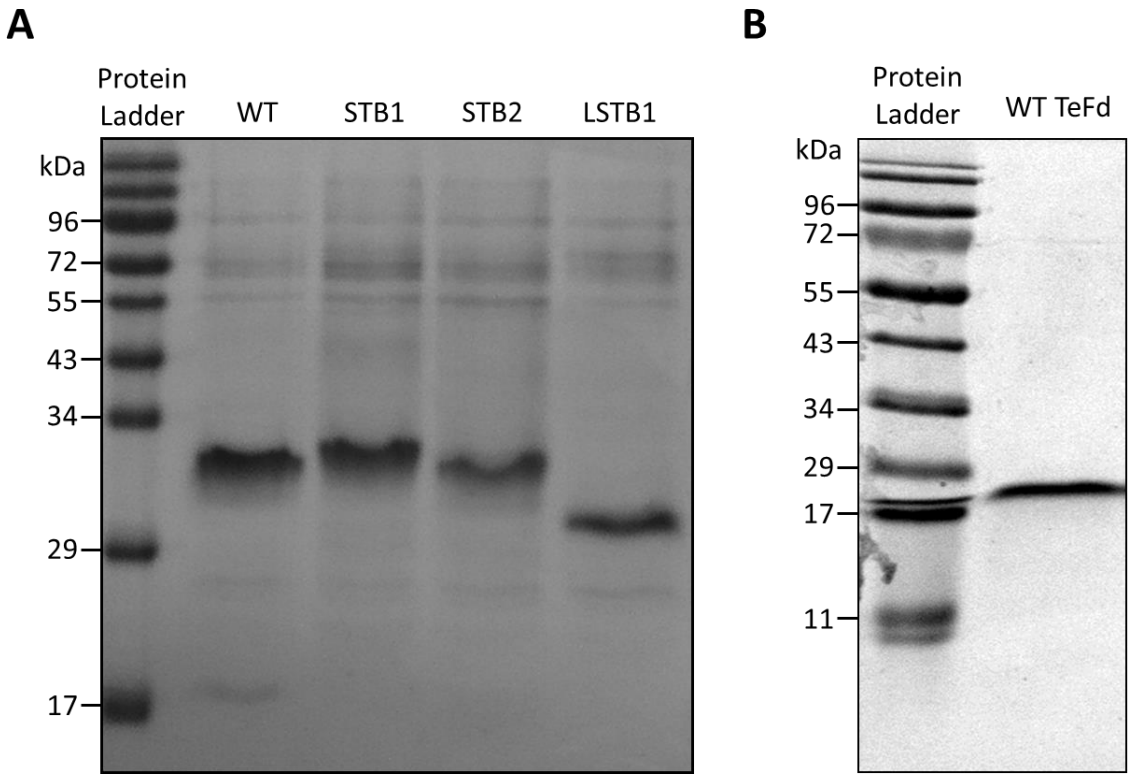

Figure 3.9 Protein purification result

A) SDS-PAGE was performed with elution of the WT TeFd (WT), STB1-TeFd (STB1), STB2-TeFd (STB2), and LSTB1-TeFd (LSTB1). Contamination bands were found at high molecular weight region; B) The purification result of WT TeFd. The elution was filtered through a 50 KDa Centrifugal Concentrator (Thermo Fisher Scientific Inc., Rockford, IL) to eliminate contamination.

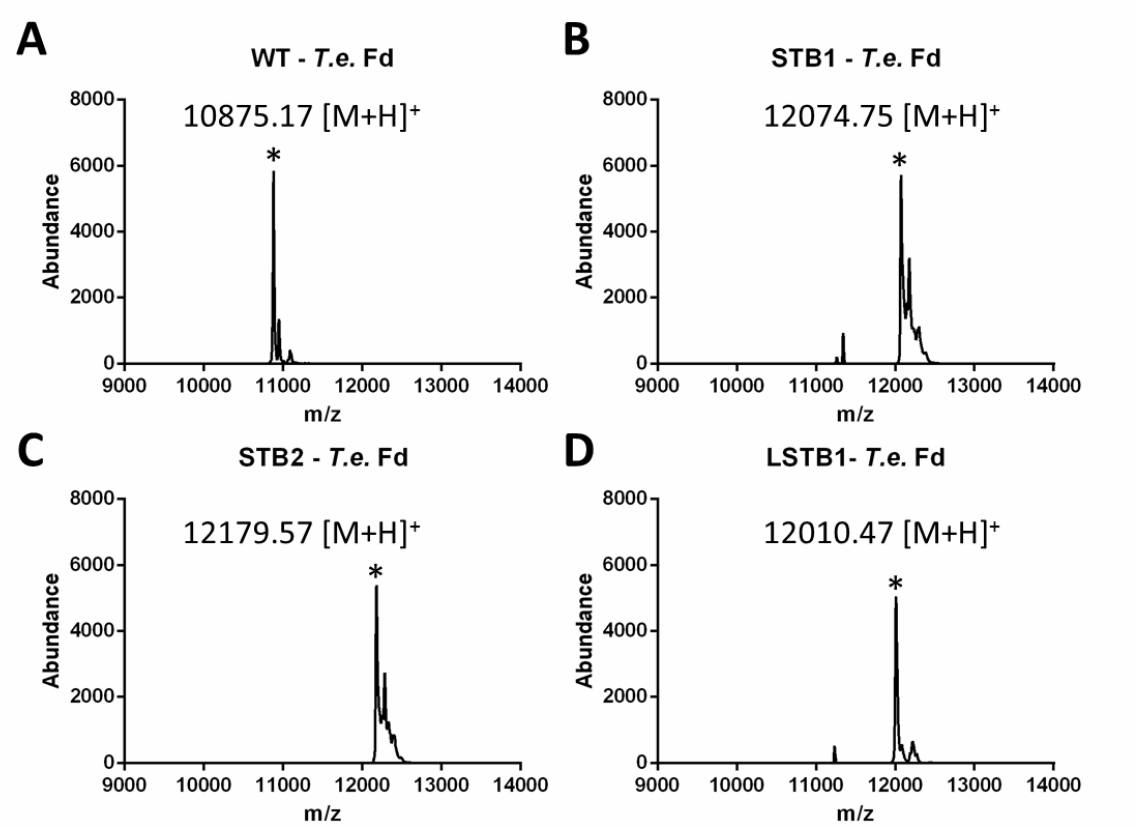

E

	WT-TeFd	STB1-TeFd	STB2-TeFd	LSTB1-TeFd
Predicted MW (Da)	10873.82	12074.18	12179.28	12010.06
MALDI result (Da)	10874.17	12073.75	12178.57	12009.47
Difference (Da)	+0.35	-0.43	-0.71	-0.59

Figure 3.10 MALDI-TOF Spectra for purified proteins

MALDI-TOF analyses of WT TeFd and the TOBiP TeFd: A) WT TeFd, B) STB1 TeFd, C) STB2 TeFd and D) LSTB1 TeFd. E) The predicated MW and MALDI calculated MW are shown to confirm the size of purified protein.

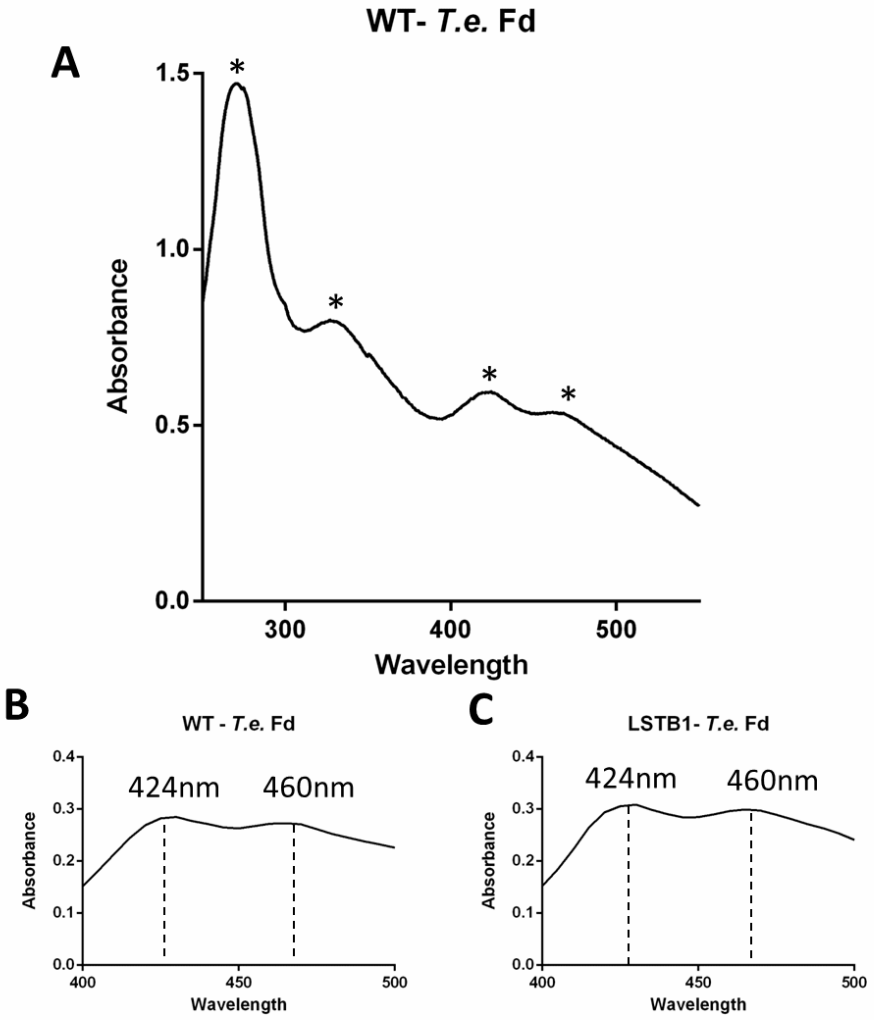

Figure 3.11 Difference spectrum of purified Fd

A) The absorbance spectrum of the oxidized state of WT TeFd. The absorbance peaks (*) are found at 278nm, 330nm, 424nm and 460nm; B) and C) The difference in absorbance between oxidized and reduced form of WT TeFd and LSTB1 TeFd respectively. The two peaks at 424nm and 460nm are labeled and characteristic of the [2Fe-2S] center in Fd.

3.6 TOBiP-Fd attachment to TiO_2 nanoparticles

After purification of the TOBiP-TeFds, their binding affinity to different TiO_2 nanoparticles were tested. Various conditions, including different TOBiP species, reaction buffer pH, additives, and TiO_2 particles were used to optimize the TOBiP-TeFd attachment to TiO_2 (Figure 3.12).

The TOBiP-TeFds were incubated with TiO_2 and then centrifuged to separate the pellet and supernatant as described in Chapter 2.9. The pellet contained TiO_2 nanoparticle and bound Fd while unbound Fd was present in supernatant. The pellet and supernatant were then analyzed using SDS-PAGE, and the binding efficiency was indicated by the percentage of bound Fd vs. total input protein. Initially, the affinity of various TOBiP-Fds for TiO_2 was probed. The assay was performed in 0.1X PBS (pH7.8) using 700 ºC TiO_2 from the University of Memphis and the results showed that LSTB1-TeFd has significantly higher affinity (47.5%) compared to STB1-TeFd (12.3%) and STB2-TeFd (18.7%) (Figure 3.12A). An interesting observation was that there was no WT-TeFd bound to TiO_2, thus indicating that binding to TiO_2 is TOBiP specific. Buffer (0.1X PBS) at various pH was used to find the optimum pH for the attachment of LSTB1-TeFd to 700 ºC TiO_2 and the pH variation test showed that highest affinity occurs at pH 7.2 (Figure 3.12B).

Different additives were used to determine their contribution to the attachment of TOBiP-TeFd to TiO_2. Various additives, including 3% PEG, 3% Glycerol, 0.3% Triton X-100, 0.3% DM and 3% DMSO were tested using LSTB1-

TeFd, 700 ºC TiO_2, and 0.1X PBS (pH 7.2). The additive test indicated 3% DMSO is most beneficial (Figure 3.12C).

All of the tested TiO_2 nanoparticles were prepared and analyzed using Scanning Electron Microscopy (SEM) (Figure 3.13). The SEM images of these TiO_2 showed significantly different appearances and may cause different binding abilities. As a result, different TiO_2 nanoparticles were assayed to determine their ability to bind TOBiP-TeFd. The attachment assay showed that the highest binding occurs when 700 ºC TiO_2 nanoparticles from the University of Memphis were used (Figure 3.12D). Consequently, the optimum conditions for the tested *in vitro* binding assay to TiO_2 are 700 ºC TiO_2 and LSTB1-TeFd in 0.1X PBS (pH7.2) containing 3% DMSO.

Figure 3.12 Optimization of TOBiP-Fd attachments to TiO_2 nanoparticle

Pellet (P) (pulled down in TiO_2) indicates the Fd that bound to TiO_2 particle while Supernatant (S) indicates the unbound Fd. The bound protein is the ratio of bound Fd to the total Fd input in percentage. A) The ability of different TOBiP-Fds to bind to TiO_2 was tested. Assay was performed in 0.1X PBS (pH7.8) with 700 ºC TiO_2 from the University of Memphis; B) Buffer (0.1X PBS) at various pH was used to find the optimum pH for the attachment of LSTB1-TeFd to 700 ºC TiO_2. PL stands for protein ladder. C) Different additives were used to determine their contribution to attach TOBiP-TeFd on TiO_2. Lanes 1-7 are no additive control, 3% PEG, 3% Glycerol, 0.3% Triton X-100, 0.3% DM, 3% DMSO respectively and 10% of total input TeFd. LSTB1-TeFd, 700 ºC TiO_2, and 0.1X PBS (pH 7.2) were used; D) Different TiO_2 particles. The assay used 3% DMSO in 0.1X PBS (pH 7.2) and LSTB1-TeFd and WT TeFd was used as control.

A

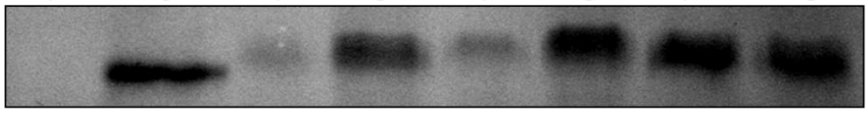

	WT	STB1	STB2	LSTB1
Bound protein (% of total input)	0	12.3	18.7	47.5

B

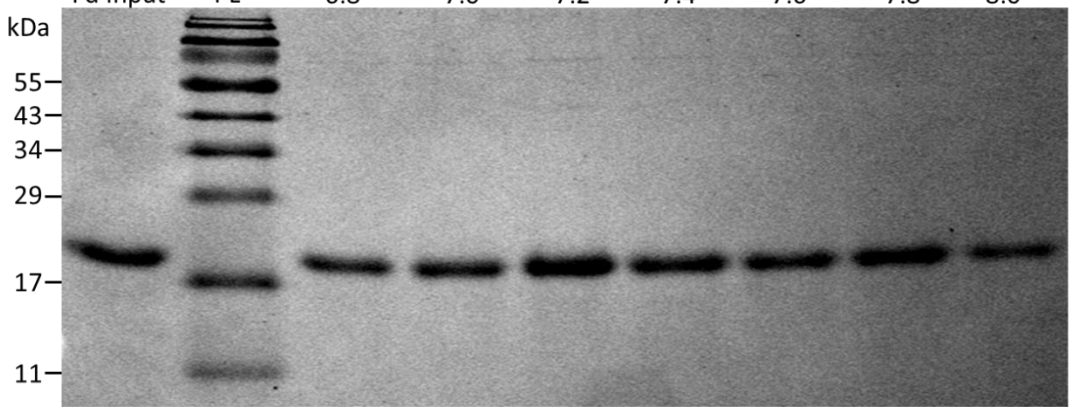

pH	6.8	7.0	7.2	7.4	7.6	7.8	8.0
Bound protein (% of total input)	16.2	20.2	29.6	22.0	17.5	22.0	12.5

C

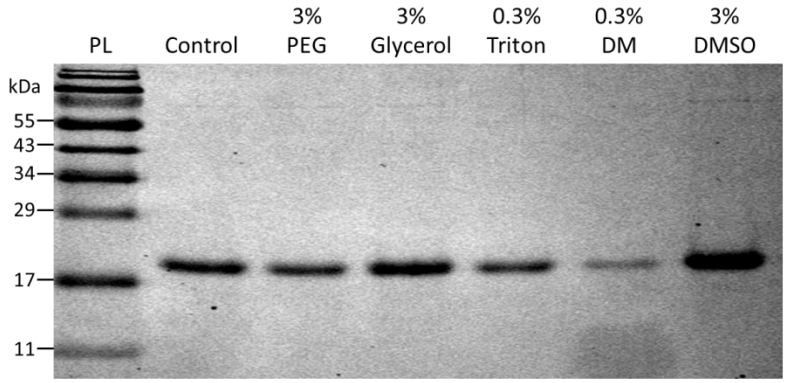

	Control	3% PEG	3% Glycerol	0.3% Triton	0.3% DM	3% DMSO
Bound protein (% of total input)	15.0%	16. 8%	29.8%	16.4%	6.9%	33.9%

D

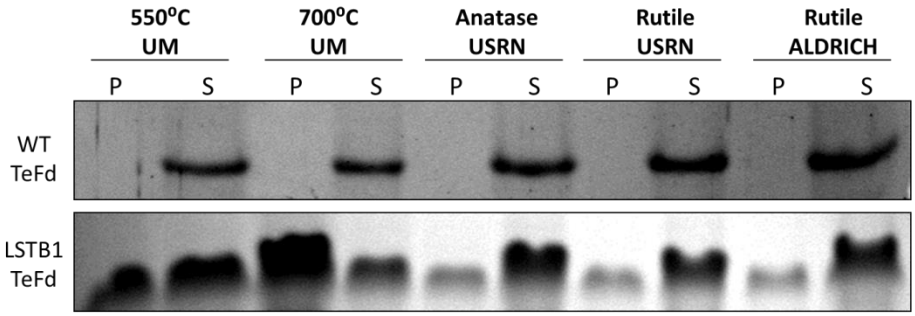

		550°C UM	700°C UM	Anatase USRN	Rutile USRN	Rutile ALDRICH
Bound protein (% of total input)	WT	0	0	0	0	0
	LSTB1	15.1	50.3	9.4	8.5	10.0

Figure 3.12 Optimization of TOBiP-Fd attachments to TiO_2 nanoparticle (continued).

`

Figure 3.13 SEM images of TiO_2 nanoparticles

SEM images for different types of TiO_2 nanoparticles. Each type of the particle has two different magnifications (upper and lower panel) to show the structure of the particle. A) and B) are made by the University of Memphis. C) and D) are made by US Research Nanomaterial, E) is made by ALDRICH.

A

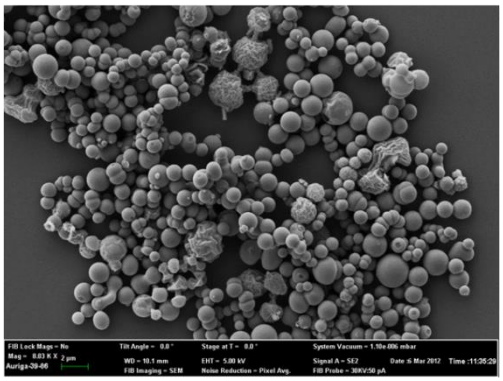

Mag = 8.03K
UM, 550 ^{o}C TiO_2

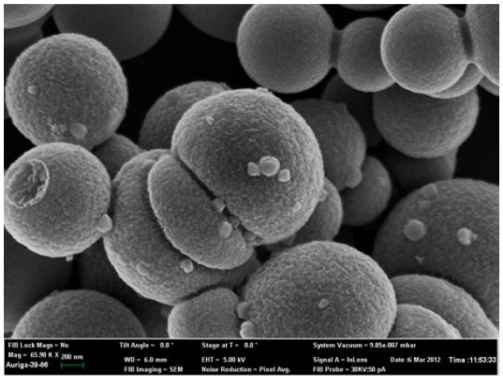

Mag = 65.98K
UM, 550 ^{o}C TiO_2

B

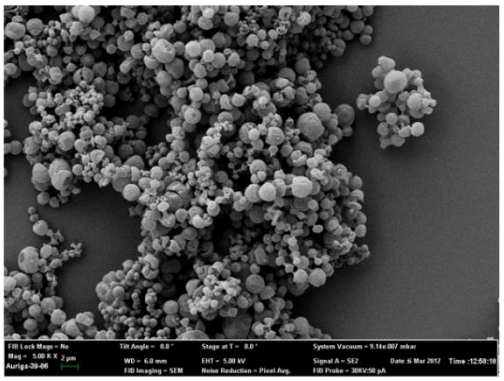

Mag = 5.00K
UM, 700 ^{o}C TiO_2

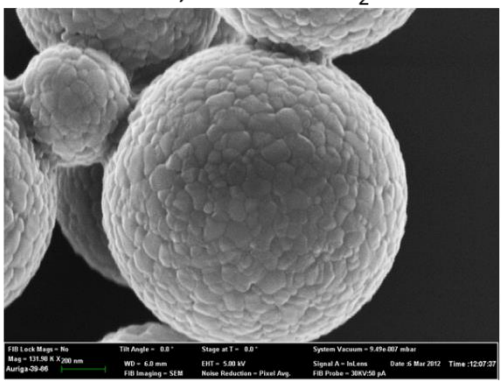

Mag = 131.98K
UM, 700 ^{o}C TiO_2

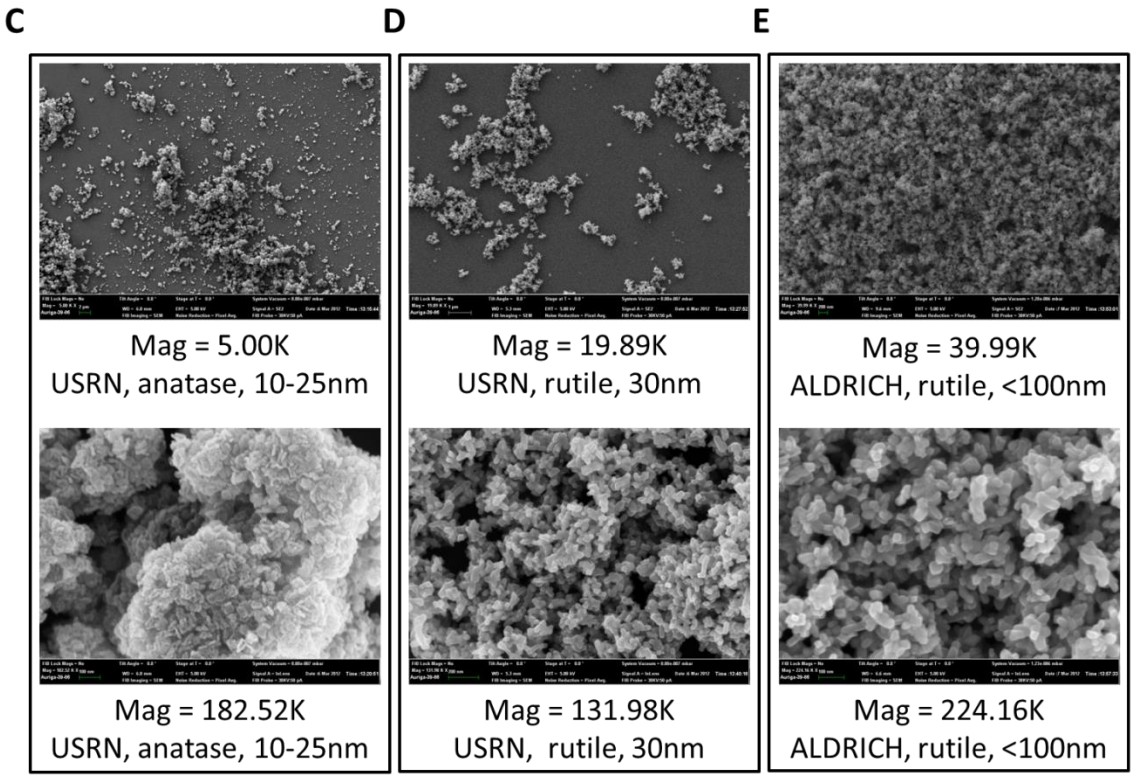

Figure 3.13 SEM images of TiO_2 nanoparticles (continued).

3.7 Fd-PSI chemical crosslinking

In order to attach PSI to TiO_2 nanoparticles via TOBiP-TeFd, a permanent connection between PSI and Fd was desired. This was achieved using chemical crosslinking, and the results were analyzed using Western blotting. To enable Western blotting analysis, purification of TeFd polyclonal antibody was performed using cyanogen bromide (CNBr)-activated Sepharose 4B (GE Healthcare Life Sciences, Piscataway, NJ). The results suggested that anti-TeFd was purified since there is no cross reacting band present after purification (Figure 3.14). The anti-PsaD and anti-PsaE were purified using the same method.

Chemical crosslinking was then performed in order to generate PSI-Fd or PSI-Fd-TOBiP crosslinked complexes as described in Chapter 2.11 (Figure 3.15). An increasing amount of WT Fd was used to crosslink to PSI. LSTB1 TeFd was also tested to confirm the N terminus LSTB1 does not interfere the crosslinking reaction between PSI and Fd. The resulting bands between PSI-WT TeFd and PSI-LSTB1 TeFd crosslinked product are largely the same excepted for a slight size shift. The slight size shift is likely due to the LSTB1 tag and thus indicates that the insertion of TOBiP to WT TeFd does not interfere with the interaction between PSI and Fd. It was observed that several unknown bands appeared in the upper region of the Western blot result. These unknown bands are likely formed due to non-specific crosslinking and are undesired for our photovoltaic device.

To solve this problem, various conditions, including reaction time, reaction temperature and PSI:Fd molar ratio, were tested to optimize the crosslinking reaction while minimizing the amount of non-specific crosslinked product (Figure 3.16). According to Figure 3.16A, time dependent crosslinking suggested that the crosslinking reaction finished within 5 sec and that longer crosslinking does not increase the desired product but rather makes the results “dirtier”. The PSI:Fd molar ratio were then tested using the conditions above except for using a 5 sec reaction time. The results indicated that too much Fd causes increased non-specific bands while too little Fd significantly decreases all crosslinked product (Figure 3.16B). In order to balance the increase of undesired bands and the decrease of all crosslinked product, a PSI:Fd molar ratio of 1:1 was selected. To further optimize the crosslinking reaction, several other conditions were also tested, such as lower reaction temperature (performing the reaction at 4^0C), lower reaction time (1 sec), less protein input (half of the previous concentration), etc. The result suggests that using lower reaction temperature, lower reaction time, and lower crosslinker concentration can reduce non-specific crosslinked products (Figure 3.16C).

In conclusion, the optimized crosslinking reaction was performed using PSI:Fd in 1:1 molar ratio, 5 mM NHS and 2.5 mM EDC at 4 ^{0}C with a 1 sec reaction time (Figure 3.17).

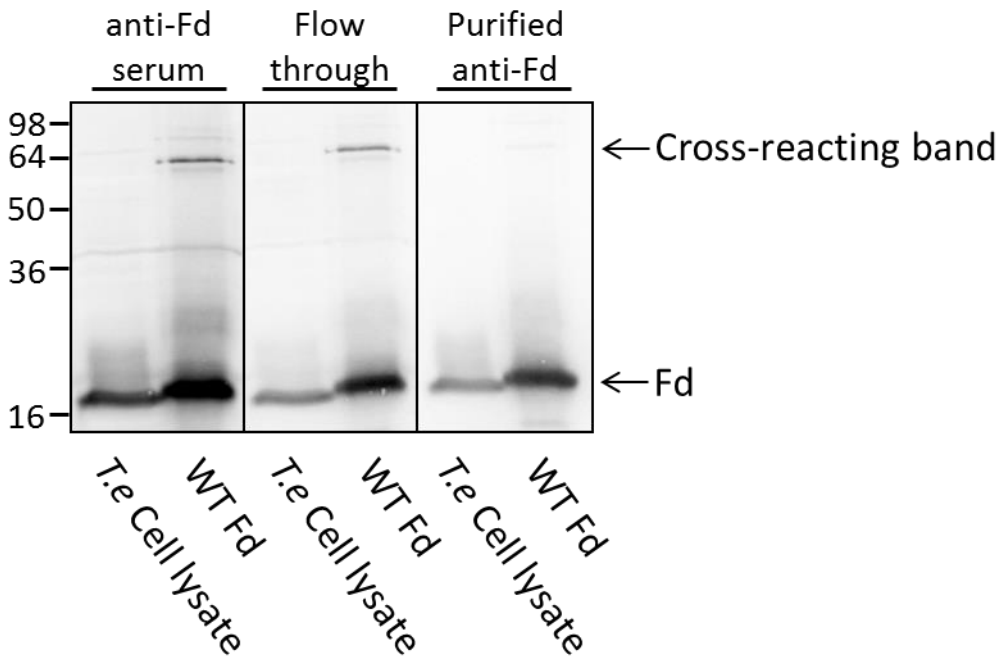

Figure 3.14 Purification of anti-TeFd

The anti-Fd serum (*T.e.*) is purified using immunoaffinity purification with cyanogen bromide (CNBr). The CNBr is coupled with purified ferredoxin (Fd), and the anti-Fd serum is then incubated on the column. The purified anti-Fd is eluted using acidic buffer (pH 2.5) and neutralized by saturated phosphate buffer. The serum, flow through and the purified antibody were tested using Western blotting.

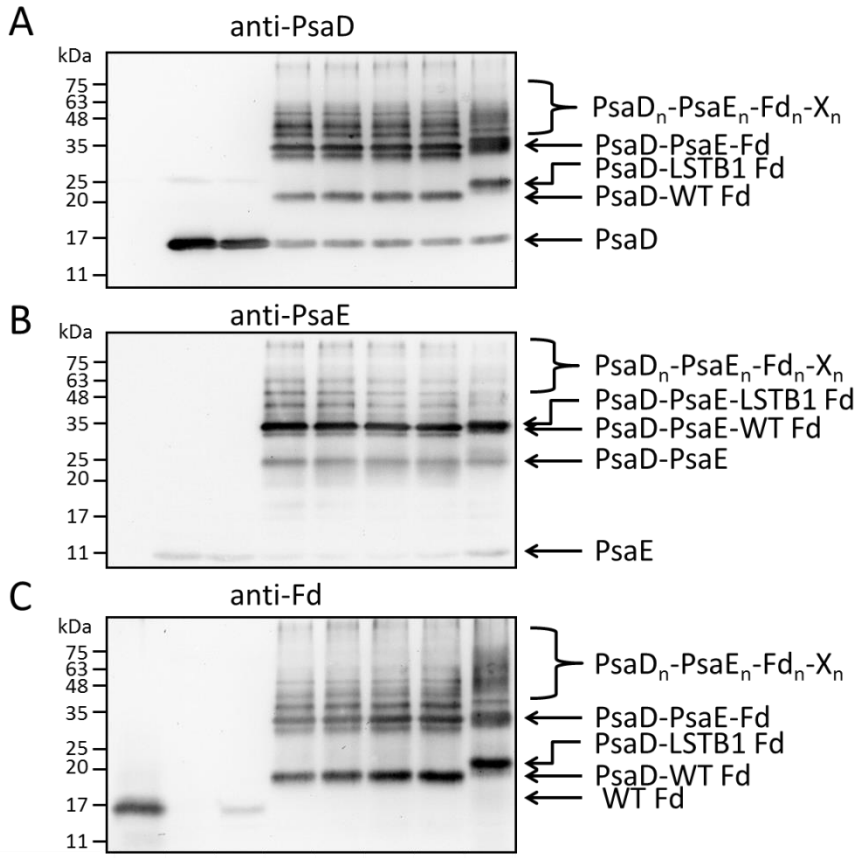

WT Fd (μg)	10	-	10	5	10	15	20	-
LSTB1 Fd (μg)	-	-	-	-	-	-	-	20
PSI	-	+	+	+	+	+	+	+
EDC-NHS	-	-	-	+	+	+	+	+

Figure 3.15 Crosslink results

The PSI-FD crosslinked result analyzed by Western blot with different antibodies. A) anti-PsaD, B) anti-PsaE, and C) anti-Fd. By comparing the crosslinked products between WT TeFd and LSTB1 TeFd, all the crosslinked bands are the same except for a slight size shift. This result further confirmed that insertion of TOBiP does not interfere with interactions between PSI and Fd.

Figure 3.16 Optimization of the crosslinking reaction

A) Time dependent crosslink result. PSI and Fd were mixed at 1:1 molar ratio and underwent chemical crosslink reaction from 5 to 300 sec. The crosslink result was analyzed by Western blot and immuno-detected using anti-PsaD, anti-PsaE, and anti-Fd. B) Different PSI:Fd molar ratios. PSI and Fd were mixed at different molar ratios and underwent chemical crosslinking for 5 sec. The crosslinking results were analyzed by Western blot and immuno-detected using anti-PsaD and anti-Fd. C) Other conditions tested to optimize the crosslinking reaction. The crosslinking results were analyzed by Western blot and immuno-detected using anti-PsaD and anti-Fd.

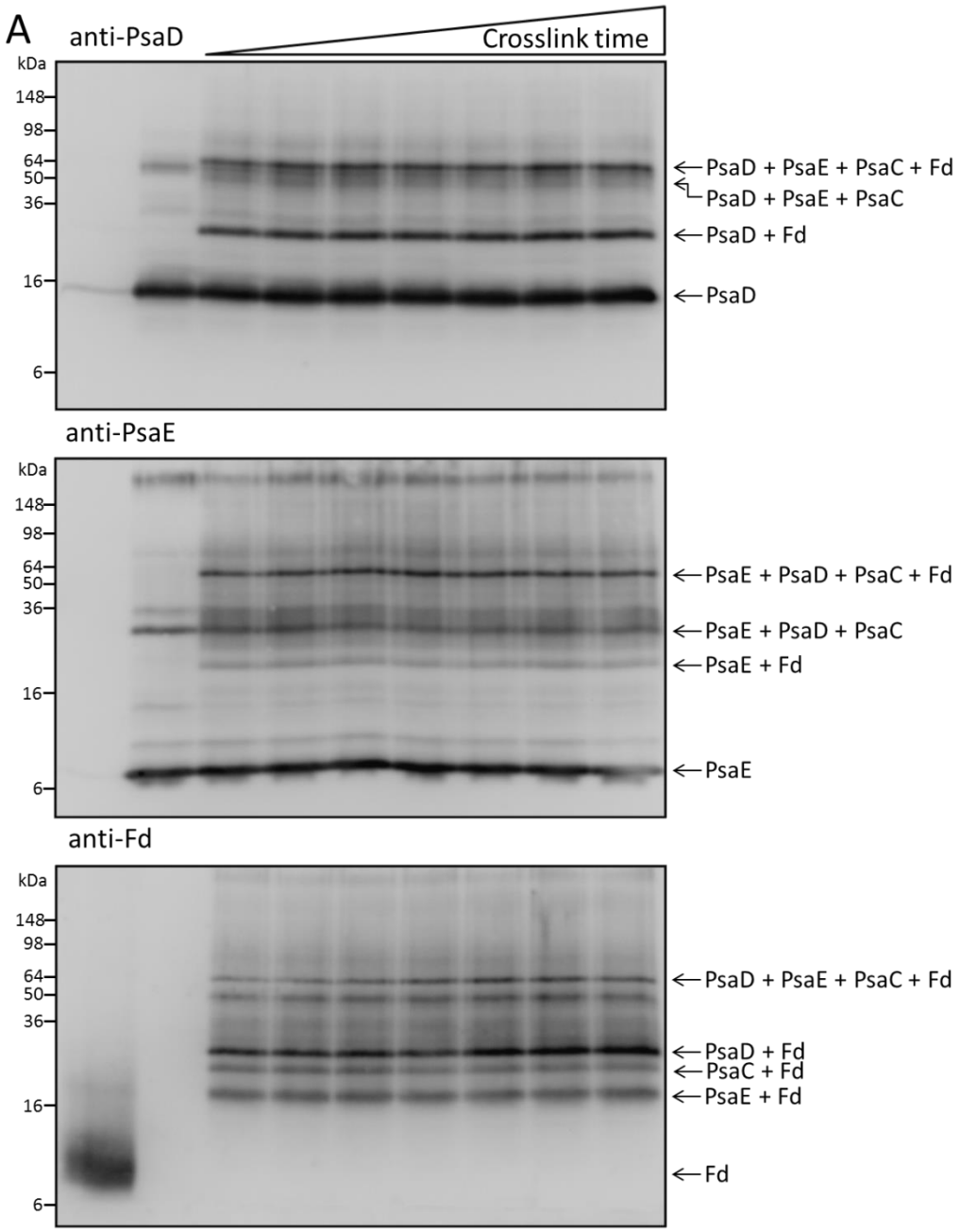

PSI	-	+	+	+	+	+	+	+	+
Fd	+	-	+	+	+	+	+	+	+
Crosslink time (second)	60	60	5	10	15	20	30	60	300

B

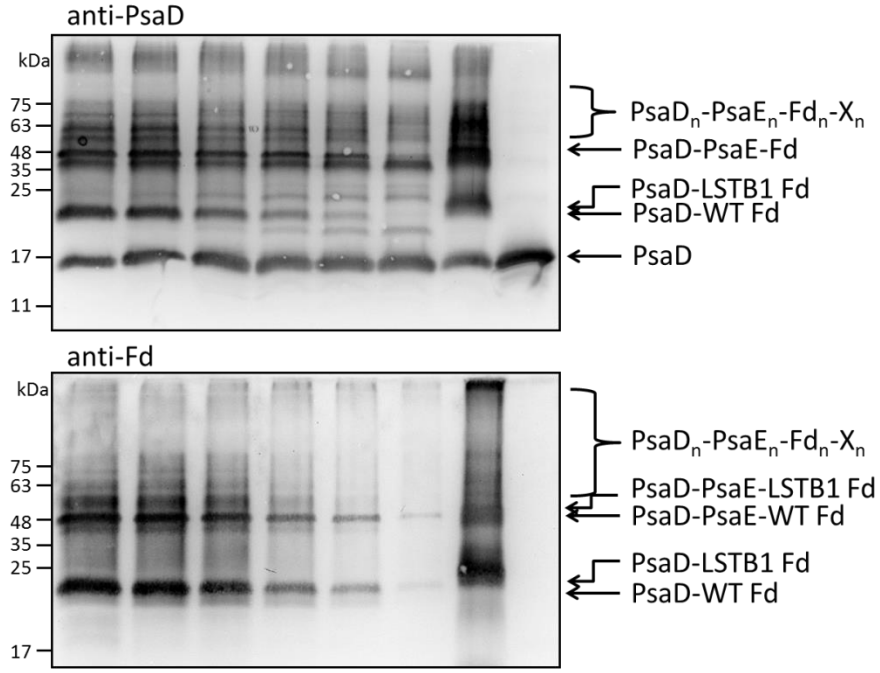

WT-Fd	+	+	+	+	+	+	-	-
LSTB1 Fd	-	-	-	-	-	-	+	-
PSI	+	+	+	+	+	+	+	+
PSI: Fd ratio	1:5	1:2	1:1	2:1	5:1	10:1	1:5	-
EDC-NHS	+	+	+	+	+	+	+	-

Figure 3.16 Optimization of the crosslinking reaction (continued)

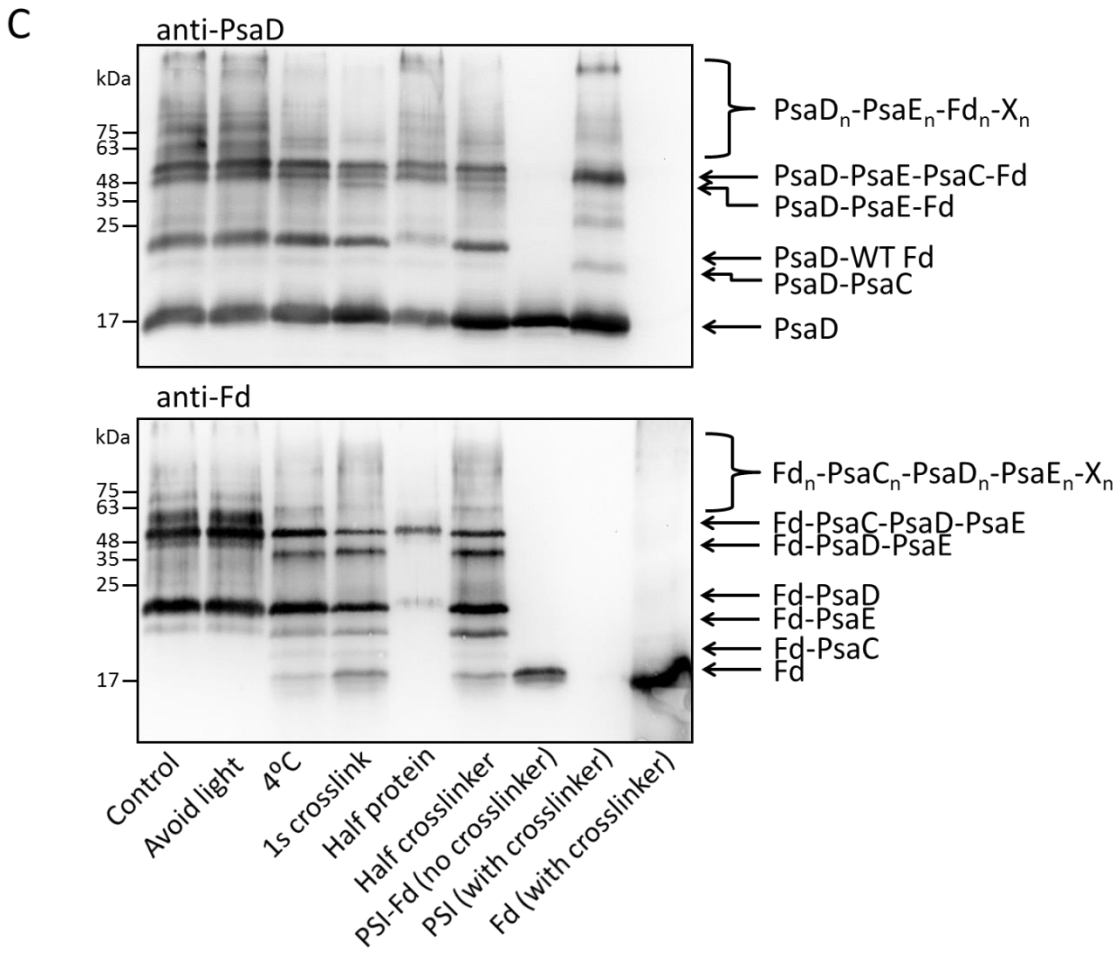

Figure 3.16 Optimization of the crosslinking reaction (continued)

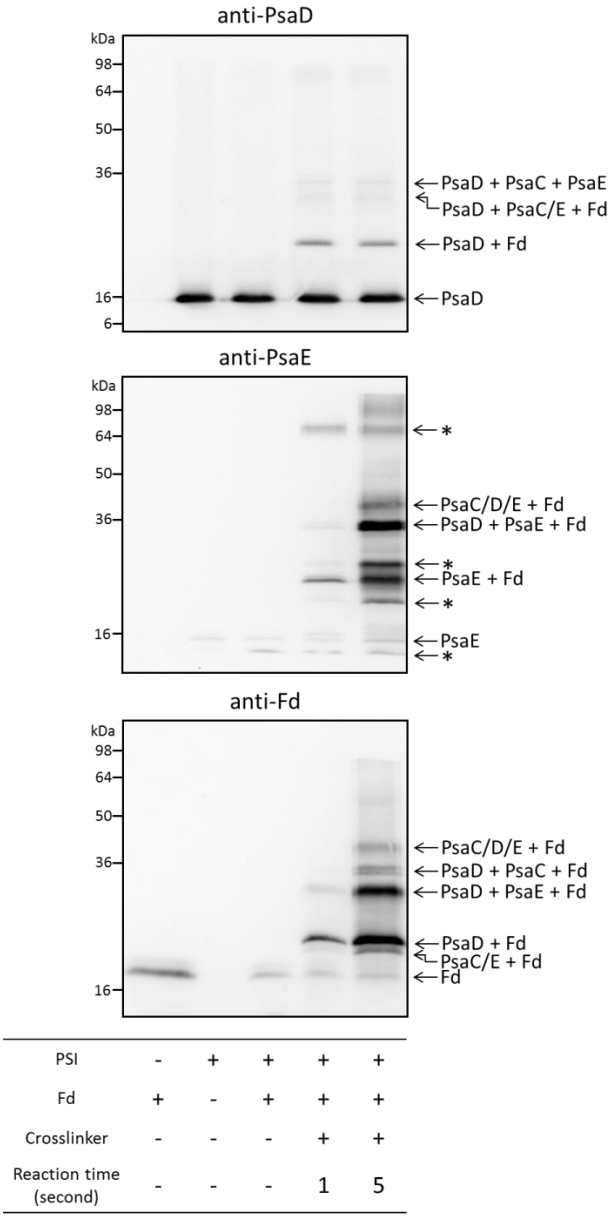

Figure 3.17 Optimized crosslink results

Using the optimized crosslinking conditions, the results were analyzed by Western blot and immuno-detected using anti-PsaD, anti-PsaE, and anti-Fd. (*) indicates unknown band.

3.8 PSI-TOBiP Fd attachment on TiO_2

The crosslinked PSI-TOBiP Fd complex was analyzed for its ability to bind TiO_2 nanoparticles. The experiment followed the same protocol as mentioned above (Chapter 2.11). The crosslinked product was then incubated with TiO_2 and bound PSI and PSI-Fd (or PSI-LSTB1 TeFd) were quantified using the standard curve (Figure 3.18). The amount of PSI (or PSI-Fd crosslinked product) attached to the TiO_2 nanoparticle was measured by Chl *a* concentration. The concentration of Chl *a* was determined using UV-Visible Spectroscopy as mentioned in Chapter 2.14. These results indicate that PSI can non-specifically bind to TiO_2 nanoparticles (Figure 3.19). By crosslinking to WT TeFd, it is possible WT TeFd interferes with regions of PSI that interact with TiO_2. The increased attachment of PSI-LSTB1 TeFd is likely due to the TOBiP engineered at the N-terminus of Fd. An increase of roughly 45% in binding was observed in LSTB1-TeFd over PSI-WT TeFd and thus supported the TOBiP-Fd fusion protein's ability to direct PSI to TiO_2.

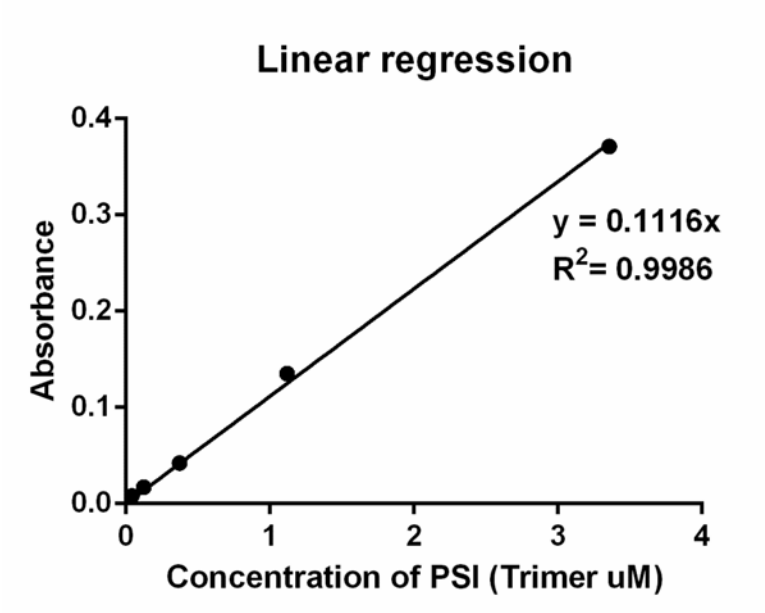

Figure 3.18 PSI Standard curve

Absorbance measurements were taken at 665 nm and used to calculate total Chl *a* content. PSI concentration was calculated based on Chl *a* concentration.

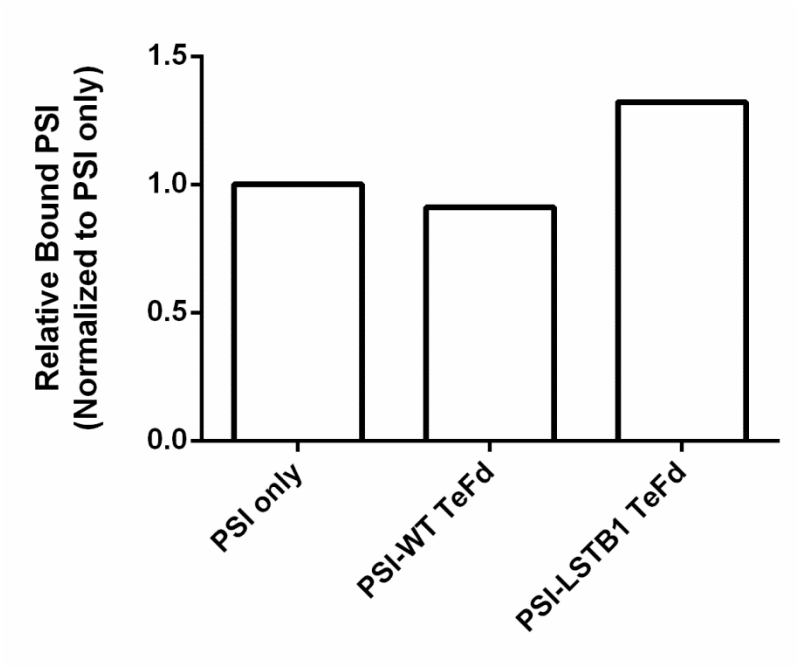

Figure 3.19 Relative amount of PSI-TOBiP Fd that is bound on TiO_2

The first column is PSI alone control, column 2 is PSI-WT TeFd crosslinked products and column 3 is PSI-LSTB1 TeFd crosslinked products.

`

Chapter 4 Discussion

4.1 Introduction

Photosynthesis is an ancient process which converts light energy into chemical energy that can be used for metabolic processes and forms the basis of life on earth (Blankenship & Hartman, 1998). Considering the increasing demands for energy and the limited fossil fuel resources, finding alternative, sustainable and clean sources of energy is a striking and urgent need (Andreiadis et al., 2011; Berardi et al., 2014; Govoni et al., 2008; Gust et al., 2009). Many efforts have attempted to convert sunlight into electricity (Berardi et al., 2014), and some investigations are focused on utilizing photosynthetic reactions to design systems to convert light into stored or electric energy. This field is called applied photosynthesis. This work has provided a possible solution for generating a biological based photovoltaic cell device by modeling the interaction between PSI and Fd, introducing TOBiP to Fd, cloning and purifying PSI and Fd (or TOBiP-Fd), chemical crosslinking and *in vitro* binding assays. In the future, it will be interesting to analyze the interaction between PSI and Fd, attach them on the TiO_2 electrode and generate a photocurrent.

4.2 Introduction of TOBiP to Fd

It is desired to develop a method which allows the conjugation of biomolecules and inorganic materials at the molecular level. Therefore, Fd was

selected to facilitate the transfer of the electron from PSI to a TiO_2 electrode (Figure 1.6).

Recently, a growing number of peptides capable of specifically recognizing inorganic materials have been reported (Thai et al., 2004). These inorganic-binding peptides have been inserted into protein structures and used to direct the assembly of hybrid materials (Sarikaya et al., 2003). Among these inorganic-binding peptides, 3 different titanium oxide binding peptides (TOBiP) have been discovered and are named STB1, STB2 and LSTB1 (Haibin Chen; Su, 2008) (Table 1). These TOBiPs were selected to be engineered to Fd and the fusion protein was expected to be able to specifically bind to TiO_2.

It is known that Fd is capable of docking on PSI as an electron acceptor (Godman & Balk, 2008; Ragsdale & Ljungdahl, 1984). Although there have been numerous studies on the interaction between PSI and Fd, the lack of a high-resolution crystal structure of the PSI-Fd complex has prevented the creation of a detailed model (Cashman et al., 2014). Due to the lack of a PSI-Fd interaction model, it was difficult to decide to which terminus TOBiP should be engineered since it is of critical importance that the engineered TOBiP does not interrupt the electron transport process from PSI and Fd.

A similar problem arose in previous studies. Investigations were performed by engineering linkers or proteins (like hydrogenase) to the C- or N-terminus of Fd. It is interesting that controversial results were generated. In one study, *Chlamydomonas reinhardtii* (a single-cell green alga) hydrogenase (Hyd)

was fused to either the N- or C- terminus of Fd, and the hydrogen production kinetics for each fusion protein were characterized (Yacoby et al., 2011). The results indicated that although the N-terminal fusion protein (Hyd-Fd) was biochemically active, they were unable to photo-produce hydrogen. In contrast, the C-terminal fusion protein (Fd-Hyd) was capable of photo-producing hydrogen. In two other investigations, opposite results were observed using Fd from bacterial and *Synechococcus elongatus Geitler* strains. Fd is functional only when the linkers or proteins are fused to the N-terminus (Agapakis et al., 2010; Wittenberg et al., 2013). This difference is likely due to the structural differences between algal and bacterial Fd (Figure 4.1) (Yacoby et al., 2011)

In order to figure out the correct terminus for fusion of Fd to TOBiP, computational modeling was used to generate predictive models describing how Fd docks to PSI in *T. elongatus*. Rigid body docking experiments were performed, and yielded several possible docking conformations of Fd to PSI which were further classified into two groups based on the orientation of Fd (Figure 3.5). One commonality existed between all the yielded conformations: the C-terminus of Fd was located in the middle of the interaction sites between PSI and Fd while the N-terminus of Fd was located away from the interaction sites. Engineering TOBiP to the N-terminus of Fd will most likely avoid interference with the interaction sites between PSI and Fd.

As a result the eight amino acid long TOBiP (Figure 3.6) was introduced to the N-terminus of TeFd. In order to increase the flexibility of the TOBiP and in

turn promote its binding affinity to TiO_2, a short linker composed of three amino acids was introduced between TOBiP and TeFd. Three TOBiP-TeFd fusion proteins were then heterologously expressed in *E. coli* 2556 strain and purified using the IMPACT system (New England Biolabs, Beverly, MA).

The hypothesis that engineering TOBiP to the N-terminus of Fd will most likely avoid interference with the interaction sites between PSI and Fd, was later supported by a chemical crosslinking experiment between PSI and TOBiP-Fd with the TOBiP tag engineered on the N-terminus of Fd (Figure 3.15). Chemical crosslinking was performed between PSI and WT Fd as well between PSI and LSTB1-Fd and analyzed using Western blotting. The crosslinking result showed no significant difference between WT Fd and LSTB1-Fd indicating that the TOBiP on the N-terminus of Fd does not interfer with the interaction between PSI and Fd.

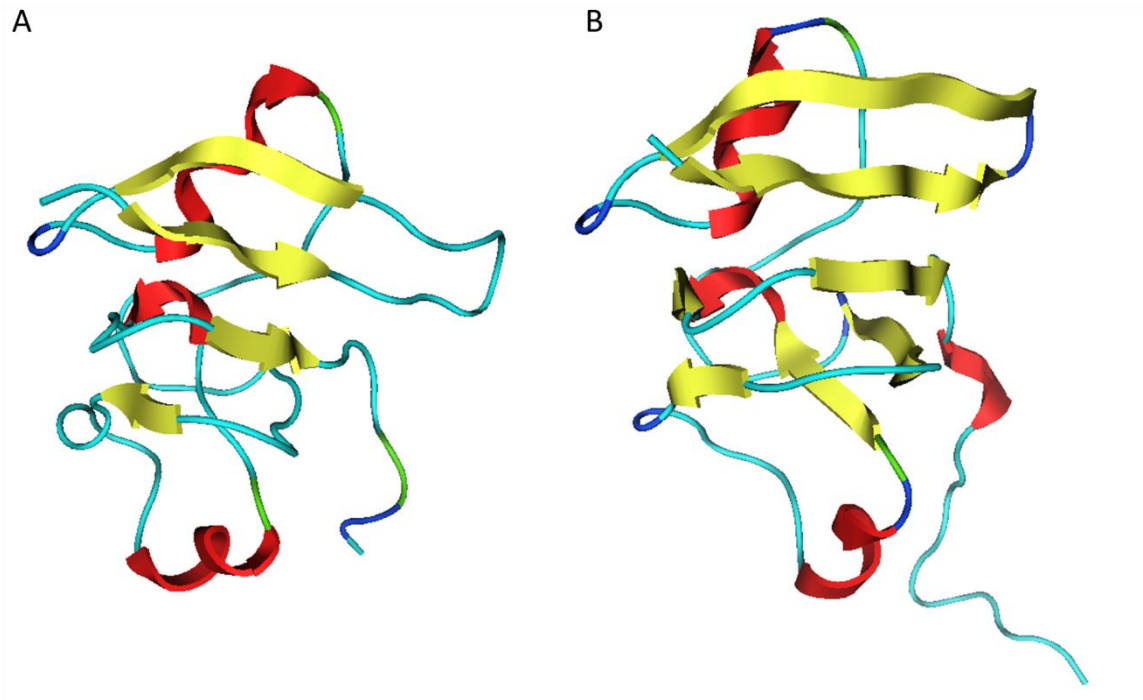

Figure 4.1 Crystal Structure of Fd from different organisms

A) *T. elongatus* Fd (PDB ID: 2CJN) composed of 98 amino acids and B) *Chlamydomonas reinhardtii* Fd (PDB ID: 4ITK) composed of 123 amino acids. The major structural difference is located at the C-terminus.

`

4.3 Functional characterize Fd

Due to the important role Fd will play in our photovoltaic device, it is necessary to characterize the purified fusion protein TOBiP-Fd. Several techniques including SDS-PAGE, MALDI-TOF MS, and difference spectroscopy were used to characterize it and confirm its functionality.

The elution from the IMPACT system was analyzed using SDS-PAGE, and the result indicated the existence of several contamination bands with apparent MW above 50 kDa. These bands are mostly likely the intein tag that was used to purify the proteins. A 50 kDa filter was used to remove the contamination (Figure 3.9B). SDS-PAGE also indicated a significant difference between the apparent MW of purified Fd and its predicted molecular weight. This difference might be due to the fact that less SDS was bound to the protein, creating less negative charge on the protein and decreasing its mobility (Hjelmeland et al., 1981). MALDI-TOF was used to confirm the MW of the purified proteins (Figure 3.10). The MALDI-TOF MW results were ± 1 Da compared to the predicted MW and confirmed that the purified protein was Fd (or TOBiP-Fd).

It is known that plant Fd exhibits absorption maxima at 465, 420, 330 and 278 nm mainly due to the [2Fe-2S] center. These specific maxima will disappear when the [2Fe-2S] is removed (Bayer et al., 1967; D. O. Hall, 1973; Rao et al., 1971). Due to the important role of the [2Fe-2S] center in the electron transport activity of Fd, difference spectroscopy was used in order to confirm the existence

of the [2Fe-2S] center in the purified protein (Figure 3.11). Similar results were observed between WT TeFd and the LSTB1-TeFd, supporting that both the purified WT TeFd and LSTB1- TeFd contain [2Fe-2S] centers that are functionally capable of transferring electrons.

Considering these results, a reasonable conclusion can be made: recombinant Fds (WT TeFd and LSTB1-TeFd) are functionally active and capable of transporting electrons between PSI and TiO_2 electrode.

4.4 In vitro binding of TOBiP-Fd to TiO_2 nanoparticle

The ability of the TOBiP to direct Fd to TiO_2 nanoparticles was tested using an *in vitro* binding assay. TOBiP-TeFd was incubated with TiO_2 nanoparticles under various conditions to characterize the optimum conditions for *in vitro* binding. The bound and unbound proteins to TiO_2 were analyzed using SDS-PAGE. The binding affinity is calculated from the ratio of bound to total protein input (Figure 3.12).

As shown in Figure 3.12A, WT TeFd showed no binding affinity while 3 TOBiP-Fd showed different affinities for the TiO_2 nanoparticle, with LSTB1-TeFd having the highest binding affinity. This result not only indicated LSTB1-TeFd has the highest binding affinity to TiO_2, but more importantly, it proved that this binding affinity was specific. Furthermore, this specificity was gained through TOBiP since WT TeFd showed no binding.

`

Along with several other conditions, inlcuding pH, additives, and TiO_2 nanoparticle species, the *in vitro* binding of TOBiP-Fd to TiO_2 nanoparticles assay was optimized.

4.5 PSI attachment to TiO_2 nanostructures via Fd-Fusion Proteins

The attachment of PSI to the electrode of a photovoltaic device requires appropriate immobilization strategies. In previous studies, researchers have attempted to immobilize PSI onto various electrode substrates. For the immobilization to be successful, two important factors must be considered: the orientation of PSI attachment and the proximity to the electrode (Nguyen & Bruce, 2014).

In order to direct PSI to the electrode with specific orientation, specific binding peptides and organothiol-based self-assembled monolayers (SAMs) were used. For example, Das *et al.* 2004 immobilized the recombinant PsaD–His_6 fusion protein on a Ni^{2+}-NTA functionalized Au surface, and this surface was then incubated with WT PSI (Figure 4.2A). In addition, Mershin *et al.* 2012 immobilized PSI using two different approaches: PSI was physisorbed to TiO_2 or self-assembled on ZnO nanowires using the PsaE-ZnO binding peptide (Figure 4.2B).

In order to enhance the photocurrent generation, it is of critical importance to optimize the process of transferring electrons from the site of charge

separation within PSI to the electrodes. Since it may be difficult to further minimize the distance between the [4Fe-4S] centers in PsaC and the electrodes, Fd may be used as an intermediary to connect PSI and the electrode, thus facilitating electron transfer.

This hypothesis was confirmed by a recent article using a similar approach to accelerate electron transport from PSI to the electron receptor. Gal Wittenberg *et al.* 2013 fused Fd to the PsaE subunit by a flexible peptide linker (PsaE-linker-Fd) and reconstituted PSI *in vitro* with the new fusion protein (Wittenberg et al., 2013). The result indicated a 10-fold increase in the electron transport rate and revealed the benefit of using closely attached Fd as an electron transporter in PSI based photovoltaic cell devices. As a result, we proposed that by directly crosslinking Fd to PSI, a faster electron transfer rate between PSI and electrode may be achieved, generating a photovoltaic device with enhanced photocurrent capabilities (Figure 4.2C).

The LSTB1-TeFd was selected based on the previous results and was chemically crosslinked to PSI using EDC and NHS as crosslinkers. Various conditions were tested to optimize the crosslinking reaction and minimize non-specific crosslinking. The crosslinked products were then incubated with TiO_2 nanoparticles, and it will be used for future photocurrent measurements.

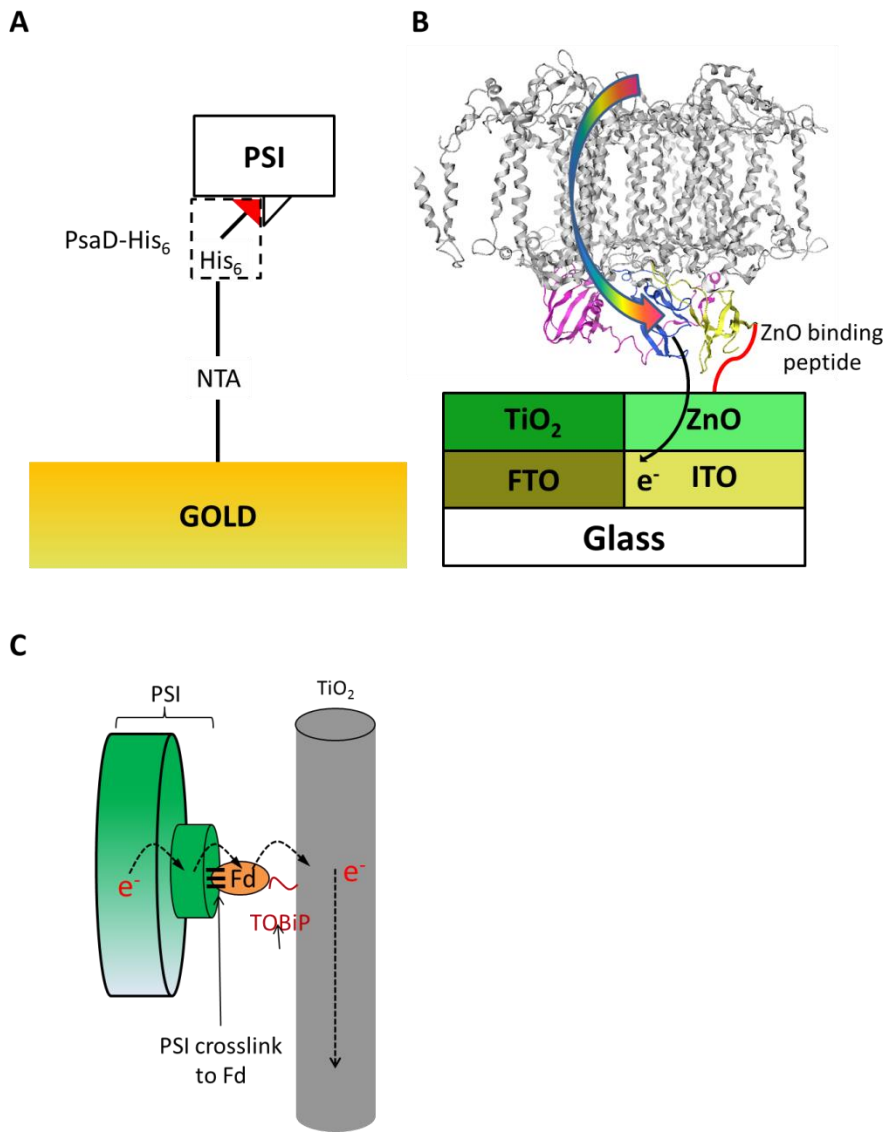

Figure 4.2 Model for PSI attachment to TiO_2 nanostructures

PSI is immobilized via A) recombinant PsaD–His_6 fusion protein on a Ni^{2+}-NTA functionalized Au surface (adopted form Das *et al.* 2004); B) physisorbed to TiO_2 or self-assembled on ZnO nanowire using the PsaE-ZnO binding peptide (adopted form Mershin *et al.* 2012); and C) crosslinked TOBiP-Fd fusion protein.

`

Chapter 5 Conclusion and Future Directions

Based on this project, many future experiments can utilize photosynthetic reaction mechanisms to convert light energy into electricity to generate a low cost, high efficient photovoltaic device. Affinity purification using the purified anti-Fd can be performed in order to purify the PSI-Fd crosslinked species from the crosslinked products. The purification process can separate the PSI-Fd crosslinked complex from free PSI, minimizing the PSI non-specific attachment found in the *in vitro* binding assay. As a result, all the bound PSI on the TiO_2 could be directed via the Fd-fusion protein to make attachment more directionally specific. Also, the *in vitro* binding assay can be further optimized to increase the binding efficiency. Various TiO_2 nanoparticles and binding conditions could be tested using Western blotting and UV-Vis spectroscopy.

Photocurrent can be measured by attaching the chemically crosslinked PSI-Fd-TOBiP complex onto the TiO_2 nanoparticle since all the required samples are prepared. Electron paramagnetic resonance (EPR) could be performed to study the electron transport in the process. Numerous conditions could be tested in order to optimize the photocurrent yield. In addition, collaboration might be necessary to produce a TiO_2 surface which could be used to further test the photocurrent in this system.

Using these low cost raw materials and relatively simple processes, we will be able to generate an affordable and efficient photovoltaic cell device. The biological materials we used originated from the thermophilic cyanobacteria, *T.*

elongatus, and can be purified in large quantities. Besides *T. elongatus*, many other sources of biological materials, including land plants, can be used for the production of PSI and Fd. Industrial-scale methods have been developed to isolate proteins from plant or bacterial extracts using polyethersulfone membranes (Liu et al., 2007; Mershin et al., 2012c). Due to these results and possiblities, the photovoltaic cell device has a promising future.

All of the above experiments will test the photocurrent generated by the device, but it would be interesting to further study the interaction sites between PSI and Fd using chemical crosslinking and LC-MS. The stromal domain of PSI has already been successfully removed from the PSI-Fd crosslinked product using urea treatment. Our lab is still working on analyzing this sample (after trypsin digestion) using LC-MS . This result could help elucidate the interactions between PSI and Fd. Together with the computational modeling we generated, more detailed interaction sites between PSI and Fd can be revealed.

`

List of References

Agapakis, C. M., Ducat, D. C., Boyle, P. M., Wintermute, E. H., Way, J. C., & Silver, P. A. (2010). Insulation of a synthetic hydrogen metabolism circuit in bacteria. *J Biol Eng, 4*, 3. doi: 10.1186/1754-1611-4-3

Altermann, W., & Kazmierczak, J. (2003). Archean microfossils: a reappraisal of early life on Earth. *Res Microbiol, 154*(9), 611-617. doi: DOI 10.1016/j.resmic.2003.08.006

Andersen, B., Scheller, H. V., & Moller, B. L. (1992). The PSI-E subunit of photosystem I binds ferredoxin:NADP+ oxidoreductase. [Research Support, Non-U.S. Gov't]. *FEBS Lett, 311*(2), 169-173.

Andreiadis, E. S., Chavarot-Kerlidou, M., Fontecave, M., & Artero, V. (2011). Artificial photosynthesis: from molecular catalysts for light-driven water splitting to photoelectrochemical cells. *Photochem Photobiol, 87*(5), 946-964. doi: 10.1111/j.1751-1097.2011.00966.x

Arnon, D. I. (1949). Copper Enzymes in Isolated Chloroplasts. Polyphenoloxidase in Beta Vulgaris. *Plant Physiol, 24*(1), 1-15.

Atsumi, S., Higashide, W., & Liao, J. C. (2009). Direct photosynthetic recycling of carbon dioxide to isobutyraldehyde. [Research Support, Non-U.S. Gov't

Research Support, U.S. Gov't, Non-P.H.S.]. *Nat Biotechnol, 27*(12), 1177-1180. doi: 10.1038/nbt.1586

Bayer, E., Josef, D., Krauss, P., Hagenmaier, H., Roder, A., & Trebst, A. (1967). [Degradation and resynthesis of the active sites of plant ferredoxins]. *Biochim Biophys Acta, 143*(2), 435-437.

Berardi, S., Drouet, S., Francas, L., Gimbert-Surinach, C., Guttentag, M., Richmond, C., . . . Llobet, A. (2014). Molecular artificial photosynthesis. *Chemical Society Reviews*. doi: 10.1039/c3cs60405e

Berg, J. M., Tymoczko, J. L., & Stryer, L. (2007). *Biochemistry (6th Edition)*. New York: W.H. Freeman & Company.

Blankenship, R. E. (2010). Early evolution of photosynthesis. [Research Support, U.S. Gov't, Non-P.H.S.

Review]. *Plant Physiol, 154*(2), 434-438. doi: 10.1104/pp.110.161687

Blankenship, R. E., & Hartman, H. (1998). The origin and evolution of oxygenic photosynthesis. [Research Support, U.S. Gov't, Non-P.H.S.

Review]. *Trends Biochem Sci, 23*(3), 94-97.

Blankenship, R. E., Tiede, D. M., Barber, J., Brudvig, G. W., Fleming, G., Ghirardi, M., . . . Sayre, R. T. (2011). Comparing photosynthetic and photovoltaic efficiencies and recognizing the potential for improvement. [Comparative Study

Research Support, Non-U.S. Gov't

Research Support, U.S. Gov't, Non-P.H.S.

Review]. *Science, 332*(6031), 805-809. doi: 10.1126/science.1200165

Bottin, H., Hanley, J., & Lagoutte, B. (2001). Role of acidic amino acid residues of PsaD subunit on limiting the affinity of photosystem I for ferredoxin. *Biochem Biophys Res Commun, 287*(4), 833-836. doi: 10.1006/bbrc.2001.5658

Brain O' Regan, & Michale Gratzel. (1991). A Low-Cost, High-Efficiency Solar-Cell Based on Dye-Sensitized Colloidal Tio2 Films. *Nature, 353*(6346), 737-740. doi: Doi 10.1038/353737a0

Brettel, K., & Leibl, W. (2001). Electron transfer in photosystem I. [Review]. *Biochim Biophys Acta, 1507*(1-3), 100-114.

Bryant, D. A., & Frigaard, N. U. (2006). Prokaryotic photosynthesis and phototrophy illuminated. *Trends Microbiol, 14*(11), 488-496. doi: DOI 10.1016/j.tim.2006.09.001

Bryngelson, J. D., & Wolynes, P. G. (1987). Spin glasses and the statistical mechanics of protein folding. [Research Support, U.S. Gov't, Non-P.H.S.]. *Proc Natl Acad Sci U S A, 84*(21), 7524-7528.

Carbone, A., Zinovyev, A., & Kepes, F. (2003). Codon adaptation index as a measure of dominating codon bias. *Bioinformatics, 19*(16), 2005-2015. doi: DOI 10.1093/bioinformatics/btg272

Cashman, D. J., Tuo Zhu, Richard F Simmerman, Cathy Scott, Barry D. Bruce, & Jerome Baudry. (2014). Molecular Interactions Between Photosystem I and Ferredoxin: An Energy Frustration-Based Model. *Journal of Molecular Recognition*.

Chang, H., Hsu, C. M., Kao, P. K., Yang, Y. J., Hsu, C. C., Cheng, I. C., & Chen, J. Z. (2014). Dye-sensitized solar cells with nanoporous TiO2 photoanodes sintered by N-2 and air atmospheric pressure plasma jets with/without air-

quenching. *J Power Sources, 251*, 215-221. doi: DOI 10.1016/j.jpowsour.2013.11.051

Chen, G., LeBlanc, G., Jennings, G. K., & Cliffel, D. E. (2013). Effect of Redox Mediator on the Photo-Induced Current of a Photosystem I Modified Electrode. *Journal of the Electrochemical Society, 160*(6), H315-H320. doi: Doi 10.1149/2.054306jes

Chen, H., Su, X., Neoh, K. G., & Choe, W. S. (2006). QCM-D analysis of binding mechanism of phage particles displaying a constrained heptapeptide with specific affinity to SiO2 and TiO2. [Research Support, Non-U.S. Gov't]. *Anal Chem, 78*(14), 4872-4879. doi: 10.1021/ac0603025

Chen, H., Su, X., Neoh, K. G., & Choe, W. S. (2008). Probing the interaction between peptides and metal oxides using point mutants of a TiO2-binding peptide. [Research Support, Non-U.S. Gov't]. *Langmuir, 24*(13), 6852-6857. doi: 10.1021/la800314p

Chevallet, M., Luche, S., & Rabilloud, T. (2006). Silver staining of proteins in polyacrylamide gels. *Nat Protoc, 1*(4), 1852-1858. doi: 10.1038/nprot.2006.288

Clayton, R. K. (1976). Photosynthesis and solar energy conversion. *Brookhaven Symp Biol*(28), 1-15.

D. O. Hall, R. C., K. K. Rao. (1973). The plant ferredoxins and their relationship to the evolution of ferredoxins from primitive life. *Pure and Applied Chemistry, 34 (1973)*(3-4), 553-578.

Das, A., & Plotkin, S. S. (2013). SOD1 exhibits allosteric frustration to facilitate metal binding affinity. *Proceedings of the National Academy of Sciences of the United States of America, 110*(10), 3871-3876. doi: 10.1073/pnas.1216597110

Das, D., & Veziroglu, T. N. (2001). Hydrogen production by biological processes: a survey of literature. *International Journal of Hydrogen Energy, 26*(1), 13-28. doi: Doi 10.1016/S0360-3199(00)00058-6

Das, R., Kiley, P. J., Segal, M., Norville, J., Yu, A. A., Wang, L. Y., . . . Baldo, M. (2004). Integration of photosynthetic protein molecular complexes in solid-state electronic devices. *Nano Letters, 4*(6), 1079-1083. doi: Doi 10.1021/Nl049579f

Deng, M. D., & Coleman, J. R. (1999). Ethanol synthesis by genetic engineering in cyanobacteria. *Appl Environ Microbiol, 65*(2), 523-528.

Des Marais, D. J. (2000). Evolution - When did photosynthesis emerge on earth? *Science, 289*(5485), 1703-1705.

Evans, B. R., & O'Neill, H. M., Hutchens, S. A., Bruce, B. D., Greenbaum, E.,. (2004). Enhanced photocatalytic hydrogen evolution by covalent attachment of plastocyanin to photosystem I. *Nano Lett, 4*(10), 1815-1819. doi: Doi 10.1021/Nl0493388

Fischer, N., Setif, P., & Rochaix, J. D. (1999). Site-directed mutagenesis of the PsaC subunit of photosystem I. F(b) is the cluster interacting with soluble ferredoxin. [Research Support, Non-U.S. Gov't]. *J Biol Chem, 274*(33), 23333-23340.

Frenkel, A., Gaffron, H., & Battley, E. H. (1950). Photosynthesis and photoreduction by the blue green alga, Synechococcus elongatus, Nag. *Biol Bull, 99*(2), 157-162.

Gaffron, H. (1939). Reduction of carbon dioxide with molecular hydrogen in green algae. *Nature, 143*, 204-205. doi: Doi 10.1038/143204a0

Ghirardi, M. L., King, P. W., Posewitz, M. C., Maness, P. C., Fedorov, A., Kim, K., . . . Seibert, M. (2005). Approaches to developing biological H-2-photoproducing organisms and processes. *Biochem Soc Trans, 33*, 70-72.

Godman, J., & Balk, J. (2008). Genome analysis of Chlamydomonas reinhardtii reveals the existence of multiple, compartmentalized iron-sulfur protein assembly machineries of different evolutionary origins. [Comparative Study

Research Support, Non-U.S. Gov't]. *Genetics, 179*(1), 59-68. doi: 10.1534/genetics.107.086033

Golbeck, J. H. (1999). A comparative analysis of the spin state distribution of in vitro and in vivo mutants of PsaC - A biochemical argument for the sequence of electron transfer in Photosystem I as F-X -> F-A -> F-B -> ferredoxin/flavodoxin. *Photosynth Res, 61*(2), 107-144. doi: Doi 10.1023/A:1006281802710

Govindjee, L. O. B. a. (2009). The evolution of photosynthesis and chloroplasts. *CURRENT SCIENCE, 96*(11).

Govoni, C., Morosinotto, T., Giuliano, G., & Bassi, R. (2008). Exploiting Photosynthesis for Biofuel Production. *Biophotonics*, 15-28. doi: Doi 10.1007/978-3-540-76782-4_2

Greenbaum, E. (1989). Photobioelectronic Studies with Thylakoid Membranes. *Appl Biochem Biotechnol, 20-1*, 813-824. doi: Doi 10.1007/Bf02936528

Gur, I., Fromer, N. A., Geier, M. L., & Alivisatos, A. P. (2005). Air-stable all-inorganic nanocrystal solar cells processed from solution. *Science, 310*(5747), 462-465. doi: 10.1126/science.1117908

Gust, D., Moore, T. A., & Moore, A. L. (2009). Solar Fuels via Artificial Photosynthesis. *Accounts of Chemical Research, 42*(12), 1890-1898. doi: Doi 10.1021/Ar900209b

Hagfeldt, A., Boschloo, G., Sun, L. C., Kloo, L., & Pettersson, H. (2010). Dye-Sensitized Solar Cells. *Chemical Reviews, 110*(11), 6595-6663. doi: Doi 10.1021/Cr900356p

Haibin Chen; Su, X. N., K; Choe, W (2008). Probing the interaction between peptides and metal oxides using point mutants of a TiO2-binding peptide. *Langmuir, 24*(13), 6852-6857. doi: Doi 10.1021/La800314p

Hammarstrom, L., & Hammes-Schiffer, S. (2009). Artificial photosynthesis and solar fuels. [Editorial

Introductory]. *Acc Chem Res, 42*(12), 1859-1860. doi: 10.1021/ar900267k

Hammond, A. L. (1972). Photovoltaic cells: direct conversion of solar energy. *Science, 178*(4062), 732-733. doi: 10.1126/science.178.4062.732

Hanley, J., Setif, P., Bottin, H., & Lagoutte, B. (1996). Mutagenesis of photosystem I in the region of the ferredoxin cross-linking site: modifications of

positively charged amino acids. *Biochemistry, 35*(26), 8563-8571. doi: 10.1021/bi960399x

Hatanaka, H., Tanimura, R., Katoh, S., & Inagaki, F. (1997). Solution structure of ferredoxin from the thermophilic cyanobacterium Synechococcus elongatus and its thermostability. [Research Support, Non-U.S. Gov't]. *J Mol Biol, 268*(5), 922-933. doi: 10.1006/jmbi.1997.1001

Hippler, M., Redding, K., & Rochaix, J. D. (1998). Chlamydomonas genetics, a tool for the study of bioenergetic pathways. [Research Support, Non-U.S. Gov't Research Support, U.S. Gov't, Non-P.H.S.

Review]. *Biochim Biophys Acta, 1367*(1-3), 1-62.

Hjelmeland, L. M., Allenmark, S., Derlan, B. A., Jackiw, B. A., Nguyen, N. Y., & Chrambach, A. (1981). Electrophoresis in Gels Containing Zwitterionic Groups. *Electrophoresis, 2*(2), 82-90. doi: DOI 10.1002/elps.1150020204

Hogewoning, S. W., Wientjes, E., Douwstra, P., Trouwborst, G., van Ieperen, W., Croce, R., & Harbinson, J. (2012). Photosynthetic Quantum Yield Dynamics: From Photosystems to Leaves. *Plant Cell, 24*(5), 1921-1935. doi: DOI 10.1105/tpc.112.097972

Ihara, M., & Nakamoto, H., Kamachi, T., Okura, I., Maeda, M.,. (2006). Photoinduced hydrogen production by direct electron transfer from photosystem I cross-linked with cytochrome c(3) to [NiFe]-hydrogenase. *Photochem Photobiol, 82*(6), 1677-1685. doi: Doi 10.1562/2006-05-07-Ra-893

Iwuchukwu, I. J. (2011). Protein engineering for the Enhanced Photoproduction of Hydrogen by Cyanobacterial Photosystem I. *Doctoral Dissertations*.

Iwuchukwu, I. J., Iwuchukwu, E., Le, R., Paquet, C., Sawhney, R., Bruce, B., & Frymier, P. (2011). Optimization of photosynthetic hydrogen yield from platinized photosystem I complexes using response surface methodology. *International Journal of Hydrogen Energy, 36*(18), 11684-11692. doi: DOI 10.1016/j.ijhydene.2011.06.068

Iwuchukwu, I. J., Vaughn, M., Myers, N., O'Neill, H., Frymier, P., & Bruce, B. D. (2010). Self-organized photosynthetic nanoparticle for cell-free hydrogen production. [Research Support, Non-U.S. Gov't

Research Support, U.S. Gov't, Non-P.H.S.]. *Nat Nanotechnol, 5*(1), 73-79. doi: 10.1038/nnano.2009.315

Jan Zarzycki, S. D. A., James N. Kinney and Cheryl A. Kerfeld. (2012). Cyanobacterial-based approaches to improving photosynthesis in plants. *Journal of Experimental Botany Advance Access*.

Jansen, R., Bussemaker, H. J., & Gerstein, M. (2003). Revisiting the codon adaptation index from a whole-genome perspective: analyzing the relationship between gene expression and codon occurrence in yeast using a variety of models. [Research Support, U.S. Gov't, P.H.S.]. *Nucleic Acids Res, 31*(8), 2242-2251.

Jenik, M., Parra, R. G., Radusky, L. G., Turjanski, A., Wolynes, P. G., & Ferreiro, D. U. (2012). Protein frustratometer: a tool to localize energetic frustration in protein molecules. [Research Support, N.I.H., Extramural

Research Support, Non-U.S. Gov't]. *Nucleic acids research, 40*(Web Server issue), W348-351. doi: 10.1093/nar/gks447

John M. Olson, R. E. B. (2004). Thinking about the evolution of photosynthesis. *Photosynth Res, 80*.

Jordan, P., Fromme, P., Witt, H. T., Klukas, O., Saenger, W., & Krauss, N. (2001a). Three-dimensional structure of cyanobacterial photosystem I at 2.5 A resolution. [Research Support, Non-U.S. Gov't]. *Nature, 411*(6840), 909-917. doi: 10.1038/35082000

Jordan, P., Fromme, P., Witt, H. T., Klukas, O., Saenger, W., & Krauss, N. (2001b). Three-dimensional structure of cyanobacterial photosystem I at 2.5 angstrom resolution. *Nature, 411*(6840), 909-917. doi: Doi 10.1038/35082000

Katoh, S., Shiratori, I., & Takamiya, A. (1962). Purification and some properties of spinach plastocyanin. *J Biochem, 51*, 32-40.

Kiley, P., Zhao, X., Vaughn, M., Baldo, M. A., Bruce, B. D., & Zhang, S. (2005). Self-assembling peptide detergents stabilize isolated photosystem I on a dry surface for an extended time. [Research Support, U.S. Gov't, Non-P.H.S.]. *PLoS Biol, 3*(7), e230. doi: 10.1371/journal.pbio.0030230

Lan, E. I., & Liao, J. C. (2011). Metabolic engineering of cyanobacteria for 1-butanol production from carbon dioxide. [Research Support, Non-U.S. Gov't]. *Metab Eng, 13*(4), 353-363. doi: 10.1016/j.ymben.2011.04.004

Lelong, C., Boekema, E. J., Kruip, J., Bottin, H., Rogner, M., & Setif, P. (1996a). Characterization of a redox active cross-linked complex between cyanobacterial photosystem I and soluble ferredoxin. *Embo Journal, 15*(9), 2160-2168.

Lelong, C., Boekema, E. J., Kruip, J., Bottin, H., Rogner, M., & Setif, P. (1996b). Characterization of a redox active cross-linked complex between cyanobacterial photosystem I and soluble ferredoxin. [Research Support, Non-U.S. Gov't]. *EMBO J, 15*(9), 2160-2168.

Lelong, C., Setif, P., Lagoutte, B., & Bottin, H. (1994). Identification of the Amino-Acids Involved in the Functional Interaction between Photosystem-I and Ferredoxin from Synechocystis Sp-Pcc-6803 by Chemical Cross-Linking. *Journal of Biological Chemistry, 269*(13), 10034-10039.

Lindberg, P., Park, S., & Melis, A. (2010). Engineering a platform for photosynthetic isoprene production in cyanobacteria, using Synechocystis as the model organism. [Research Support, Non-U.S. Gov't]. *Metab Eng, 12*(1), 70-79. doi: 10.1016/j.ymben.2009.10.001

Liu, J. G., Lu, J. R., Zhao, X. B., Lu, J. R., & Cui, Z. F. (2007). Separation of glucose oxidase and catalase using ultrafiltration with 300-kDa polyethersulfone membranes. *Journal of Membrane Science, 299*(1-2), 222-228. doi: DOI 10.1016/j.memsci.2007.04.044

Macwan, D. P., Dave, P. N., & Chaturvedi, S. (2011). A review on nano-TiO2 sol-gel type syntheses and its applications. *Journal of Materials Science, 46*(11), 3669-3686. doi: DOI 10.1007/s10853-011-5378-y

Matsubara, H., Sasaki, R. M., & Chain, R. K. (1967). The amino Acid sequence of spinach ferredoxin. *Proc Natl Acad Sci U S A, 57*(2), 439-445.

Mershin, A., Matsumoto, K., Kaiser, L., Yu, D., Vaughn, M., Nazeeruddin, M. K., . . . Zhang, S. (2012a). Self-assembled photosystem-I biophotovoltaics on nanostructured TiO(2)and ZnO. *Scientific reports, 2*, 234. doi: 10.1038/srep00234

Mershin, A., Matsumoto, K., Kaiser, L., Yu, D., Vaughn, M., Nazeeruddin, M. K., . . . Zhang, S. (2012b). Self-assembled photosystem-I biophotovoltaics on nanostructured TiO(2)and ZnO. *Sci Rep, 2*, 234. doi: 10.1038/srep00234

Mershin, A., Matsumoto, K., Kaiser, L., Yu, D. Y., Vaughn, M., Nazeeruddin, M. K., . . . Zhang, S. G. (2012c). Self-assembled photosystem-I biophotovoltaics on nanostructured TiO2 and ZnO. *Sci Rep, 2*. doi: Artn 234

Doi 10.1038/Srep00234

Miao, X., & Wu, Q. (2006). Biodiesel production from heterotrophic microalgal oil. [Research Support, Non-U.S. Gov't]. *Bioresour Technol, 97*(6), 841-846. doi: 10.1016/j.biortech.2005.04.008

Millsaps, J. F., Bruce, B. D., Lee, J. W., & Greenbaum, E. (2001). Nanoscale photosynthesis: photocatalytic production of hydrogen by platinized photosystem I reaction centers. [Research Support, Non-U.S. Gov't

Research Support, U.S. Gov't, Non-P.H.S.]. *Photochem Photobiol, 73*(6), 630-635.

Mulkidjanian, A. Y., Koonin, E. V., Makarova, K. S., Mekhedov, S. L., Sorokin, A., Wolf, Y. I., . . . Galperin, M. Y. (2006). The cyanobacterial genome core and the origin of photosynthesis. [Research Support, N.I.H., Intramural

Research Support, Non-U.S. Gov't]. *Proc Natl Acad Sci U S A, 103*(35), 13126-13131. doi: 10.1073/pnas.0605709103

Mussgnug, J. H., Thomas-Hall, S., Rupprecht, J., Foo, A., Klassen, V., McDowall, A., . . . Hankamer, B. (2007). Engineering photosynthetic light capture: impacts on improved solar energy to biomass conversion. [Research Support, Non-U.S. Gov't]. *Plant Biotechnol J, 5*(6), 802-814. doi: 10.1111/j.1467-7652.2007.00285.x

Nakamura, Y., Kaneko, T., Sato, S., Ikeuchi, M., Katoh, H., Sasamoto, S., . . . Tabata, S. (2002). Complete genome structure of the thermophilic cyanobacterium Thermosynechococcus elongatus BP-1. [Research Support, Non-U.S. Gov't]. *DNA Res, 9*(4), 123-130.

Nelson, N. (2009). Plant photosystem I--the most efficient nano-photochemical machine. *J Nanosci Nanotechnol, 9*(3), 1709-1713.

Nguyen, K., & Bruce, B. D. (2014). Growing green electricity: Progress and strategies for use of Photosystem I for sustainable photovoltaic energy conversion. [Review]. *Biochim Biophys Acta*. doi: 10.1016/j.bbabio.2013.12.013

Onuchic, J. N., Luthey-Schulten, Z., & Wolynes, P. G. (1997). Theory of protein folding: the energy landscape perspective. [Research Support, Non-U.S. Gov't
Research Support, U.S. Gov't, Non-P.H.S.
Research Support, U.S. Gov't, P.H.S.
Review]. *Annu Rev Phys Chem, 48*, 545-600. doi: 10.1146/annurev.physchem.48.1.545

Orkin, S. (1990). Molecular-Cloning - a Laboratory Manual, 2nd Edition - Sambrook,J, Fritsch,Ef, Maniatis,T. *Nature, 343*(6259), 604-605. doi: Doi 10.1038/343604a0

Page, C. C., Moser, C. C., Chen, X., & Dutton, P. L. (1999). Natural engineering principles of electron tunnelling in biological oxidation-reduction. [Research Support, U.S. Gov't, P.H.S.]. *Nature, 402*(6757), 47-52. doi: 10.1038/46972

Ragsdale, S. W., & Ljungdahl, L. G. (1984). Characterization of ferredoxin, flavodoxin, and rubredoxin from Clostridium formicoaceticum grown in media with high and low iron contents. [Research Support, Non-U.S. Gov't
Research Support, U.S. Gov't, Non-P.H.S.
Research Support, U.S. Gov't, P.H.S.]. *J Bacteriol, 157*(1), 1-6.

Rao, K. K., Cammack, R., Hall, D. O., & Johnson, C. E. (1971). Mossbauer effect in Scenedesmus and spinach ferredoxins. The mechanism of electron transfer in plant-type iron-sulphur proteins. *Biochem J, 122*(3), 257-265.

Raven, J. A. (1969). Action Spectra for Photosynthesis and Light-Stimulated Ion Transport Processes in Hydrodictyon Africanum. *New Phytologist, 68*(1), 45-+. doi: DOI 10.1111/j.1469-8137.1969.tb06418.x

Raven, J. A. (1970). Role of Cyclic and Pseudocyclic Photophosphorylation in Photosynthetic C-1402 Fixation in Hydrodictyon-Africanum. *J Exp Bot, 21*(66), 1-&. doi: Doi 10.1093/Jxb/21.1.1

Rochaix, J. D. (2011). Regulation of photosynthetic electron transport. [Research Support, Non-U.S. Gov't

Review]. *Biochim Biophys Acta, 1807*(3), 375-383. doi: 10.1016/j.bbabio.2010.11.010

Sarikaya, M., Tamerler, C., Jen, A. K. Y., Schulten, K., & Baneyx, F. (2003). Molecular biomimetics: nanotechnology through biology. *Nat Mater, 2*(9), 577-585. doi: Doi 10.1038/Nmat964

Sasaki, R. M., & Matsubara, H. (1967). Molecular weight and amino acid composition of Chromatium ferredoxin. *Biochem Biophys Res Commun, 28*(3), 467-473.

Scott, S. A., Davey, M. P., Dennis, J. S., Horst, I., Howe, C. J., Lea-Smith, D. J., & Smith, A. G. (2010). Biodiesel from algae: challenges and prospects. [Research Support, Non-U.S. Gov't

Review]. *Curr Opin Biotechnol, 21*(3), 277-286. doi: 10.1016/j.copbio.2010.03.005

Setif, P., Fischer, N., Lagoutte, B., Bottin, H., & Rochaix, J. D. (2002). The ferredoxin docking site of photosystem I. [Comparative Study]. *Biochim Biophys Acta, 1555*(1-3), 204-209.

Setif, P., Harris, N., Lagoutte, B., Dotson, S., & Weinberger, S. R. (2010a). Detection of the photosystem I:ferredoxin complex by backscattering interferometry. *Journal of the American Chemical Society, 132*(31), 10620-10622. doi: 10.1021/ja102208u

Setif, P., Harris, N., Lagoutte, B., Dotson, S., & Weinberger, S. R. (2010b). Detection of the photosystem I:ferredoxin complex by backscattering interferometry. *J Am Chem Soc, 132*(31), 10620-10622. doi: 10.1021/ja102208u

Shih, P. M., Wu, D. Y., Latifi, A., Axen, S. D., Fewer, D. P., Talla, E., . . . Kerfeld, C. A. (2013). Improving the coverage of the cyanobacterial phylum using diversity-driven genome sequencing. *Proc Natl Acad Sci U S A, 110*(3), 1053-1058. doi: DOI 10.1073/pnas.1217107110

Sonoike, K., Hatanaka, H., & Katoh, S. (1993). Small Subunits of Photosystem-I Reaction Center Complexes from Synechococcus-Elongatus .2. The Psae Gene-Product Has a Role to Promote Interaction between the Terminal Electron-Acceptor and Ferredoxin. *Biochim Biophys Acta, 1141*(1), 52-57. doi: Doi 10.1016/0005-2728(93)90188-L

Stuart, T. S., & Gaffron, H. (1972). Mechanism of Hydrogen Photoproduction by Several Algae .1. Effect of Inhibitors of Photophosphorylation. *Planta, 106*(2), 91-&. doi: Doi 10.1007/Bf00383989

Sugimoto, T., Zhou, X., & Muramatsu, A. (2003). Synthesis of uniform anatase TiO2 nanoparticles by gel-sol method. 4. Shape control. *J Colloid Interface Sci, 259*(1), 53-61.

Tagawa, K., & Arnon, D. I. (1962). Ferredoxins as electron carriers in photosynthesis and in the biological production and consumption of hydrogen gas. *Nature, 195*, 537-543.

Thai, C. K., Dai, H., Sastry, M. S., Sarikaya, M., Schwartz, D. T., & Baneyx, F. (2004). Identification and characterization of Cu(2)O- and ZnO-binding polypeptides by Escherichia coli cell surface display: toward an understanding of metal oxide binding. [Research Support, U.S. Gov't, Non-P.H.S.]. *Biotechnol Bioeng, 87*(2), 129-137. doi: 10.1002/bit.20149

Toporik, H., Carmeli, I., Volotsenko, I., Molotskii, M., Rosenwaks, Y., Carmeli, C., & Nelson, N. (2012). Large photovoltages generated by plant photosystem I crystals. [Research Support, Non-U.S. Gov't]. *Adv Mater, 24*(22), 2988-2991, 2987. doi: 10.1002/adma.201200039

Wang, Z., Zhu, X. G., Chen, Y., Li, Y., Hou, J., & Liu, L. (2006). Exploring photosynthesis evolution by comparative analysis of metabolic networks between chloroplasts and photosynthetic bacteria. [Comparative Study

Research Support, Non-U.S. Gov't]. *BMC Genomics, 7*, 100. doi: 10.1186/1471-2164-7-100

Wittenberg, G., Sheffler, W., Darchi, D., Baker, D., & Noy, D. (2013). Accelerated electron transport from photosystem I to redox partners by covalently linked

ferredoxin. [Research Support, Non-U.S. Gov't]. *Phys Chem Chem Phys, 15*(45), 19608-19614. doi: 10.1039/c3cp53264j

Yacoby, I., Pochekailov, S., Toporik, H., Ghirardi, M. L., King, P. W., & Zhang, S. G. (2011). Photosynthetic electron partitioning between [FeFe]-hydrogenase and ferredoxin:NADP(+)-oxidoreductase (FNR) enzymes in vitro. *Proc Natl Acad Sci U S A, 108*(23), 9396-9401. doi: DOI 10.1073/pnas.1103659108

Yamaoka, T., Satoh, K., & Katoh, S. (1978). Photosynthetic Activities of a Thermophilic Blue-Green-Alga. *Plant and Cell Physiology, 19*(6), 943-954.

Yehezkeli, O., Tel-Vered, R., Michaeli, D., Willner, I., & Nechushtai, R. (2013). Photosynthetic reaction center-functionalized electrodes for photo-bioelectrochemical cells. *Photosynthesis research*. doi: 10.1007/s11120-013-9796-3

Zanetti, G., & Merati, G. (1987). Interaction between Photosystem-I and Ferredoxin - Identification by Chemical Cross-Linking of the Polypeptide Which Binds Ferredoxin. *European Journal of Biochemistry, 169*(1), 143-146. doi: DOI 10.1111/j.1432-1033.1987.tb13591.x

Zilber, A. L., & Malkin, R. (1988). Ferredoxin Cross-Links to a 22-Kd Subunit of Photosystem-I. *Plant Physiology, 88*(3), 810-814. doi: Doi 10.1104/Pp.88.3.810

Zouni, A., Witt, H. T., Kern, J., Fromme, P., Krauss, N., Saenger, W., & Orth, P. (2001). Crystal structure of photosystem II from Synechococcus elongatus at 3.8 A resolution. [Research Support, Non-U.S. Gov't]. *Nature, 409*(6821), 739-743. doi: 10.1038/35055589

`

Appendix

`

Appendix 1 Wild type and codon optimize TeFd sequence

WT TeFd:

ATG GCA ACC TAC AAA GTA ACG CTA GTG CGT CCT GAT GGA GGC GAA ACA ACA ATT GAC GTG CCC GAA GAT GAG TAC ATT CTG GAT GTG GCC GAA GAG CAA GGC CTA GAC TTG CCC TTC TCC TGC CGT GCT GGT GCT TGC TCC ACC TGT GCC GGT AAG CTC CTG GAA GGA GAA GTG GAT CAG TCG GAT CAG TCC TTC TTG GAT GAT GAC CAA ATT GAG AAG GGC TTT GTG CTT ACC TGT GTA GCC TAT CCC CGT TCT GAC TGC AAA ATC CTC ACC AAC CAA GAG GAA GAG CTT TAC

C.O. TeFd

ATG GCT ACC TAC AAA GTT ACT CTG GTT CGT CCG GAT GGT TCT GAA ACC ACC ATC GAC GTG CCG GAA GAT GAA TAT ATC CTG GAC GTT GCT GAA GAG CAG GGC CTG GAC CTG CCG TTC AGC TGC CGT GCG GGC GCT TGC TCT ACT TGT GCG GGT AAA CTG CTG GAA GGC GAA GTT GAT CAG TCC GAC CAG TCT TTC CTG GAC GAC GAC CAG ATC GAG AAA GGC TTC GTA CTG ACC TGC GTA GCA TAT CCG CGT TCT GAT TGC AAA ATC CTG ACC AAC CAG GAA GAA GAA CTG TAC

`

Appendix 2 Primer list

M13 Forward: 5’- CGCCAGGGTTTTCCCAGTCACGAC -3’

M13 reverse: 5’- TCACACAGGAAACAGCTATGAC -3’

T7 Promoter F: 5’- AATACGACTCACTATAGGG -3’

T7 Terminator R: 5’- CTGCTAACAAAGCCCGAAAGGAA -3’

STB1-C.O.TeFd Forward: 5’- GGTCATATGTGCCATAAAAAACCGAGCAAAAG

CTGCGGCGGCAGCGCTACCTACAAAGTT -3’

STB2-C.O.TeFd Forward: 5’- GGTCATATGTGCACCAAACGCAACAACAAACG

CTGCGGCGGCAGCGCTACCTACAAAGTT -3’

LSTB1-C.O.TeFd Forward: 5’- GGTCATATGGCGCATAAAAAACCGAGCAAAA

GCGCGGGCGGCAGCGCTACCTACAAAGTT -3’

TOBiP-C.O.TeFd Reverse: 5’- CAAAGCACCCGGGGTACAGTTCTTC -3’

`

Appendix 3 HPLC method for Te PSI purification

Method Editor : MV_PSI_05-29-09.met Multi-Method : (UnTitled)

File Multi Method Edit Display Options OnBoard Analysis Template Window

EQ L W EL C S G I AI P Add Event Multi Method

Elapsed		Block	Event
			General Settings: Set Detectors Inline
			General Settings: Set Column Offline
			General Settings: UV Detector Wavelength = 280 nM and 430 nM
			General Settings: Flow Rate = 18.00 ml/min
			General Settings: Turn UV Detector Lamp On
			Pump On
0.00	min		Method Start
0.00	min	[01]	Equil Block
0.00	min		(A) Purge with Equilibration Buffer
0.00	min		0.00 ml Set Column Offline
0.00	min		0.00 ml Set Solvent Blend 80.0% A:H2O 20.0% B:PSI buffer
0.00	min		0.00 ml Set Flow Rate = 30.00 ml/min
0.00	min		0.00 ml Reset Fraction Collector*
0.50	min		15.00 ml Set Flow Rate = 18.00 ml/min
0.58	min		16.50 ml Set Column 1 Inline
0.58	min		
0.58	min		(B) Eq column w/ Eq buffer
0.58	min		0.00 CV Set Solvent Blend 80.0% A:H2O 20.0% B:PSI buffer
1.23	min		7.00 CV Zero UV Detector*
1.23	min		7.00 CV End Solvent Blend 80.0% A:H2O 20.0% B:PSI buffer
1.23	min		
1.23	min		————————————————————
1.23	min	[02]	Load Block
1.23	min		(A) Step Segment
1.23	min		0.00 ml Load through Pump 100% C
1.79	min		10.00 ml Set Flow Rate = 10.00 ml/min*
1.79	min		10.00 ml Load through Pump 100% C
1.79	min		
1.79	min		————————————————————
1.79	min	[03]	Wash Block
1.79	min		(A) Wash sucrose out of column
1.79	min		0.00 CV Set Solvent Blend 80.0% A:H2O 20.0% B:PSI buffer
2.45	min		4.00 CV Set Flow Rate = 15.00 ml/min*
3.34	min		12.00 CV End Solvent Blend 80.0% A:H2O 20.0% B:PSI buffer
3.34	min		
3.34	min		————————————————————
3.34	min	[04]	Elute Block

3.34	min	(A)	Gradient segment
3.34	min		0.00 CV Start Gradient 80.0% A:H2O 20.0% B:PSI buffer
4.00	min		6.00 CV Start Fraction Collection Peak 1.00ml Thr 0.500 Slp 0.200*
4.44	min		10.00 CV End Gradient 70.0% A:H2O 20.0% B:PSI buffer 10.0% D:MgSO4
4.44	min		
4.44	min	(B)	Step Segment
4.44	min		0.00 CV Set Solvent Blend 70.0% A:H2O 20.0% B:PSI buffer 10.0% D:MgSO4
5.55	min		10.00 CV End Solvent Blend 70.0% A:H2O 20.0% B:PSI buffer 10.0% D:MgSO4
5.55	min		
5.55	min	(C)	Elution gradient
5.55	min		0.00 CV Start Gradient 70.0% A:H2O 20.0% B:PSI buffer 10.0% D:MgSO4
6.88	min		12.00 CV End Gradient 50.0% A:H2O 20.0% B:PSI buffer 30.0% D:MgSO4
6.88	min		
6.88	min	(D)	Step Segment
6.88	min		0.00 CV Set Solvent Blend 20.0% A:H2O 20.0% B:PSI buffer 60.0% D:MgSO4
7.44	min		5.00 CV End Solvent Blend 20.0% A:H2O 20.0% B:PSI buffer 60.0% D:MgSO4
7.44	min		
7.44	min	———	———
7.44	min	[05]	Clean Block
7.44	min	(A)	Rinse Column with H2O
7.44	min		0.00 CV Set Solvent Blend 100% A:H2O
7.77	min		3.00 CV Stop Fraction Collection*
7.78	min		3.10 CV Reset Fraction Collector*
7.99	min		5.00 CV End Solvent Blend 100% A:H2O
7.99	min		
7.99	min	(B)	Acid wash column
7.99	min		0.00 CV Set Solvent Blend 90.0% A:H2O 10.0% E:HCl
8.54	min		5.00 CV End Solvent Blend 90.0% A:H2O 10.0% E:HCl
8.54	min		
8.54	min	(C)	Rinse out acid with H2O
8.54	min		0.00 CV Set Solvent Blend 100% A:H2O
9.32	min		7.00 CV End Solvent Blend 100% A:H2O
9.32	min		
9.32	min	(D)	Restore column pH
9.32	min		0.00 CV Set Solvent Blend 60.0% A:H2O 40.0% B:PSI buffer
10.98	min		15.00 CV End Solvent Blend 60.0% A:H2O 40.0% B:PSI buffer
10.98	min		Thresholds [pH > 5.5, Delay 0.00 CV]

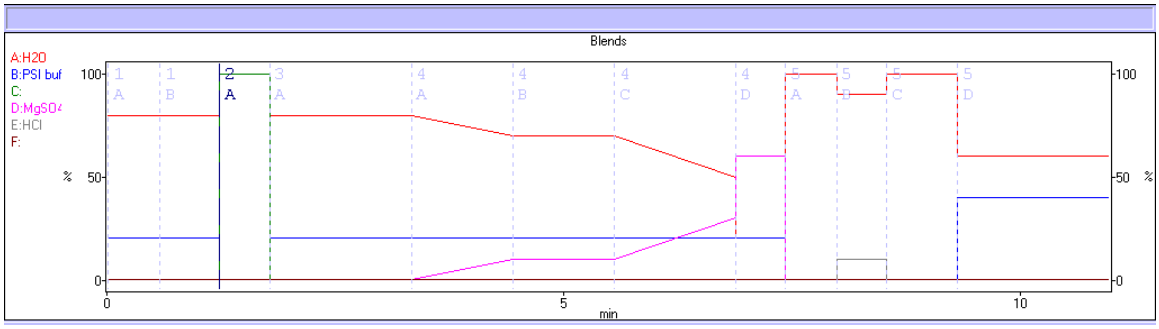

`

Vita

Tuo Zhu was born in Xianyang, China on February 18th, 1989. He attended primary school at Tianwang Primary School and went to Weicheng High School in Xianyang, China. He graduated from Weicheng High School in 2003 and joined Wuhan University, China in the same year. He obtained his Bachelor's Degree in the Biological Sciences from the Wuhan University in 2010. He joined the graduate program in the Biochemistry and Cellular and Molecular Biology Department of the University of Tennessee, Knoxville in the fall of 2010. He joined Dr. Barry D. Bruce's laboratory in the fall of 2011 and conducted research on engineering of photosystem I attachment to TiO_2 nanostructures via ferredoxin-fusion proteins. After completing his Master's Degree in May of 2014, he plans to work as a research scientist in Philadelphia.